CT-898-591
DON. 7015

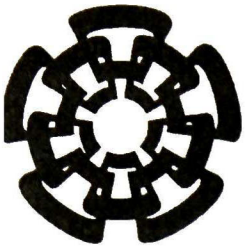

Centro de Investigación y de Estudios Avanzados
del Instituto Politécnico Nacional
Unidad Guadalajara

Diseño de la estructura y el control de área amplia del sistema de potencia

Tesis que presenta:
Evaristo Noé Reyes Pérez

para obtener el grado de:
Doctor en Ciencias

en la especialidad de:
Ingeniería Eléctrica

Director de Tesis
Dr. Arturo Román Messina

CINVESTAV del IPN Unidad Guadalajara, Guadalajara, Jalisco, Febrero de 2015.

CT00705
CT-898-551
14-10-2015
DONE 2015
$

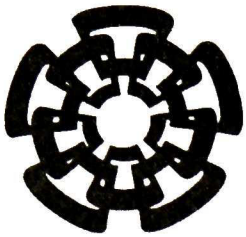

Centro de Investigación y de Estudios Avanzados del I.P.N.

Unidad Guadalajara

Wide-area power system control and structure design

A thesis presented by·
Evaristo Noé Reyes Pérez

to obtain the degree of:
Doctor in Science

in the subject of:
Electrical Engineering

Thesis Advisor:
Dr. Arturo Román Messina

Guadalajara, Jalisco, February 2015.

Diseño de la estructura y el control de área amplia del sistema de potencia

Tesis de Doctorado en Ciencias
Ingeniería Eléctrica

Por:
Evaristo Noé Reyes Pérez
Maestro en Ciencias en Ingeniería Eléctrica
CINVESTAV Guadalajara 2000-2002

Becario de CONACYT, expediente no. 35325

Director de Tesis
Dr. Arturo Román Messina

CINVESTAV del IPN Unidad Guadalajara, Febrero de 2015.

Wide-area power system control and structure design

Doctor of Science Thesis
In Electrical Engineering

By·
Evaristo Noé Reyes Pérez
Master of Sciences in Electrical Engineer
Centro de Investigación y de Estudios Avanzados del I. P N.,
Unidad Guadalajara
2000-2002

Scholarship granted by CONACYT, No. 35325

Thesis Advisor:
Dr. Arturo Román Messina

CINVESTAV del IPN Unidad Guadalajara, February, 2015.

Acknowledgments

Special thanks to CONACYT and the Center of Researching and Advanced Studies of IPN (CINVESTAV) for their supports.

A mi padre, Evaristo Reyes Bautista, desaparecido físicamente desde hace más de una década, quien me enseñó todo el grado cultural, económico, social, histórico del que gozo.

Al Dr. Arturo Román Messina, quien me enseñó la moral y la ética en la investigación.

Al Lic. Andrés Manuel López Obrador, quien ha enfrentado de manera incansable a los tecnócratas neoliberales de este país, y que me enseñó la congruencia y el pudor de la vida pública de México.

Diseño de la estructura y el control de área amplia del sistema de potencia

Resumen

En esta tesis, se propone un marco de trabajo general analítico para diseñar simultáneamente la estructura y el control de área amplia del sistema de potencia para amortiguar oscilaciones inter área. Primero, se propone una formulación general basada en el valor singular estructurado, la cual permite evaluar el efecto de la incertidumbre compleja en la robustez de la estabilidad. Entonces, se desarrolla una nueva técnica para determinar los mejores pares entrada salida para controladores de área amplia multivariables basado en la ganancia por bloques relativa.

En este contexto, la teoría de control robusto multivariable es aplicada para generar controles descentralizados o parcialmente descentralizados que garantizan un rendimiento con respecto a las incertidumbres en la estructura de la red y las condiciones de operación. La técnica es particularmente adecuada para sistemas de potencia grandes y complejos, en los cuales varios controladores del sistema de potencia son usados para amortiguar simultáneamente los modos inter área y locales de las diferentes frecuencias que aparecen simultáneamente.

Finalmente, las técnicas de desigualdades lineales matriciales son empleadas para diseñar controladores de área amplia. En general, esta plataforma de trabajo permite una mejor coordinación de las capacidades del control, y el uso de las medidas de interacción permite ayudar en la elección de la estructura y localización del control.

La eficacia de la configuración de control jerárquica propuesta para mejorar los modos oscilatorios críticos del sistema es examinado en un modelo real del sistema interconectado mexicano. Son investigados en detalle los efectos de latencia, incertidumbre y la interacción del control en el comportamiento del sistema. Simulaciones de tiempo no lineales detalladas son realizadas para verificar la eficiencia de las metodologías de diseño propuestos.

Wide-area power system control and structure design

Abstract

In this dissertation, a general analytical framework for simultaneously designing wide-area power system control and structure for damping inter-area oscillations is proposed. First, a general formulation based on the mixed structural singular value, which allows to assess the effect of complex uncertainty on stability robustness is introduced. Then, a novel technique to determine the best input-output pairings for multivariate wide-area controllers based on the block relative gain is developed.

In this framework, multivariable robust control theory is applied to generate decentralized or partially centralized controls that guarantee performance with respect to uncertainties in network structure and operating conditions. The technique is particularly well suited for large, complex power systems in which several power system controllers are used to simultaneously damp local and inter-area modes of different frequencies appearing simultaneously.

Linear matrix inequality techniques are finally employed to design wide-area damping controllers. In general, this framework allows for a better coordination of control capabilities, and the use of interaction measures allows to help in the choice of control location and structure.

The effectiveness of the proposed hierarchical control configuration to enhance damping of critical system oscillatory modes is tested on a realistic model of the Mexican interconnected system. The effects of latency, uncertainty and control interaction on system behavior are investigated in detail. Detailed nonlinear time simulations are conducted to verify the efficiency of the proposed design methodologies.

Contents

List of Figures

List of Tables

Abbreviations

SISO	Single-input single-output.
MIMO	Multi-input multi-output.
RGA	Relative gain array.
DRGA	Dynamic relative gain array.
GDRG	Generalized dynamic relative gain.
RIA	Relative interaction array.
LFT	Linear fractional transformation.
SSV	Structured singular value.
SVD	Singular value decomposition.
LTI	Linear time invariant system.
BRG	Block relative gain.
RHP	Right half plane.
arg	Argument of a function.
LMI	Linear matrix inequality.
NPhard	Non-deterministic polynomial-time hard.
NRG	Non-square relative gain.
LQG	Linear quadratic Gaussian.
DFT	Discrete Fourier transform.
PMU	Phasor measurement unit.
WAMS	Wide-area measurement system.
WADC	Wide-area measurement system.
FACTS	Flexible alternating current transmission system.
PSS	Power system stabilizer.
HVDC	High-voltage direct current.
MIS	Mexican interconnected system.

Symbols

j	Unit imaginary number.
ω	Frequency.
$\mathbf{u}(s)$	Input.
$\mathbf{y}(s)$	Output.
$\mathbf{e}(s)$	Control error.
$\mathbf{r}(s)$	Reference.
$\mathbf{w}(s)$	Perturbation.
$\mathbf{G}(s)$	Plant transfer function.
$\mathbf{K}(s)$	Controller transfer function.
$\mathbf{K}_{ii}(s)$	Closed loop transfer function with the k-th open control loop.
$\left[\begin{array}{c\|c} \mathbf{A} & \mathbf{B} \\ \hline \mathbf{C} & \mathbf{D} \end{array}\right]$	State space realization of $\mathbf{C}(s\mathbf{I}-\mathbf{A})^{-1}\mathbf{B}+\mathbf{D}$.
$\mathbf{A}$, $\mathbf{B}$, $\mathbf{C}$, $\mathbf{D}$	State space matrices.
$\langle\cdot,\cdot\rangle$	Inner product.
$\|\mathbf{A}\|$	Norm of $\mathbf{A}$.
$\mathcal{H}_\infty$	Space of all functions $\mathbf{F}(s)$ which are analytic in $\mathrm{Re}(s)>0$, take values in $\mathbb{C}^{m\times n}$ and are bounded in the right half plane.
$\mathcal{RH}_\infty$	The real rational subspace of $\mathcal{H}_\infty$.
$\bar{\sigma}[\mathbf{A}]$	Largest singular value of $\mathbf{A}$.
$F_l[\mathbf{P}(s),\mathbf{K}(s)]$	Lower LFT.
$F_u[\mathbf{P}(s),\mathbf{\Delta}(s)]$	Upper LFT.
$\rho[\mathbf{A}]$	The spectral radius of $\mathbf{A}$.
$\rho_{\mathbb{R}}[\mathbf{A}]$	The real spectral radius of $\mathbf{A}$.
$\mathbf{D}(\omega)$, $\mathbf{G}(\omega)$	Scaling matrices for computing the structured singular value.
$\mathbf{D}(s)$	Scaling used in D-K iteration.
$\mathbf{G}(s)$, $\mathbf{G}_h(s)$	Additional scaling in D-G-K iteration.
$\mathbf{\Gamma}(s)$, $\gamma(s)$	Additional scaling in μ-K iteration.
$\mu_{\mathrm{M}}[\mathbf{A}]$	The mixed structured singular value of $\mathbf{A}$.
$\mu_{\mathrm{C}}[\mathbf{A}]$	The complex structured singular value of $\mathbf{A}$.
$\mu_S[\mathbf{A}]$	The skewed structured singular value of $\mathbf{A}$.
$\mathbf{\Delta}(s)$	Block diagonal perturbation structure used with μ.
$\det[\mathbf{A}]$	Determinant of complex matrix $\mathbf{A}$.
$[\boldsymbol{\lambda}(s)]_{11}$	The BRG array for pairing $\mathbf{y}_1(s)-\mathbf{u}_1(s)$
$[\tilde{\boldsymbol{\lambda}}(s)]_{11}$	The block GDRG for pairing $\mathbf{y}_1(s)-\mathbf{u}_1(s)$.
$\frac{1}{s}\Big\|_{s=0}$	Integral feedback control evaluated at $s=0$.
$\mathbf{H}^i(0)$	The closed loop function at $s=0$ to the pairing $y_i(0)-u_i(0)$
$\mathbf{K}^i(0)$	The diagonal matrix of controllers with $k_{ii}(s)=0$.

Chapter 1
Introduction

1.1 Introduction and motivation

Power system oscillatory behavior has received a great deal of attention in recent research. The critical dynamics are often associated with inter-area and local oscillation modes associated with the exchange of kinetic energy among system generators. Under some circumstances, these oscillations can result in system instability and blackout. Unfortunately, power systems are complex networks that defy predictions with any degree of certainty due to the vast number of generators and transmission lines that make the analysis and control of power system oscillatory behavior difficult [1-3].

As a result of the size of the power system, linear methodologies are preferred to analyze and design power system controllers. Using linear analysis approaches, wide-area controllers can be represented by transfer functions for local input-output or multiple-input multiple-output (MIMO) channels. In general, these characteristics must be considered during linear analysis and design of controllers.

Decentralized controllers are preferred in large linear systems because they result in local feedback signals and simpler control structures. A single-input single–output (SISO) decentralized controller design, however, neglects loop interactions due to the off-diagonal elements of a plant, which can lead to performance deterioration and even instability. This motivates this research work.

Ideally, a multivariable plant would be controlled by a centralized controller where the control action of each manipulated variable is a function of all the measurements, but it is preferable to design SISO controllers.

In the last decades, multivariable controllers have been avoided in favor of simpler decentralized controllers due to the fact that power system generator controllers are decentralized through power system stabilizers (PSSs). The basic function of a PSS is to add damping to the generator rotor oscillations by controlling its excitation using auxiliary stabilizing signals. To provide damping, the PSS must produce a component of electrical torque in phase with the rotor speed deviations [1]. In addition, with the incorporation of flexible alternating current transmission system (FACTS) devices have been possible to design supplementary controllers to enhance power system stability in addition to their main principal function of power flow.

It is further assumed that the nominal scenario of a power system is stable to design supplementary controllers, which can be expressed in frequency domain. Unfortunately, the high degree of nonlinearity of power systems and continuous change in operating points make very difficult to achieve a controller design using only a single nominal model. These limitations have lead to the development of robust decentralized controllers which can incorporate uncertainties for robust performance and analysis.

Another related problem in power systems is the location of the most suitable input-output signals for control configurations. In the last decade, with the incorporation of phasor measurement units (PMUs) and satellite communications, wide-area measurement system (WAMS) technology has made it possible to implement multi-level control configurations for damping electromechanical modes through remote measurements.

Much of recent research has therefore focused on developing new methods to assess and select input-output signals for wide-area damping controllers. Although wide-area damping controller (WADC) devices have the potential to improve the damping of inter-area oscillations, the use of hierarchical configurations also introduces new challenges into the synthesis of controllers and loop interactions to damp local modes.

Uncertainties arise due to varying parameters, unmodeled or neglected dynamics in linear systems, etc. Robust stability and robust performance are essential in electric power systems to mitigate electromechanical oscillations through robust decentralized controllers. Structured and unstructured uncertainty representations in power systems are useful in describing load flow changes, variations in network topology and changes in operating conditions, deregulation in the sector, and neglected dynamics

This thesis discusses the problem of simultaneous wide-area control/structure design and robustness.

The main motivations behind this research include:

- In contrast to conventional PSSs and FACTS devices, the implementation of wide-area controllers is much more effective for damping inter-area oscillations because it suffices to choose of a set of global signals and the associated most suitable input-output pairings.

- Multi-level hierarchical control structures can be used to simultaneously damp local and inter-area modes or inter-area modes of different frequencies appearing simultaneously

- The analysis and evaluation of robust stability in the presence of unmodeled dynamics and variations in power system operating conditions is a problem of increasing importance in centralized/decentralized wide-area control design.

1.2 Statement of the problem

Control structure design is an important first step in the design of robust power system controllers. Characterization of dynamic loop interactions is required for both, the selection of control structure and the minimization of adverse control interactions. In addition, an important requirement for a practical control system is robustness with respect to uncertain plant parameters.

Robust control theory provides a rich class of control configurations and methods to design controllers such as: μ [36-37, 48], $\mathcal{H}_\infty$ [7], and $\mathcal{H}_2/\mathcal{H}_\infty$ [50] techniques. Current research suggests that while the problem is hard in general, certain classes of robust controllers with special information structures are tractable via convex optimization techniques. Among them, $\mathcal{H}_2/\mathcal{H}_\infty$ method have been applied in several researches with good results.

The implementation of efficient algorithms using linear matrix inequalities (LMIs) and μ-synthesis in power systems has been developed in previous research to damp electromechanical modes. In general, the application of these methods provides attractive characteristics to design MIMO and SISO controllers. Two types of methodologies have been applied by most researchers to represent uncertainty in power systems to compute the structure singular value (SSV) [33]: the structure uncertainty based on percent representation which can include unstructured uncertainty, and the polynomial representation derived from least square minimization [25-28, 40].

The first uncertainty representation is more conservative and limited to each coefficient of linear matrix equations. In general, the SSV have been introduced in the literature to evaluate the robust stability and the robust performance.

If a power system does not have robust stability, the main objective is to find a robust controller to mitigate power system oscillations including robust performance. Unfortunately, to achieve these objectives, robust controllers must be carefully designed to achieve robust stability of the electromechanical modes without reducing the damping of other modes with weighting functions.

The relative gain array (RGA) is a tool to describe interactions among control loops, and is very easy to implement in large power systems. Furthermore, the selection and location of input-output signals, which play an important role in the stability of control devices, is crucial to stabilize inter-area and local modes. This method, however, does not provide additional information about MIMO loop interactions. In many applications several control configurations are modeled by MIMO systems, such as WADCs which take into account MIMO signals. Then, a solution for this problem must be given based on interaction measures. Finally, another drawback of the classical RGA analysis is the concept of phase.

It is therefore necessary to use a technique that could capture the uncertainties and include them into the model. Furthermore, a technique to describe interaction among control loops in frequency domain is deemed necessary.

1.3 Review of previous work

Over the last few years, research in robust control design, interactions measures and power systems has led to the development of many different tools for the design of robust SISO controllers and WADCs.

A brief review of these approaches is presented next in the context of this research.

1.3.1 Loop interactions and the RGA analysis

The problem of control loop interaction has been addressed using two interrelated approaches [4-5]: choosing suitable input-output pairs that will lead to the least interaction among control loops, and designing control strategies that will attenuate the effects of the interaction.

One of the earliest measures of interaction was the relative gain array (RGA). This original technique was introduced by Bristol [6]. The Bristol method has been extensively used to design decentralized controls by assuming that the control has a proportional integral (PI) feedback. The RGA, however, is a conservative and empirical method because it uses knowledge of the steady-state process and lacks dynamic information [7-8], which may result in wrong pairings and inaccurate indication of the amount of loop interaction present.

The above limitations have led some researchers to develop dynamic measures with the ability to improve the pairing capabilities of the steady state RGA in cases where the RGA changes substantially with frequency [9]. In the literature this method is called dynamic relative gain (DRGA). Other related works in the process control literature have been motivated by the goal of evaluating loop interaction in the frequency domain [10-14].

There is a large and growing literature on control loop interaction analysis. Two main approaches for choosing input-output pairings for PSSs and FACTS devices have emerged: modal analysis and frequency methods. The first approach involves the calculation of the eigenvalues and residues of the system, while the latter can be derived using the singular value decomposition or frequency methods [15-16].

The notion of interaction measures has been used for some time in designing and locating power system controllers [17-18]. In [19], a decentralized method to mitigate adverse interaction between controllers and electromechanical oscillations based on the notion of a dynamic RGA was proposed.

More recently, the RGA in [20, 21] was used to evaluate the capability, control structure and the bifurcation subsystems of a μ-synthesis power system stabilizer design. References [22, 23] examine the use of various analytical methods to select signals for FACTS devices and locate controllers.

A more recent and interesting development, has been the use of DRGA-based techniques to assess and select suitable inputs for FACTS and high-voltage direct current (HVDC) devices in wide-area control schemes [24]. In most cases, however, the selection of the input-output variables for the design of WADCs has been based on single-input single-output models.

1.3.2 Robust analysis using the structured singular value

Generally, in the literature two linear methodologies have been applied by most researches to determine stability in linear power systems: small signal stability that uses the eigenvalues analysis and robust techniques that use the SSV [25-28]. However, small signal stability is limited on a few selected points from the wide range of possible operating points. Then, the task is based in experience and on engineering judgment. Furthermore, these methods do not consider structured and unstructured uncertainty. Then, it is possible to design robust controllers to modify a mode of oscillation by feedback, but the size of the system must be considered to evaluate these techniques.

The use of the SSV in power systems has emerged as an alternative to quantify the robust stability and the robust performance in linear systems. This linear methodology presents an elegant technique to represent the nominal scenario and the structured uncertainty. Uncertainty is represented using the LFT representation which naturally unify the frequency-domain and state space methods [29-31]. Nevertheless, the structured uncertainty representation in power systems has a strong computational demand and arise due to changes in loads, transmission lines of the network, neglected dynamics, etc.

An essential and sometimes underrated concept regarding to the SSV is the difference between the complex and the mixed SSV. The complex case was derived using upper and lower bounds out of real parametric uncertainties [32-33]. Unfortunately, the gap among these bounds can be conservative. In fact, the mathematical formulation of the complex SSV shows that it may be considered as a first approximation with respect to the mixed SSV.

On the other hand, in [34] the robustness framework for multimachine power systems using $\mathcal{L}_\infty$ was developed. The main advantage of this approach is the simplicity of the derived conditions for robustness, which consists of computing the spectral radius of a certain nonnegative matrix.

The mixed SSV has been the focus of some researches due to the fact that it incorporates real parametric uncertainties [35-38]. A solution is to reformulate the upper and lower bounds with new scaling matrices. However, the computational burden of the procedure grows and the mixed SSV is discontinuous. This means that the possibility of missing a point does exist. A partial solution for the discontinuity behavior of the mixed SSV is to incorporate a percent of complex uncertainty, but this will result in an increase of the uncertainty [39].

1.3.3 Design of WADCs in power systems

There exist several robust linear methodologies to design robust controllers or optimal in some sense in power systems. One approach was developed using a set of LMIs [40-42]. This approach presents multi objectives characteristics derived from disturbance rejection, pole-placement, minimum damping ratio, etc. However, the nominal system is represented by unstructured uncertainty and balanced reduced-order model. Furthermore, in [43-44] similar results for unstructured uncertainty was derive using $\mathcal{H}_\infty$ and the polynomial approach. In [45], the normalized coprime factorization approach for loop-shaping design was proposed to design robust controllers. Essentially, all these methodologies describe unstructured uncertainties as the standard state space $\mathcal{H}_\infty$.

The introduction of techniques with μ-synthesis to design robust controllers has been applied in different researches [46-47]. In all these methodologies, the synthesis process is supporting with complex μ using D-K iteration. Nevertheless, the structured uncertainty is modelled as real parametric. These limitations emerge due fact to represent the structured uncertainty as a complex uncertainty.

For system models which incorporate real parametric uncertainties, it was developed the D-G-K iteration as a consequence of the mixed structured singular value [48-49]. However, in large power systems the D-G-K iteration increases the computational burden due to due to the scaling matrices of the mixed and complex SSV upper bounds.

1.4 Objectives of the dissertation

In this dissertation a common mathematical framework for decentralized, quasi-decentralized control and multilevel of large interconnected power systems is provided. A systematic analytical procedure based on the concept of the block relative gain (BRG) and block generalized dynamic relative gain (GDRG) is used to design block-decentralized controllers to damp electromechanical oscillations. The method allows to identify the most suitable pairing loops for MIMO WADCs and avoids degradation of performance and stability among designed controllers.

In a first stage the damping factor of electromechanical modes are studied using the small-signal analysis. Then the complex and mixed SSV are computed to evaluate and compare the robust stability. From the results obtained from modal analysis, the input-output selection criterion for MIMO controllers using the BRG is described. The use of the BRG method extends the conventional use of the RGA for interacting control systems, to the BRG to analyze interactions among MIMO controllers.

This gives candidate sets for supplementary controllers which are solved using the LMI techniques and evaluated in closed loop to evaluate interactions. Finally, in order to quantify the effectiveness of controllers an eigenvalue analysis of the closed-loop system is necessary. Then, the robust stability of designed controllers are computed using the SSV and non-linear simulations are simulated in a power system with real specifications.

1.5 Contributions of this dissertation

The main contributions of this dissertation are:

- A framework to evaluate the robust stability in power systems using the complex and mixed SSV is proposed and tested. Moreover, the incorporation of a percent of complex perturbations to real parameters to avoid the semi continuity of the mixed SSV for large power systems.

- A block decentralized control perspective to design WADCs which include hierarchical control configurations in power systems using LMI techniques is suggested.

- A systematic methodology to study interactions derived from the MIMO linear systems is developed. This document proposes the use of the BRG and block GDRG methodologies to select the more suitable input-outputs pairings for MIMO controllers.

- In addition, the concept of phase for interaction measures in SISO control loops is introduced.

1.6 Outline of the dissertation

This document is organized as follows: Chapter 2 introduces the robust control theory for unstructured and structure uncertainty and their criterions in linear systems; emphasis is placed on the difference between the complex SSV and mixed SSV In addition, via incorporating a percent of complex perturbations to real parameters, the semicontinuity of the mixed SSV for large power systems is avoided. Then, a general modeling approach for modeling real-valued parametric uncertainty in power systems is presented.

The problem of selecting the input-output pairings in large systems is treated in chapter 3. This problem emerges as a necessity to choose the most suitable input-output signals for MIMO and SISO controllers. Then, basic criterions are developed using the BRG.

Furthermore, this chapter proposes the use of the skewed SSV to measure the interaction impact due to the nominal model. Finally, a new method is proposed to select MIMO pairings for wide-area damping controllers and the development of new measures for interaction that account for more realistic operating conditions and control structures.

In chapter 4, a rigorous review of the robust control synthesis methods is presented. These topic includes, the LMI technique, the D-K iteration, the D-G-K iteration and the μ-K iteration and their respective limitations. The objective of this review is to have a general idea of the numerical limitations for large power systems.

Finally, chapter 5 discusses the proposed control scheme of block decentralized controllers on a realistic 5-area model of a practical test system. Furthermore, robust performance simulations using the mixed and complex SSV are included to evaluate the linear system and large disturbances are simulated to evaluate the performance of controllers.

1.7 Publications

Summited papers

1. E. N. Reyes, A. R. Messina, and M. A. G. Perez, "Design of wide-area damping controllers using the block relative gain array," *Electric Power Systems Research*, 2014.

2. E. N. Reyes, A. R. Messina, and A. J. Zavala, "Selection of multiple input/output signals for wide-area damping controllers in hierarchical configurations," *Electric Power Systems Research*, 2015.

Refereed journal papers

1. Arturo R. Messina, Noé Reyes, Ismael Moreno, and Marco A. Pérez., "A statistical data-fusion-based framework for Wide-area Oscillation monitoring," *Electric Power Components and Systems. Special Issue: The smart grid-state-of-art and future trends.* Vol. 42, Issue 3-4, Feb. 2014.

Papers on conference proceedings

1. E. N. Reyes., M. A. G. Perez, and A. R. Messina, "A framework or decentralized design of system controllers using an extended relative gain approach," presented at North American Power Symposium, 2013, Paper IEEE-978-1-4799-1255-1, pp. 1-6.

2. E. N. Reyes., M. A. G. Perez, and A. R. Messina, "Assessing robust stability of power systems using the complex and mixed SSV," presented at the Proc. Power and Energy, 2013, Paper 806-32, pp. 1-6.

1.8 References

[1] P. Kundur, *Power System Stability and Control*, McGraw-Hill, 1994, ISBN 0-07-035958-X.

[2] G. Rogers, *Power System Oscillations*, Kluwer Academic Publishers, 2000, ISBN 978-0-7923-7712-2.

[3] P W. Sauer and M. A. Pai, *Power System Dynamics and Stability*, Prentice Hall, 1998, ISBN 0-13-678830-0.

[4] P J. Campo, and M. Morari, "Achievable closed loop properties of systems under decentralized control: Conditions involving the steady state gain, *IEEE Trans. Automatic Control*, vol. 39, no. 5, pp. 932-943, 1994.

[5] A. Khali-Sedigh, and B. Moaveni, *Control configuration selection for multivariable plants*, Springer-Verlag Berlin Heidelberg, 2009, ISBN 978-3-642-03193-9.

[6] E. H. Bristol "On a new measure of interaction for multivariable process control,' *IEEE Trans. Automat. Contr.*, vol. 11, pp. 133-134, Jan. 1966.

[7] S. Skogestad, and I. Postlethwaite, *Multivariable Feedback Control: Analysis and Design*, John Wiley and Sons, 1996, ISBN 0-471-94277-4.

[8] S. Skogestad, and M. Morari, "Implications of large RGA elements on control performance," *Ind. Eng. Chem. Res.*, vol. 26, pp. 2323-2330, Nov. 1987.

[9] E. H. Bristol "RGA 1977: "Dynamic effects of interaction, *in Proc. 16th Conf. Decision and Contr.*, New Orleans, Louisiana, pp. 1096-1100, Dec. 1977.

[10] H.-P. Huang, M. Ohshima and L. Hashimoto, "Dynamic interaction and multiloop control system design,' *J. Proc. Cont.*, vol. 4, pp. 15-27, 1994.

[11] H. Lau, J. Alvarez, and K. F. Jensen, "Synthesis of control structures by singular value analysis: Dynamic measure of sensitivity and interaction" *AIChe J.*, vol. 31, pp. 427-439, Mar. 1985.

[12] Z-X. Zhu "Variable pairing selection based on individual and overall interaction measures, *Ind. Eng. Chem. Res.*, vol. 35, pp. 4091-4099, 1996.

[13] Z-X Zhu "Structural analysis and stability conditions of decentralized control systems," *Ind. Eng. Chem. Res.*, vol. 35, pp. 736-745., 1996.

[14] M. Van de Wal, and B. De Jaber, "A review of methods for input/ouput selection,' *Automatica,* vol. 37, pp. 487-510, Abr. 2001.

[15] F L. Pagola, I. J. Pérez-Arriaga and G. C. Verghese, "On sensitivities, residues, and participations," *IEEE Trans. Power Syst.*, vol. 4, pp. 278-285, Feb. 1989.

[16] A. Heniche, and I. Kamwa "Control loops selection to damp inter-area oscillations of electrical networks," *IEEE Trans. Power Syst.*, vol. 17, pp. 378-384, May. 2002.

[17] P. Zhang, A. R. Messina, A. Coonick and B. J. Cory, "Selection of locations and input signals for multiple SVC damping controllers in large power systems," presented at the Proc. 1998 IEEE/Power Eng. Soc. Winter Meeting, Paper IEEE-0-7803-4403-0, pp. 667-670.

[18] J. V Milanovic, and A. C. S. Duque "Identification of electromechanical modes and placement of PSSs using relative gain array," *IEEE Trans. Power Syst.*, vol. 19, pp. 410-417, Feb. 2004.

[19] A. R. Messina, O. Begovich, J. H. López, E. N. Reyes, "Design of multiple facts controllers for damping inter-area oscillations: a decentralized control approach, Electric Power and Energy Systems, vol. 26, pp. 19-29, Dec. 2004.

[20] M. Yue, and R. A. Schlueter, "μ-synthesis power system stabilizer design using a bifurcation subsystem based methodology," *IEEE Trans. Power Systems*, vol. 18, pp. 1497-1506, Nov. 2003.

[21] M. Yue, and R. A. Schlueter, "Robust control designs for multiple bifurcations, *IEEE Trans. Power Systems*, vol. 20, pp. 301-311, Feb. 2005.

[22] M. M. Farsangi, Y. H. Song, and Kwang Y. Lee "Choice of FACTS device control inputs for damping interarea oscillations,' *IEEE Trans. Power Syst.*, vol. 19, pp. 1135-1143, May. 2004.

[23] M. M. Farsangi, H. Nezamabadi-pour, Y. H. Song, and K. Y. Lee, "Placement of SVCs and selection of stabilizing singnals in power systems,' *IEEE Trans. Power Syst.*, vol. 22, pp. 1061-1071, Aug. 2007.

[24] Y. Li, C. Rehtanz, S. R. L. Luo, and Y. Cao, "Assessment and choice of input signals for multiple HVDC and FACTS wide-area damping controllers,' *IEEE Trans. Power Syst.*, vol. 27, pp. 1969-1977, Nov. 2012.

[25] G. Rogers, *Power System Oscillations*, Kluwer Academic Publishers, 2000, ISBN 978-1-4615-4561-3.

[26] M. Djukanovic, M. H. Khammash, and V Vittal, "Application of structured singular value theory for robust stability and control analysis in multimachine power systems part-I: Framework development, *IEEE Trans. Power Systems*, vol. 13, pp. 1311-1316, Nov. 1998.

[27] M. Djukanovic, M. H. Khammash, and V Vittal, "Application of structured singular value theory for robust stability and control analysis in multimachine power systems part-II: Numerical simulations and results," *IEEE Trans. Power Systems*, vol. 13, pp. 1317-1322, Nov. 1998.

[28] R. Castellanos, A. R. Messina, and H. Sarmiento, "Robust stability analysis of large power systems using the structured singular value theory," *Electric Power and Energy Systems*, vol. 27, pp. 389-397, Jun. 2005.

[29] M. K. H. Fan, A. L. Tits, "Characterization and efficient computation of the structured singular value" *IEEE Trans. Automat. Contr.*, vol. 31, pp. 734-743, Aug. 1986.

[30] D. W. Gu, P. Hr Petkov, M. M. Konstantinov, *Robust control Design with Matlab* (Springer, 2005), ISBN 10-1852339837.

[31] R. R. E. De Gaston, M. G. Safonov, "Exact calculation of the multiloop stability margin, structured singular value,' *IEEE Trans. Automat. Contr.*, vol. 33, pp. 156-171, Feb. 1988.

[32] A. Packard, J. C. Doyle, "The complex structured singular value,' *Automatica*, vol. 29, pp. 71-109, Jan. 1993.

[33] K. Zhou, J. C. Doyle and K. Glover, *Robust and optimal control*, Prentice Hall, 1995, ISBN-10: 0134565673.

[34] M. H. Khammash, V Vittal, and C. D. Pawloski "Analysis of control performance for stability robustness of power systems," *IEEE Trans. Power Systems*, vol. 9, pp. 1861-1866, Nov. 1994.

[35] M. K. H. Fan, A. L. Tits, J. C: Doyle, "Robustness in the presence of mixed parametric uncertainty and unmodeled dynamics," *IEEE Trans. Automat. Contr.*, vol. 36, pp. 25-38, Jan. 1991.

[36] P. M. Young, J. C. Doyle, "Properties of the mixed μ problem and its bounds,' *IEEE Trans. Automat. Contr.*, vol. 41, pp. 155-159, Jan. 1996.

[37] P. M. Young, "Robustness with parametric dynamic uncertainty", Ph. D. Thesis, California Institute of Technology, 1993.

[38] G. J. Balas, J. C. Doyle, K. Glover, A, Packard, R. Smith, *μ-analysis and synthesis toolbox*, 1998.

[39] S. L. Gatley, D.G. Bates, M. J. Hayes, I. Postlethwaite, "Robustness analysis of an integrated flight and propulsion control system using μ and the u-gap metric," *Control Eng. Practice*, vol. 10, 261-275, Mar. 2002.

[40] B. Pal, and B. Chaudhuri, *Robust control in power systems*, Springer, 2005, ISNB 0-387-25949-X.

[41] P. S. Rao, and I. Sen, "Robust pole placement stabilizer design using linear matrix inequalities,' *IEEE Trans. Power Systems*, vol. 15, pp. 313-319, Feb. 2000.

[42] R. V. De Oliveira, R. A. Ramos and N. G. Bretas, "A mixed procedure based on classical and modern control to design robust damping controllers, *IEEE Trans. Power Systems*, vol. 22, pp. 1231-1239, Aug. 2007.

[43] M. Klein, L. X. Lee, G. J. Rogers, S. Farrokhpay and N. J. Balu, "$\mathcal{H}_\infty$ damping controller design in large power systems,' *IEEE Trans. Power Systems*, vol. 10, pp. 1317-1322, Feb. 1995.

[44] K. A. Folly, N. Yorino, and H. Sasaki, "Improving the robustness of $\mathcal{H}_\infty$ PSSs using the polynomial approach," *IEEE Trans. Power Systems*, vol. 13, pp. 1359-1364, Nov. 1998.

[45] C. Zhu, M. Khammash, V. Vittal and W. Qiu, "Robust power system stabilizer design using $\mathcal{H}_\infty$ loop shaping approach," *IEEE Trans. Power Systems*, vol. 18, pp. 810-818, May. 2003.

[46] M. Djukanovic, M. Khammash, V. Vittal, "Sequential synthesis of structured singular value based decentralized controllers in power systems," *IEEE Trans. Power Systems*, vol. 14, pp. 635-641, May. 1999.

[47] X. Yu, M. Khammash, V. Vittal, "Robust design of a damping controller for static var compensators in power systems,' *IEEE Trans. Power Systems*, vol. 16, pp. 456-462, Aug. 2001.

[48] K. Zhou, J. C. Doyle, *Essentials of Robust Control*, Prentice Hall, 1998, ISBN-0135258332.

[49] S. Toffner-Clausen, *System Identification and Robust Control: A Synergistic Approach*, 1996, Springer, ISBN 3540760873.

[50] M. Chilali and P. Gahinet, "$\mathcal{H}_\infty$ design with pole placement constraints: an LMI approach,' *IEEE Trans. Automat. Contr.*, vol. 41, pp. 358-367, Mar. 1996.

Chapter 2

Robust Stability and Robust Performance Analysis of Linear Systems Using the Structured Singular Value

The analysis of stability and performance robustness to variations in uncertain system parameters represents a major issue in system design and operation of power systems. Robustness refers to the ability of a system to preserve system characteristics, stability or performance in the presence of unknown perturbations and noise. Robust stability and robust system behavior have to be guaranteed for the entire expected working range.

This chapter examines the problem of robust stability and robust performance analysis in plants with parametric uncertainty using the concept of structured singular value and discusses basic robust control theory. Using this approach, stability can be guaranteed for all parameter combinations modeled and perturbations which includes $\mathcal{H}_\infty$ and the multivariable gain margin as special cases.

A general modeling approach for modeling real-valued parametric uncertainty in power systems is presented. Numerical issues associated with the application of robustness analysis techniques are also discussed. Finally, this chapter concludes with a formal statement of a general framework to include a percent of complex uncertainty for large power systems.

2.1 Introduction

In many studies, uncertainty arises as a natural expression of unmodeled dynamics, parameter variations, and nonlinear variations. In general, uncertainty can lead to instability or performance problems. In addition, the investigation of the closed-loop subject to model uncertainty is an important issue to assure stability and performance robustness of a designed control as well as to describe and forecast uncertain behavior in control processes.

Uncertainty can be modeled within the framework of linear fractional transformation (LFT) theory and can be broadly divided into two types: structured uncertainty associated with parametric uncertainty quantified by assuming that each uncertainty is bounded with some region, and unstructured uncertainty associated with neglected or unmodeled dynamics [1-2].

In the control literature, the concept of unstructured uncertainty is based on the description of the model uncertainty as a transfer function which is norm-bounded, but otherwise unknown using the small gain theorem and the singular value decomposition (SVD). This kind of unstructured uncertainty can be additive, multiplicative, or other uncertainty. These methods, however, do not capture the parametric uncertainties and present various limitations [1-2].

In order to overcome the limitations of unstructured uncertainty, the structured singular value (SSV) theory was developed by Doyle [3]. Unfortunately, the exact value of the SSV has shown to be *NPhard* (Non-deterministic polynomial-time hard) and in practice its exact value cannot be computed for large systems except for very low order systems. Consequently, these constraints have led some researchers to improve an upper and lower bound to approximate the SSV.

Algorithms for computing lower and upper bounds have been documented in several publications [4-10]. Furthermore, in the theory of the SSV an essential difference is the relation between the complex and mixed SSV

The complex SSV is derived using upper and lower bounds without real parametric uncertainties. Unfortunately, the gap between these bounds can be conservative. That is, the mathematical expression of the complex SSV can be considered as a first approximation of real parametric uncertainties. The mixed SSV has been the focus of research due to the fact that incorporates real parametric uncertainties [11-16].

In the case where μ has real parametric uncertainties, a solution is to reformulate the upper and lower bounds of the complex SSV. However, the computational cost of the procedure grows and the mixed SSV is discontinuous. This means that there exists the possibility of missing a point. A partial solution for the discontinuity of the mixed SSV is to incorporate a percentage of complex uncertainty in each block [17-18].

This chapter reviews existing methodologies for computing the complex and mixed SSV for large power systems models. The main focus is to avoid the discontinuities of the mixed SSV.

2.2 The parametric uncertainty modeling problem

In order to gain insight into the problem of robust stability and robust performance analysis, consider a finite dimensional linear time-invariant (LTI) dynamical system described by the linear constant coefficient differential equation:

$$\dot{\mathbf{x}}(t) = \mathbf{A}\mathbf{x}(t) + \mathbf{B}\mathbf{u}(t), \mathbf{x}(t_0) = \mathbf{x_0} \tag{2.1}$$
$$\mathbf{y}(t) = \mathbf{C}\mathbf{x}(t) + \mathbf{D}\mathbf{u}(t)$$

where $\mathbf{x}(t) \in \mathbb{R}^n$ is the vector of system states, $\mathbf{x}(t_0)$ is the initial condition of the system, $\mathbf{u}(t) \in \mathbb{R}^{p_u}$ is the vector of system inputs, and $\mathbf{y}(t) \in \mathbb{R}^{q_y}$ is the vector of system output; $\mathbf{A} \in \mathbb{R}^{n\times n}$, $\mathbf{B} \in \mathbb{R}^{n\times p}$ $\mathbf{C} \in \mathbb{R}^{q\times n}$, $\mathbf{D} \in \mathbb{R}^{q\times p}$ are the state, input, output matrices, respectively.

The corresponding frequency response $\mathbf{G}(j\omega) \in \mathbb{C}^{q\times p}$ of the transfer matrix from $\mathbf{u}(s)$ to $\mathbf{y}(s)$ is given by

$$\mathbf{y}(s) = \mathbf{G}(s)\mathbf{u}(s) = [\mathbf{C}(s\mathbf{I} - \mathbf{A})^{-1}\mathbf{B} + \mathbf{D}]\mathbf{u}(s) \tag{2.2}$$

where $\mathbf{u}(s)$ and $\mathbf{y}(s)$ are in the frequency domain.

For uncertain analysis, assume that the uncertain system models (2.1) and (2.2) can be expressed in the form

$$\dot{\mathbf{x}}(t) = [\mathbf{A} + \mathbf{\Delta A}(\mathbf{p})]\mathbf{x}(t) \tag{2.3}$$
$$\mathbf{y}(s) = [\mathbf{G}(s) + \mathbf{\Delta}(s)]\mathbf{u}(s) \tag{2.4}$$

where $\mathbf{\Delta A}(\mathbf{p})$ represents an unknown real perturbation term, and $\mathbf{p}$ is a vector of uncertain parameters, combining all uncertainties. On the other hand, the complex matrix $\mathbf{\Delta}(s)$ can be a block diagonal transfer function matrix. In practice, the uncertainty matrix $\mathbf{\Delta}(s)$ is confined to a certain bounded set as discussed below.

These approaches allow for perturbations in the coefficients of the state space model, and enable the connection between system identification and robust control theories to be examined.

The main problem in (2.3) and (2.4) consists in approximating these expressions including uncertainty in a robust stability and robust performance framework that allows the use of the SSV.

2.3 Basic concepts

A key concept to evaluate and describe the performance specifications of a control system is in terms of the size of certain signals of interest. For this purpose, in this section is introduced the holomorphic Hardy space $\mathcal{H}_\infty$. In general, these Hilbert spaces can specify in robust control theory the requirements and objectives of controllers, when the loops of transfer functions through the uncertainties are closed. A few definitions are needed [9].

Suppose a vector space with an inner product which is called an inner product. This inner product induces a norm with the next properties:

i. $\langle x, \alpha y + \beta z \rangle = \alpha \langle x, y \rangle + \beta \langle x, z \rangle$

ii. $\langle x, y \rangle = \overline{\langle y, x \rangle}$

iii. $\langle x, y \rangle > 0$ if $x \neq 0$.

A sequence $\{f_n\}$ in a normed space V converges to $f \in V$. and f is the limit of the sequence, if the sequence of real positive numbers $\|f - f_n\|$ converges to zero and $n \to \infty$. Essentially, this definition says that in any neighborhood around the limit point, f, there exist an infinite number of points. If such f exists, then the sequence is convergent.

A sequence $\{f_n\}$ in V is called a Cauchy sequence if for each $\varepsilon > 0$ there exists a natural number $n_0 \in \mathbb{N}$ such that for $n, m \geq n_0$ and $n, m \to \infty$ then $\|f_n - f_m\| \leq \varepsilon$. A normed space $(V, \langle \cdot, \cdot \rangle)$ is said to be complete if every Cauchy sequence is convergent. A pre-Hilbert space $(V, \langle \cdot, \cdot \rangle)$ is said to be complete with respect to the norm induced by the scalar product $\langle \cdot, \cdot \rangle$. A complete normed space is called a Banach space and a complete pre Hilbert space is denoted a Hilbert space.

$\mathcal{L}_\infty(j\mathbb{R})$ is the space of all functions $\mathbf{F}(j\omega)$, defined on the imaginary axis, which take values in $\mathbb{C}^{m \times n}$ and are bounded on the imaginary axis. $\mathcal{L}_\infty(j\mathbb{R})$ is a Banach space under the norm

$$\|\mathbf{F}(j\omega)\|_\infty = \sup_{\omega\in\mathbb{R}} \|\mathbf{F}(j\omega)\|_2 = \sup_{\omega\in\mathbb{R}} \bar{\sigma}[\mathbf{F}(j\omega)]$$

Here, $\mathcal{H}_\infty$ is the space of all functions $\mathbf{F}(s)$ which are analytic in $\mathrm{Re}(s) > 0$ take values in $\mathbb{C}^{m\times n}$ and are essentially (*ess*) bounded in the right half plane (RHP):

$$\sup_{\mathrm{Re}>0} \|\mathbf{F}(s)\|_2 = ess\ \sup_{\omega\in\mathbb{R}} \bar{\sigma}[\mathbf{F}(j\omega)]$$

The real rational subspace of $\mathcal{H}_\infty$ is denoted by $\mathcal{RH}_\infty$, which consists of all proper and real rational stable transfer matrices. It then follows that, for a transfer function $\mathbf{G}(s) \in \mathcal{RH}_\infty$

$$\|\mathbf{F}(s)\|_\infty = \sup_{\omega\in\mathbb{R}} \bar{\sigma}[\mathbf{F}(j\omega)] \tag{2.5}$$

The above equation (2.5) for a stable transfer function $\|\mathbf{G}(s)\|_\infty$ is induced by the operator $\|\cdot\|_{(2,2)}$ and $\bar{\sigma}$ is the maximal gain. If $\mathbf{F}(s) \in \mathcal{H}_\infty$ and $\mathbf{u}(t) \in \mathcal{H}_2$, then $\mathbf{y}(t) \in \mathcal{H}_2$ and the induced operator 2-norm of $\mathbf{u}(t)$ on $\mathbf{y}(t)$ equals the $\mathcal{H}_\infty$ norm$\|\mathbf{F}(s)\|_\infty$. This means that a stable linear system maps bounded energy inputs onto bounded energy outputs. In addition, $\mathcal{L}_\infty(j\mathbb{R})$ is defined only on the imaginary axis, its domain is $j\mathbb{R}$.

2.4 Nominal stability and nominal performance

The requirement of internal stability in a feedback system is essential to get robust stability and robust performance. To illustrate these ideas considered the feedback configuration shown in Fig. 2.1. Here, $\mathbf{d}_i(s)$ is the plant input disturbance, $\mathbf{d}(s)$ is the plant output disturbance, $\mathbf{n}(s)$ is the noise, $\mathbf{r}(s)$ is the reference, $\mathbf{u}(s)$ is the control input, and $\mathbf{u}_p(s)$ is the plant input.

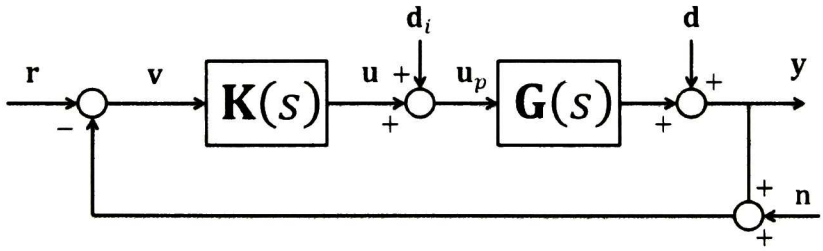

Figure 2.1. General feedback control configuration.

Disregarding input and output disturbances, $\mathbf{d}(s)$, $\mathbf{d}_i(s)$, and noise $\mathbf{n}(s)$, the system has internal stability, $\mathbf{G}(s) \in \mathcal{RH}_\infty$ and $\mathbf{K}(s) \in \mathcal{RH}_\infty$. The next generalized Nyquist stability criterion is derived for multiple-input multiple-output (MIMO) systems.

Theorem 2.1 (The generalized Nyquist stability criterion) [19]. If the open loop transfer function matrix $\mathbf{G}(s)\mathbf{K}(s)$ has p poles in the right-half s-plane, then the closed loop system is stable if and only if the map of $\det(\mathbf{I} + \mathbf{G}(s)\mathbf{K}(s))$, as s traverses the Nyquist $\mathcal{D}$ contour once, encircles the origin p times anti-clockwise assuming no right-half s –plane zero-pole cancellations have occurred forming the product $\mathbf{G}(s)\mathbf{K}(s)$.

With reference to Fig. 2.1, it is convenient to define the input loop transfer function matrix $\mathbf{L}_i(s) = \mathbf{K}(s)\mathbf{G}(s)$ and the output loop transfer function matrix, $\mathbf{L}_o(s) = \mathbf{G}(s)\mathbf{K}(s)$ with $\mathbf{G}(s) \in \mathcal{RH}_\infty$ and $\mathbf{K}(s) \in \mathcal{RH}_\infty$. Also of interest, the input sensitivity is defined as the transfer function from $\mathbf{d}_i(s)$ to $\mathbf{u}_p(s)$, *i.e.* $\mathbf{u}_p(s) = \mathbf{S}_i(s)\mathbf{d}_i(s)$ where $\mathbf{S}_i(s) = (\mathbf{I} + \mathbf{L}_i(s))^{-1}$ and the output sensitivity is defined as $\mathbf{y}(s) = \mathbf{S}_o(s)\mathbf{d}(s)$ where $\mathbf{S}_o(s) = (\mathbf{I} + \mathbf{L}_o(s))^{-1}$

Furthermore, the input and output complementary sensitivity are defined as:

$$\mathbf{T}_i(s) = \mathbf{I} - \mathbf{S}_i(s) = \mathbf{L}_i(s)(\mathbf{I} + \mathbf{L}_i(s))^{-1} \tag{2.6}$$

$$\mathbf{T}_o(s) = \mathbf{I} - \mathbf{S}_o(s) = \mathbf{L}_o(s)(\mathbf{I} + \mathbf{L}_o(s))^{-1} \tag{2.7}$$

$$\mathbf{T}_o(s) + \mathbf{S}_o(s) = \mathbf{I} \tag{2.8}$$

Straightforward analysis yields

$$\mathbf{y}(s) = \mathbf{T}_o(s)[\mathbf{r}(s) - \mathbf{n}(s)] + \mathbf{S}_o(s)\mathbf{G}(s)\mathbf{d}_i(s) + \mathbf{S}_o(s)\mathbf{d}(s) \tag{2.9}$$

$$\mathbf{r}(s) - \mathbf{y}(s) = \mathbf{e}(s) = \mathbf{S}_o(s)[\mathbf{r}(s) - \mathbf{d}(s)] + \mathbf{T}_o(s)\mathbf{n}(s) - \mathbf{S}_o(s)\mathbf{G}(s)\mathbf{d}_i(s) \tag{2.10}$$

$$\mathbf{u}(s) = \mathbf{K}(s)\mathbf{S}_o(s)[\mathbf{r}(s) - \mathbf{n}(s)] - \mathbf{K}(s)\mathbf{S}_o(s)\mathbf{d}(s) - \mathbf{T}_i(s)\mathbf{d}_i(s) \tag{2.11}$$

$$\mathbf{u}_p(s) = \mathbf{K}(s)\mathbf{S}_o(s)[\mathbf{r}(s) - \mathbf{n}(s)] - \mathbf{K}(s)\mathbf{S}_o(s)\mathbf{d}(s) - \mathbf{S}_i(s)\mathbf{d}_i(s) \tag{2.12}$$

The following observations can be made about this model [8]:

- For disturbances $\mathbf{d}_i(s)$ and $\mathbf{d}(s)$ to affect the output $\mathbf{y}(s)$ to the least extent, (2.9) shows that the sensitivity $\mathbf{S}_o(s)$ should be small.
- For good disturbance error reduction due to the disturbances $[\mathbf{r}(s) - \mathbf{d}(s)]$ and $\mathbf{d}(s)$ to the least extent, (2.10) shows that the sensitivity $\mathbf{S}_o(s)$ should be small.
- For disturbances $[\mathbf{r}(s) - \mathbf{n}(s)]$ and $\mathbf{d}(s)$ to affect the inputs $\mathbf{u}(s)$ and $\mathbf{u}_p(s)$ to the least extent, (2.11) and (2.12) show that the sensitivity $\mathbf{S}_o(s)$ should be small.

However, due to the equation (2.8) $\mathbf{S}_o(s)$ and $\mathbf{T}_o(s)$ cannot both be small in the same frequency range. For good rejection $\mathbf{d}(s)$ at output $\mathbf{y}(s)$, it will be required that $\|\mathbf{S}_o(s)\|_\infty << 1$. Similarly, for good rejections $\mathbf{r}(s)$ and $\mathbf{n}(s)$ at output, it will be required that $\|\mathbf{T}_o(s)\|_\infty << 1$. Fortunately, the limitations in (2.8) can be avoided with proper choice of weighting functions, and physical reasons. On the other hand, the sensitivity is a very good indicator of closed loop performance [8].

A feedback control configuration with weighting functions is shown in Fig. 2.2. The weighting functions are chosen to reflect the design objectives and knowledge of the disturbances and sensors noise. In practice, the selection of weighting functions should be guided by the expected system inputs and the relative importance of the outputs.

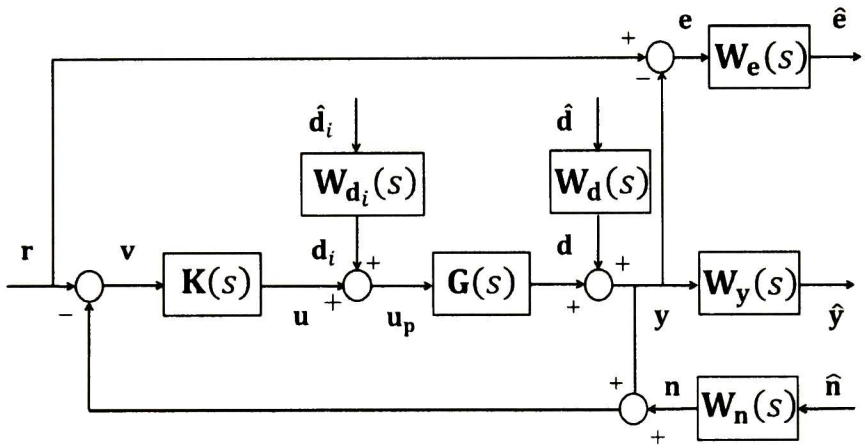

Figure 2.2. Feedback control configuration with weighting functions.

Definition 2.1 [19]. The nominal performance problem is, given weighting functions $\mathbf{W}_y(s)$ and $\mathbf{W}_d(s)$, to design a stabilizing controller $\mathbf{K}(s)$ such that the cost function

$$\|\mathbf{W}_y(s)\mathbf{S}_o(s)\mathbf{W}_d(s)\|_\infty \tag{2.13}$$

is minimized.

Thus,

$$\mathbf{K}(s) = \arg\min_{\mathbf{K}(s)\in\mathcal{K}_s} \|\mathbf{W}_y(s)\mathbf{S}_o(s)\mathbf{W}_d(s)\|_\infty$$

where $\mathcal{K}_s$ denotes the set of all stabilizing controllers and $\mathcal{H}_\infty$ represents a control problem. If a controller can achieve $\|\mathbf{W}_y(s)\mathbf{S}_o(s)\mathbf{W}_d(s)\|_\infty < 1$, it is said that the closed loop system has nominal performance.

2.5 Robust stability and robust performance with unstructured uncertainty

A $m \times m$ complex-value norm-bounded unstructured perturbation Δ_C is the set of $m \times m$ transfer functions $\boldsymbol{\Delta}(s): \mathbb{C} \rightarrow \mathbb{C}^{m \times m}$ which are analytic in the closed right half-plane and have a norm-bound less than or equal to some given positive function $\bar{\delta}^C(\omega): \mathbb{R} \rightarrow \mathbb{R}^+$ then $\Delta_C = \{\boldsymbol{\Delta}(s) \in \mathcal{RH}_\infty | \bar{\sigma}[\boldsymbol{\Delta}(j\omega)] \leq \bar{\delta}^C(\omega), \omega \in (-\infty, \infty)\}$ with $\bar{\sigma}$ as the maximum singular value. The normalized uncertainty set is given by $B\Delta_C = \{\boldsymbol{\Delta}(s) \in \mathcal{RH}_\infty | \bar{\sigma}[\boldsymbol{\Delta}(j\omega)] \leq 1, \omega \in (-\infty, \infty)\}$.

From the above definition it can be established a frequency dependent magnitude bound uncertainty to describe many types of uncertainty. The basic representations of unstructured uncertainty models are: additive uncertainty $\mathbf{G}_T(s) = \mathbf{G}(s) + \tilde{\boldsymbol{\Delta}}(s)$, input multiplicative uncertainty $\mathbf{G}_T(s) = \mathbf{G}(s)\left(\mathbf{I} + \tilde{\boldsymbol{\Delta}}(s)\right)$, output multiplicative uncertainty $\mathbf{G}_T(s) = \left(\mathbf{I} + \tilde{\boldsymbol{\Delta}}(s)\right)\mathbf{G}(s)$, inverse input multiplicative uncertainty $\mathbf{G}_T(s) = \mathbf{G}(s)\left(\mathbf{I} + \tilde{\boldsymbol{\Delta}}(s)\right)^{-1}$ and inverse output multiplicative uncertainty $\mathbf{G}_T(s) = \left(\mathbf{I} + \tilde{\boldsymbol{\Delta}}(s)\right)^{-1}\mathbf{G}(s)$, where

$$\tilde{\boldsymbol{\Delta}}(s) = \mathbf{W}_{u2}(s)\boldsymbol{\Delta}(s)\mathbf{W}_{u1}(s) \tag{2.14}$$

Equation (2.14) has two weighting matrices $\mathbf{W}_{u1}(s)$ and $\mathbf{W}_{u2}(s)$. Using the SVD for the perturbation model, $\boldsymbol{\Delta}(s)$ is normalized and $\|\boldsymbol{\Delta}(s)\|_\infty < 1$. These weighting matrices are natural expressions of the uncertainty model, but it is important their normalization. In the literature, the unstructured uncertainty $\boldsymbol{\Delta}(s)$ is simple called a full complex block.

Theorem 2.2 (Small gain theorem) [9]. Suppose $\mathbf{M}(s) \in \mathcal{RH}_\infty$ and let $\gamma > 0$. Then the interconnection system shown in Fig. 2.3 is well-posed and internally stable for all $\boldsymbol{\Delta}(s) \in \mathcal{RH}_\infty$ with $\|\boldsymbol{\Delta}(s)\|_\infty \leq \frac{1}{\gamma}$ if and only if $\|\mathbf{M}(s)\|_\infty < \gamma$ or $\|\boldsymbol{\Delta}(s)\|_\infty < \frac{1}{\gamma}$ if and only if $\|\mathbf{M}(s)\|_\infty \leq \gamma$.

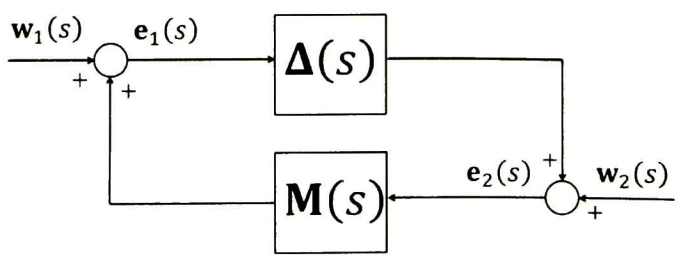

Figure 2.3. $\mathbf{M}(s) - \boldsymbol{\Delta}(s)$ loop for stability analysis.

For a given controller, $\mathbf{K}(s)$, the small gain theorem therefore guarantees the stability of the closed loop system with unstructured uncertainties. The small gain theorem, which requires that the modulus of $\mathbf{M}(s) - \mathbf{\Delta}(s)$ be less than 1 for all frequencies, plays an important role in robust control and is shown graphically in Fig 2.4.

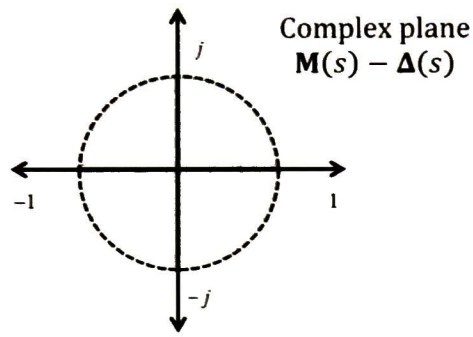

Figure 2.4. Small gain theorem in the complex plane $\mathbf{M}(s) - \mathbf{\Delta}(s)$.

In general, the small gain theorem provides only a sufficient condition for stability and is therefore potentially conservative. It then follows that using the small gain theorem $\|\mathbf{M}(s)\mathbf{\Delta}(s)\|_\infty < 1$ for all $\omega \in \mathbb{R}$, and

$$\bar{\sigma}\,[\mathbf{M}(s)\mathbf{\Delta}(s)] = |\mathbf{M}(s)\mathbf{\Delta}(s)| = |\mathbf{M}(s)||\mathbf{\Delta}(s)| = \bar{\sigma}\,[\mathbf{M}(s)]\bar{\sigma}\,[\mathbf{\Delta}(s)]$$

Finally, the next expression can be written for different types of unstructured uncertainty:

$$\bar{\sigma}\,[\mathbf{M}(j\omega)]\bar{\sigma}\,[\mathbf{\Delta}(j\omega)] < 1 \tag{2.15}$$

Consider the linear fractional transformation in Fig 2.5, where $\|\mathbf{\Delta}(s)\|_\infty \leq 1$, $\mathbf{w}(s)$ and $\mathbf{z}(s)$ are the exogenous inputs and the exogenous outputs, respectively. It is assumed that uncertainty is extracted, the control is absorbed. Then, from the small gain theorem, the next important theorem for robust stability can be derived:

Theorem 2.3 [19]. Assume that the interconnection of $\mathbf{M}(s) \in \mathcal{RH}_\infty$ and $\mathbf{\Delta}(s)$ is of such a form that the perturbed close loop system is stable if and only if the map of $\det(\mathbf{I} + \mathbf{G}(s)\mathbf{K}(s))$ as s traverses the $\mathcal{D}$ contour does not encircle the origin. Then the closed loop system has robust stability for all perturbations $\mathbf{\Delta}(s)$ with $\bar{\sigma}\,[\mathbf{\Delta}(j\omega)] \leq 1$ if and only if $\|\mathbf{M}(s)\|_\infty < 1$.

The nominal open-loop interconnected transfer function matrix $\mathbf{P}(s)$ in Fig. 2.5 does not consider the controller $\mathbf{K}(s)$ and the perturbation $\mathbf{\Delta}(s)$. Let $\mathbf{P}(s)$ may be partitioned as

$$\mathbf{P}(s) = \begin{bmatrix} \mathbf{P}_{11}(s) & \mathbf{P}_{11}(s) & \mathbf{P}_{11}(s) \\ \mathbf{P}_{11}(s) & \mathbf{P}_{11}(s) & \mathbf{P}_{11}(s) \\ \mathbf{P}_{11}(s) & \mathbf{P}_{11}(s) & \mathbf{P}_{11}(s) \end{bmatrix}$$

The signals $\mathbf{y}(s)$ and $\mathbf{u}(s)$ represent the feedback signals and the control signal, respectively.

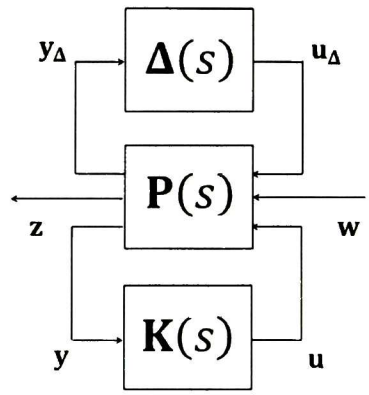

Figure 2.5. General framework of the linear system.

It then follows that the relationship between $\mathbf{N}(s)$ in Fig. 2.6 and $\mathbf{P}(s)$ can be obtained by a lower LFT as

$$F_l[\mathbf{P}(s), \mathbf{K}(s)] = \mathbf{N}(s)[\mathbf{P}(s), \mathbf{K}(s)] = \begin{bmatrix} \mathbf{N}_{11}(s) & \mathbf{N}_{12}(s) \\ \mathbf{N}_{21}(s) & \mathbf{N}_{22}(s) \end{bmatrix}$$

$$= \begin{bmatrix} \mathbf{P}_{11}(s) & \mathbf{P}_{12}(s) \\ \mathbf{P}_{21}(s) & \mathbf{P}_{22}(s) \end{bmatrix} + \begin{bmatrix} \mathbf{P}_{13}(s) \\ \mathbf{P}_{23}(s) \end{bmatrix} \mathbf{K}(s)\big(\mathbf{I} - \mathbf{P}_{33}(s)\mathbf{K}(s)\big)^{-1} [\mathbf{P}_{31}(s) \quad \mathbf{P}_{32}(s)] \tag{2.16}$$

where $\mathbf{N}(s)$ is written as $\mathbf{N}(s)[\mathbf{P}(s), \mathbf{K}(s)]$ to show that $\mathbf{N}(s)$ is formed by $\mathbf{P}(s)$ and $\mathbf{K}(s)$; $F_l[\mathbf{P}(s), \mathbf{K}(s)]$ represents the lower LFT. In the literature Fig. 2.6 is sometimes called the $\mathbf{N}(s) - \boldsymbol{\Delta}(s)$ framework for robust analysis.

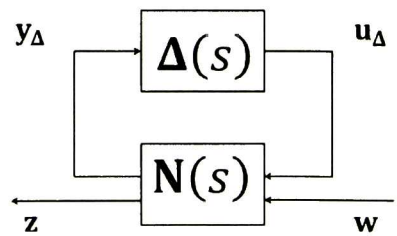

Figure 2.6. $\mathbf{N}(s) - \boldsymbol{\Delta}(s)$ framework for robust analysis.

Hence, the robust stability of equation (2.16) is given by $\mathbf{M}(s) = \mathbf{N}_{11}(s)$ into the $\mathbf{M}(s) - \boldsymbol{\Delta}(s)$ framework for robust stability shown in Fig. 2.7.

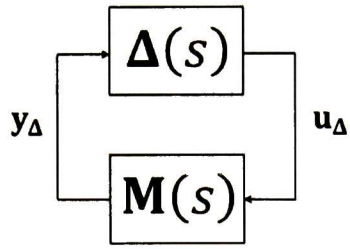

Figure 2.7. $\mathbf{M}(s) - \boldsymbol{\Delta}(s)$ framework for robust stability.

Assume now that the augmented perturbation matrix is described by $\widetilde{\boldsymbol{\Delta}}(s) = diag[\boldsymbol{\Delta}(s), \boldsymbol{\Delta}_p(s)]$, then the fundamental importance of this representation is expressed in the following theorem.

Theorem 2.4 [19]. Assume that the interconnection $F_l[\mathbf{P}(s), \mathbf{K}(s)]$ is stable and that the perturbation $\widetilde{\boldsymbol{\Delta}}(s)$ is of such a form that the perturbed closed loop system in Fig. 2.8 is stable if and only if the map of $\det\left(\mathbf{I} - [F_l[\mathbf{P}(s), \mathbf{K}(s)]]\widetilde{\boldsymbol{\Delta}}(s)\right)$ as s traverses the $\mathcal{D}$ contour does not encircle the origin. Then the system $F_u[F_l[\mathbf{P}(s), \mathbf{K}(s)], \boldsymbol{\Delta}(s)]$ will satisfy the robust performance criterion $F_u[F_l[\mathbf{P}(s), \mathbf{K}(s)], \boldsymbol{\Delta}(s)] < 1$ if and only if $F_l[\mathbf{P}(s), \mathbf{K}(s)]$ is stable for all perturbations $\widetilde{\boldsymbol{\Delta}}(s)$ with $\bar{\sigma}[\widetilde{\boldsymbol{\Delta}}(j\omega)] \leq 1$.

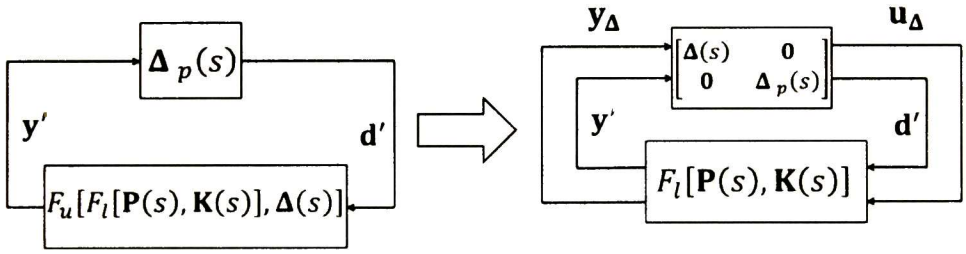

Figure 2.8. Diagram structure for robust performance analysis.

In general from the above theorem, the optimal robust performance problem can be expressed as

$$\mathbf{K}(s) = \arg\min_{\mathbf{K}(s)\in\mathcal{K}_s} \sup_{\boldsymbol{\Delta}(s)\exists\|\boldsymbol{\Delta}(s)\|_\infty\leq 1} \|F_u[F_l[\mathbf{P}(s), \mathbf{K}(s)], \boldsymbol{\Delta}(s)]\|_\infty \qquad (2.17)$$

if $\|F_u[F_l[\mathbf{P}(s), \mathbf{K}(s)], \boldsymbol{\Delta}(s)]\|_\infty < 1$, for all $\boldsymbol{\Delta}(s)$ with $\|\boldsymbol{\Delta}(s)\|_\infty \leq 1$, it is said that the closed loop system has robust performance. The equation $F_u[F_l[\mathbf{P}(s), \mathbf{K}(s)], \boldsymbol{\Delta}(s)]$ satisfies the robust performance condition if and only if it is robustly stable for a norm bounded matrix perturbation $\boldsymbol{\Delta}_p(s)$ with $\|\boldsymbol{\Delta}_p(s)\|_\infty \leq 1$.

Systems with unmodelled dynamics can be represented in the standard $\mathbf{M}(s) - \mathbf{\Delta}(s)$ configuration. The robust stability and the robust performance analysis developed in this section are necessary, conservative, sufficient conditions, and vary with the assumptions of the unstructured uncertainty descriptions and the robust performance requirements.

The last limitations lead to the definition of the SSV, which is a unified framework to treat exactly the robust stability and the robust performance problems for systems with multiple sources of uncertainties.

2.6 Theory and computing of the complex and mixed SSV

The structured uncertainty can include complex parametric uncertainties, real parametric uncertainties and individual sources of uncertainty that are identified and represented directly. That is, if the uncertainty modeling results in structural zeros in entries of Δ_C, the uncertainty is called "structured" This representation leads to an uncertainty description with multiple perturbations. The differences between some of these uncertainties, including the ones used here, are described in [2, 4, 8-9].

Suppose that a $r \times r$ complex-value repeated perturbation Δ_c is defined as

$$\Delta_c = \{\mathbf{\Delta} | \mathbf{\Delta} = \delta^c \mathbf{I}, |\delta^c| \leq \bar{\delta}^c\} \tag{2.18}$$

with $\bar{\delta}^c \in \mathbb{R}^+$ being some real number. Then, the normalized version is

$$B\Delta_c = \{\mathbf{\Delta} | \mathbf{\Delta} = \delta^c \mathbf{I}, |\delta^c| \leq 1\} \tag{2.19}$$

In the preceding equations $\mathbf{I}$ is the $r \times r$ identity matrix and Δ_c is restricted to square uncertainty matrices. Any non-square uncertainty can be made square adding zero rows or columns. In addition, the maximum SVD of Δ_c can vary whit frequency while the maximum SVD of Δ_c, which is equal to maximum absolute value, is fixed.

Lemma 2.1 Let $\mathbf{\Delta}(s)$ be a structured set $\mathbf{M}(s) \in \mathcal{RH}_\infty$. Then

$$\sup_{s \in \bar{\mathbb{C}}_+} \mu_{\mathbf{\Delta}}[\mathbf{M}(s)] = \sup_{s \in \mathbb{C}_+} \mu_{\mathbf{\Delta}}[\mathbf{M}(s)] = \sup_{\omega} \mu_{\mathbf{\Delta}}[\mathbf{M}(j\omega)] \tag{2.20}$$

where $\mu_{\mathbf{\Delta}}$ is called the SSV

Consider repeated complex scalars and full blocks for uncertainty, and two nonnegative integers, S_c and F, which denote the number of repeated scalar blocks and the number of full blocks, respectively. It is necessary that $\{m = S_c + F\} \leq n$. Then, the block structure is an m −tuple

$$\mathrm{C} = (r_1, \ldots, r_{S_c}, m_1, \ldots, m_F) \tag{2.21}$$

Equation (2.21) specifies the dimensions of the perturbation blocks. For consistency among all the dimensions, $\sum_{j=1}^{S_c} r_j + \sum_{l=1}^{F} m_l = n$ [12]. Once this notation has been given, define $\mathrm{X_C}$ as a general uncertainty as

$$\mathrm{X_C} = \left\{ diag\left[\delta_1^c \mathbf{I}_{r_1}, \ldots, \delta_{S_c}^c \mathbf{I}_{r_{S_c}}, \mathbf{\Delta}_{m_1}^C, \ldots, \mathbf{\Delta}_{m_F}^C\right] : \delta_j^c \in \mathbb{C}, \mathbf{\Delta}_{m_l}^C \in \mathbb{C}^{m_l \times m_l} \right\} \tag{2.22}$$

The unit ball is introduced in the space of transfer matrices

$$B\mathrm{X_C} = \left\{ \mathbf{\Delta} = diag\left[\delta_1^c \mathbf{I}_{r_1}, \ldots, \delta_{S_c}^c \mathbf{I}_{r_{S_c}}, \mathbf{\Delta}_{m_1}^C, \ldots, \mathbf{\Delta}_{m_F}^C\right] : \bar{\sigma}\,[\mathbf{\Delta}] \leq 1 \right\} \tag{2.23}$$

Note that the relation $\bar{\sigma}\,[\mathbf{\Delta}] \leq 1$ can be expressed as $\left|\delta_j^c\right| \leq 1$ and $\bar{\sigma}\left[\mathbf{\Delta}_{m_l}^C\right] \leq 1$. Then, the complex SSV can be defined as:

Definition 2.2 [6]. For $\mathbf{M} \in \mathbb{C}^{n \times n}$, $\mu_{\mathrm{C}}[\mathbf{M}]$ is the complex structural singular value and can be expressed as:

$$\mu_{\mathrm{C}}[\mathbf{M}] = \frac{1}{\min\limits_{\mathbf{\Delta} \in \mathrm{X_C}} \{\bar{\sigma}\,[\mathbf{\Delta}] : \det[\mathbf{I} + \mathbf{M\Delta}] = 0\}} \tag{2.24}$$

unless no $\mathbf{\Delta} \in \mathrm{X_C}$ makes $\mathbf{I} + \mathbf{M\Delta}$ singular, in which case $\mu_{\mathrm{C}}[\mathbf{M}] = 0$.

The complex SSV has the next properties

a) If $\mathrm{X_C} = \{\delta \mathbf{I} : \delta \in \mathbb{C}\}$, then $\mu_{\mathrm{C}}[\mathbf{M}] = \rho[\mathbf{M}]$.

b) If $\mathrm{X_C} = \mathbb{C}^{n \times n}$, then $\mu_{\mathrm{C}}[\mathbf{M}] = \bar{\sigma}[\mathbf{M}]$.

c) $\mu_{\mathrm{C}}[\alpha \mathbf{M}] = |\alpha| \mu_{\mathrm{C}}[\mathbf{M}]$ for any complex scalar α.

d) Let $\mathbf{\Delta} \in \mathrm{X_C}$, $\mathbf{\Delta} = diag\{\mathbf{\Delta}_1, \mathbf{\Delta}_2\}$ be a block-diagonal perturbation, and let $\mathbf{M}$ be partitioned accordingly. Then $\mu_{\mathrm{C}}[\mathbf{M}] \geq \max\{\mu_{\mathrm{C}}[\mathbf{M}_{11}], \mu_{\mathrm{C}}[\mathbf{M}_{22}]\}$.

e) $\mu_{\mathrm{C}}[\mathbf{M}]$ is bounded by the spectral radius and the singular value (spectral norm):

$$\rho[\mathbf{M}] \leq \mu_{\mathrm{C}}[\mathbf{M}] \leq \bar{\sigma}[\mathbf{M}] \tag{2.25}$$

Using (2.25), it is possible to describe an upper bound and a lower bound. The gap between ρ and $\bar{\sigma}$ can be arbitrarily large; however, it can be refined with transformations on $\mathbf{M}$ that do not affect $\mu_{\mathrm{C}}[\mathbf{M}]$, but do affect ρ and $\bar{\sigma}$. To do this, define subsets on $\mathbb{C}^{n \times n}$ $\delta_1^c \mathbf{I}_{r_1}, \ldots, \delta_{S_c}^c \mathbf{I}_{r_{S_c}}, \mathbf{\Delta}_{m_1}^C, \ldots, \mathbf{\Delta}_{m_F}^C$

$$\mathrm{U_C} = \{\mathbf{U} \in \mathrm{X_C} : \mathbf{U}\mathbf{U}^* = \mathbf{I}_n\} \tag{2.26}$$

$$\mathrm{D} = \left\{ \begin{matrix} diag[\mathbf{D}_1, \ldots, \mathbf{D}_{S_c}, d_1\mathbf{I}_{m_1}, \ldots, d_F\mathbf{I}_{m_F}]: \\ \mathbf{D}_j \in \mathbb{C}^{r_j \times r_j}, \mathbf{D}_j = \mathbf{D}_j^* > 0, d_l \in \mathbb{R}, d_l > 0 \end{matrix} \right\}. \tag{2.27}$$

For any $\mathbf{\Delta} \in \mathrm{X_C}$, $\mathbf{U} \in \mathrm{X_C}$, and $\mathbf{D} \in \mathrm{D}$

$$\mathbf{U}^* \in \mathrm{U_C},\ \mathbf{U\Delta} \in \mathrm{X_C},\ \mathbf{\Delta U} \in \mathrm{X_C},\ \bar{\sigma}[\mathbf{U\Delta}] = \bar{\sigma}[\mathbf{\Delta U}] = \bar{\sigma}[\mathbf{\Delta}] \tag{2.28}$$

$$\mathbf{D\Delta} = \mathbf{\Delta D} \tag{2.29}$$

Therefore, the bounds in (2.25) can be tightened to

$$\max_{\mathbf{U}\in\mathrm{U_C}} \rho[\mathbf{UM}] \le \max_{\mathbf{\Delta}\in\mathrm{X_C}} \rho[\mathbf{\Delta M}] = \mu_{\mathrm{C}}[\mathbf{M}] \le \inf_{\mathbf{D}\in\mathrm{D}} \bar{\sigma}[\mathbf{DMD}^{-1}] \tag{2.30}$$

Hence, without affecting the loop properties it can insert an identity matrix into the loop affected by $\mathbf{UU}^* = \mathbf{U}^*\mathbf{U} = \mathbf{I}$ where $\mathbf{U}$ is a unitary matrix. Then, the lower bound can be increased trough $\mathbf{U}$ and $\mathbf{U}^*$ in the loop such that the uncertainty block $\mathbf{\Delta}$ is unchanged while the $\mathbf{M}$ part is maximized in ρ. This method for the lower bound is shown in Fig. 2.9.

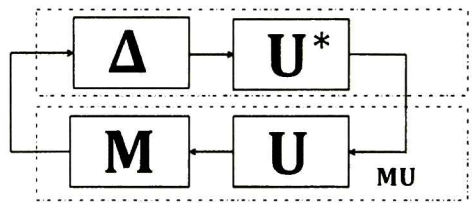

Figure 2.9. Structure of $\mathbf{U}$ related to $\mathbf{\Delta}$ for the lower bound where $\mathbf{U\Delta} \in \mathrm{X_C}$.

On the other hand, the upper bound is minimized trough $\mathbf{\Delta}$ with $\mathbf{D}$ as shown in Fig 2.10.

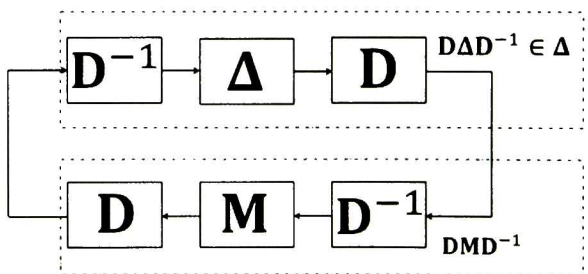

Figure 2.10. Structure of $\mathbf{D}$ related to $\mathbf{\Delta}$ for the upper bound where $\inf_{\mathbf{D}\in\mathrm{D}} \bar{\sigma}[\mathbf{DMD}^{-1}]$.

The limitations imposed with repeated complex scalars in structured uncertainty for the complex SSV leads to the mixed SSV It is natural then to express repeated real scalars in structured uncertainty. However, data analysis and computation will be more complex.

Assume that a $k \times k$, real-value repeated perturbation Δ_r is defined as

$$\Delta_r = \{\Delta | \Delta = \delta^r \mathbf{I}, \delta \in [-\bar{\delta}, +\bar{\delta}]\} \tag{2.31}$$

with $\bar{\delta} \in \mathbb{R}$ being some real number. The normalized version is

$$B\Delta_r = \{\Delta | \Delta = \delta^r \mathbf{I}, \delta \in [-1, +1]\} \tag{2.32}$$

in both equations $\mathbf{I}$ is the $k \times k$ identity matrix.

The mixed SSV considers three types of blocks: repeated real scalar, repeated complex scalar and full blocks. Three nonnegative integers: S_r, S_c and F.

$$\sum_{i=1}^{S_r} k_i + \sum_{j=1}^{S_c} r_j + \sum_{l=1}^{F} m_l = n$$

The block structure can be defined as $\mathrm{M} = (k_1, \ldots, k_{S_r}, r_{S_r+1}, \ldots, r_{S_r+S_c}, m_{S_r+S_c+1}, \ldots, m_F)$. Hence the normalized uncertainty is given by

$$B\mathbf{X}_\mathrm{M} = \left\{\Delta = diag\left[\delta_1^r \mathbf{I}_{k_1}, \ldots, \delta_{S_r}^r \mathbf{I}_{k_{S_r}}, \delta_1^c \mathbf{I}_{r_1}, \ldots, \delta_{S_c}^c \mathbf{I}_{r_{S_c}}, \Delta_{m_1}^C, \ldots, \Delta_{m_F}^C\right] : \bar{\sigma}[\Delta] \leq 1\right\} \tag{2.33}$$

The purely complex case corresponds to $S_r = F = 0$ and the purely real case corresponds to $S_c = F = 0$.

The last observations lead to the next important definition.

Definition 2.3 [12]. The mixed structured singular value, $\mu_\mathrm{M}[\mathbf{M}]$ of a matrix $\mathbf{M} \in \mathbb{C}^{n \times n}$ with respect to a block structure $\boldsymbol{\Delta}$ is defined as

$$\mu_\mathrm{M}[\mathbf{M}] = \frac{1}{\min\limits_{\Delta \in \mathbf{X}_\mathrm{M}} \{\bar{\sigma}[\Delta] : \det[\mathbf{I} + \mathbf{M}\Delta] = 0\}} \tag{2.34}$$

With $\mu_\mathrm{M}[\mathbf{M}] = 0$ if no $\boldsymbol{\Delta} \in \mathrm{X}_\mathrm{M}$ solves $\det[\mathbf{I} + \mathbf{M}\boldsymbol{\Delta}] = 0$.

The mixed SSV has the next some important properties:

$$S_r = 0, S_c = 0, F = 1 \rightarrow \mu_\mathrm{M}[\mathbf{M}] = \bar{\sigma}[\mathbf{M}] \tag{2.35}$$

$$S_r = 0, S_c = 1, F = 0 \rightarrow \mu_\mathrm{M}[\mathbf{M}] = \rho[\mathbf{M}] \tag{2.36}$$

$$S_r = 1, S_c = 0, F = 0 \rightarrow \mu_\mathrm{M}[\mathbf{M}] = \rho_\mathbb{R}[\mathbf{M}] \tag{2.37}$$

Note from equation (2.35) that $\mu_\mathrm{M}[\mathbf{M}]$ reduces to the maximum singular value, and in property (2.36) that $\mu_\mathrm{M}[\mathbf{M}]$ is the complex spectral radius. Finally, $\mu_\mathrm{M}[\mathbf{M}]$ can be considered as a generalization of $\bar{\sigma}[\mathbf{M}]$ and $\rho_\mathbb{R}[\mathbf{M}]$. The following sequence of inequalities holds

$$\rho_{\mathbb{R}}[\mathbf{M}] \leq \mu_{\mathrm{M}}[\mathbf{M}] \leq \bar{\sigma}[\mathbf{M}] \tag{2.38}$$

It is necessary to define new subsets

$$\mathrm{Q}_k = \left\{\boldsymbol{\Delta} \in \mathrm{X}_{\mathrm{M}} : \delta_i^r \in [-1,1], \delta_j^{c*}\delta_j^c = 1, \boldsymbol{\Delta}_l^{C*}\boldsymbol{\Delta}_l^C = \mathbf{I}_{m_l}\right\} \tag{2.39}$$

$$\mathrm{U}_{\mathrm{M}} = \{\mathbf{U} \in \mathrm{Q}_{\mathrm{M}} : \mathbf{U}\mathbf{U}^* = \mathbf{I}_n\} \tag{2.40}$$

$$\mathrm{D} = \left\{ \begin{matrix} diag\left[\widetilde{\mathbf{D}}_1, \ldots, \widetilde{\mathbf{D}}_{S_r}, \mathbf{D}_1, \ldots, \mathbf{D}_{S_c}, d_1\mathbf{I}_{m_1}, \ldots, d_F\mathbf{I}_{m_F}\right]: \\ \widetilde{\mathbf{D}}_i \in \mathbb{C}^{k_i \times k_i}, \widetilde{\mathbf{D}}_i = \widetilde{\mathbf{D}}_i^* > 0, \mathbf{D}_j \in \mathbb{C}^{r_j \times r_j}, \mathbf{D}_j = \mathbf{D}_j^* > 0, d_l \in \mathbb{R}, d_l > 0 \end{matrix} \right\} \tag{2.41}$$

$$\mathrm{G}_{\mathrm{M}} = \left\{ \begin{matrix} diag\left[\mathbf{G}_1, \ldots, \mathbf{G}_{S_r}, 0_1, \ldots, 0_{m_F}\right]: \\ \mathbf{G}_i = \mathbf{G}_i^* \in \mathbb{C}^{k_j \times k_j} \end{matrix} \right\} \tag{2.42}$$

These subsets lead to the consideration of the next properties

a) For all $\boldsymbol{\Delta} \in \mathrm{X}_{\mathrm{M}}$, $\mathbf{Q} \in \mathrm{Q}_{\mathrm{M}}$, then $\mathbf{Q}\boldsymbol{\Delta} \in \mathrm{X}_{\mathrm{M}}$, $\boldsymbol{\Delta}\mathbf{Q} \in \mathrm{X}_{\mathrm{M}}$ with $\bar{\sigma}[\mathbf{Q}\boldsymbol{\Delta}] \leq \bar{\sigma}[\boldsymbol{\Delta}], \bar{\sigma}[\boldsymbol{\Delta}\mathbf{Q}] \leq \bar{\sigma}[\boldsymbol{\Delta}]$.

b) For all $\boldsymbol{\Delta} \in \mathrm{X}_{\mathrm{M}}$, $\mathbf{U} \in \mathrm{U}_{\mathrm{M}}$, then $\mathbf{U}\boldsymbol{\Delta} \in \mathrm{X}_{\mathrm{M}}$, $\boldsymbol{\Delta}\mathbf{U} \in \mathrm{X}_{\mathrm{M}}$ with $\bar{\sigma}[\mathbf{U}\boldsymbol{\Delta}] = \bar{\sigma}[\boldsymbol{\Delta}], \bar{\sigma}[\boldsymbol{\Delta}\mathbf{U}] = \bar{\sigma}[\boldsymbol{\Delta}]$.

c) $\mu_{\mathrm{M}}[\mathbf{QM}] = \mu_{\mathrm{M}}[\mathbf{MQ}] \leq \mu_{\mathrm{M}}[\mathbf{M}]$ for all $\mathbf{M} \in \mathbb{C}^{n\times n}$ and $\mathbf{Q} \in \mathrm{Q}_{\mathrm{M}}$.

d) $\mu_{\mathrm{M}}[\mathbf{UM}] = \mu_{\mathrm{M}}[\mathbf{MU}] = \mu_{\mathrm{M}}[\mathbf{M}]$ for all $\mathbf{M} \in \mathbb{C}^{n\times n}$ and $\mathbf{U} \in \mathrm{U}_{\mathrm{M}}$.

The above properties show that $\mu_{\mathrm{M}}[\mathbf{M}]$ is not necessary invariant to matrices in Q_k which may not to be unitary, since the real parameters are not restricted to be on the boundary of the allowable set. Then, the following upper and lower bounds are derived

$$\max_{\mathbf{Q}\in\mathrm{Q}_k} \rho_{\mathbb{R}}[\mathbf{QM}] \leq \mu_{\mathrm{M}}[\mathbf{M}] \leq \inf_{\mathbf{D}\in\mathrm{D}} \bar{\sigma}[\mathbf{DMD}^{-1}] \tag{2.43}$$

The lower bound is not necessarily a continuous function, while the upper bound is semicontinuous. From equation (2.43), the upper bound can be reformulated:

$$\max_{\mathbf{Q}\in\mathrm{Q}_k} \rho_{\mathbb{R}}[\mathbf{QM}] \leq \mu_{\mathrm{M}}[\mathbf{M}] \leq \inf_{\mathbf{D}\in\mathrm{D}} \min_{0\leq\beta\in\mathbb{R}} \{\beta : \mathbf{M}^*\mathbf{DM} - \beta^2\mathbf{D} \leq 0\} \tag{2.44}$$

Note however that (2.44) does not use the phase information that is present in the real perturbations, and hence this upper bound is frequently conservative for mixed problems. Then, the next upper bound was proposed in the literature [12].

$$\mathbf{M}^*\widehat{\mathbf{D}}\mathbf{M} + j\left[\widehat{\mathbf{G}}\mathbf{M} - \mathbf{M}^*\widehat{\mathbf{G}}\right] - \beta^2\widehat{\mathbf{D}} \leq 0 \tag{2.45}$$

where $\widehat{\mathbf{D}} = \mathbf{D}^2 \in \mathrm{D}$ and $\widehat{\mathbf{G}} = \mathbf{DGD} \in \mathrm{G}_{\mathrm{M}}$. Minimizing (2.44) over β and the $\widehat{\mathbf{D}}$, $\widehat{\mathbf{G}}$ scaling matrices, it is possible to derive the next theorem.

Theorem 2.5 (Mixed $\mu_M[\mathbf{M}]$ upper bound) [12]. Let $\mathbf{M} \in \mathbb{C}^{n\times n}$ and $\mathbf{\Delta} \in \mathrm{X}_{\mathrm{M}}$. Then

$$\mu_{\mathrm{M}}[\mathbf{M}] \leq \inf_{\mathbf{D}\in\mathrm{D},\mathbf{G}\in\mathrm{G}_{\mathrm{M}}} \min_{0\leq\beta\in\mathbb{R}} \{\beta : \mathbf{M}^*\mathbf{DM} + j[\mathbf{GM} - \mathbf{M}^*\mathbf{G}] - \beta^2\mathbf{D} \leq 0\} \qquad (2.46)$$

The upper bound in equation can be interpreted in terms of covering the real parameter uncertainty with complex or disk uncertainty, but now **G** leads to use off-axis disks. This can be shown in Fig. 2.11.

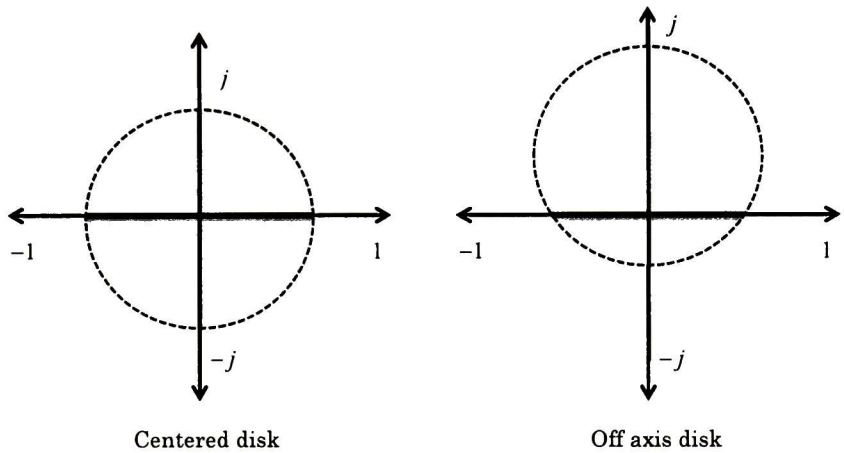

Figure 2.11. Covering real parameters with disks.

Let $\mathbf{M} \in \mathbb{C}^{n\times n}$ partitioned as

$$\mathbf{M} = \begin{bmatrix} \mathbf{M}_{11} & \mathbf{M}_{12} \\ \mathbf{M}_{21} & \mathbf{M}_{22} \end{bmatrix} \qquad (2.47)$$

and suppose there are two block structures, $\mathrm{X}_{\mathrm{M}_1}$ and $\mathrm{X}_{\mathrm{M}_2}$which are compatible with $\mathbf{M}_{11}$ and $\mathbf{M}_{22}$, respectively. The perturbation $\mathbf{M} - \mathbf{\Delta}$ is divided in two parts and shown in Fig. 2.12. Define a third block structure X_{M} as

$$\mathrm{X}_{\mathrm{M}} = \begin{bmatrix} \mathbf{\Delta}_1 & \mathbf{0} \\ \mathbf{0} & \mathbf{\Delta}_2 \end{bmatrix} : \mathbf{\Delta}_1 \in B\mathrm{X}_{\mathrm{M}_1}, \mathbf{\Delta}_2 \in B\mathrm{X}_{\mathrm{M}_2} \qquad (2.48)$$

then the LFT $F_l[\mathbf{M}, \mathbf{\Delta}_2]$ is well posed for all $\mathbf{\Delta}_2 \in B\mathrm{X}_{\mathrm{M}_2}$ if and only if $\mu_{\mathrm{M}_{\Delta_2}}[\mathbf{M}] < 1$.

Theorem 2.6 (Main loop theorem) [12]. Let $\mathbf{M} \in \mathbb{C}^{n\times n}$ and $0 < \beta \in \mathbb{R}$. Then $\mu_{\mathrm{M}}[\mathbf{M}] < \beta$ if and only if $\mu_{\mathrm{M}_{\Delta_2}}[\mathbf{M}_{22}] < \beta$ and for all $\mathbf{\Delta}_2 \in \mathrm{X}_{\mathrm{M}_2}$, $\bar{\sigma}[\mathbf{\Delta}_2] \leq \frac{1}{\beta}$ it has $\mu_{\mathrm{M}_{\Delta_1}}[F_l[\mathbf{M}, \mathbf{\Delta}_{22}]] < \beta$.

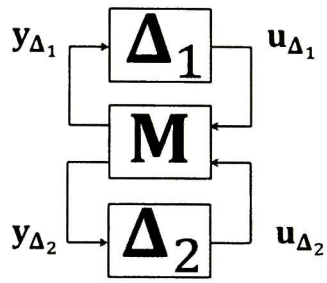

Figure. 2.12. Structure $\mathbf{M} - \boldsymbol{\Delta}$ divided in $\boldsymbol{\Delta}_1$ and $\boldsymbol{\Delta}_2$.

It should be noticed that that if $\boldsymbol{\Delta}_2 \in B\mathrm{X}_{\mathrm{M}_2}$ then $\max_{\boldsymbol{\Delta}_2 \in B\mathrm{X}_{\mathrm{M}_2}} \mu_{\mathrm{M}_{\Delta_1}}[F_l[\mathbf{M}, \boldsymbol{\Delta}_2]] < 1$. This last theorem forms the basis for all uses of μ in linear systems robustness analysis.

This statement can be rewritten in the more useful form

$$\mu_{\mathrm{M}}[\mathbf{M}] < 1 \leftrightarrow \left\{\mu_{\mathrm{M}_{\Delta_1}}[\mathbf{M}_{22}] < 1, \text{ and } \max_{\boldsymbol{\Delta}_2 \in B\mathrm{X}_{\mathrm{M}_2}} \mu_{M_{\Delta_1}}[F_l[\mathbf{M}, \boldsymbol{\Delta}_2]] < 1\right\}$$

2.7 Robust stability and robust performance with μ

The analysis presented in section 2.5 assumes unstructured uncertainty, and it was implicitly considered that $\|\boldsymbol{\Delta}(s)\|_\infty < 1$ in frequency domain. In the definition of the SSV, there is a general structure that considers $\|\boldsymbol{\Delta}(s)\|_\infty < 1$ as a special case, but this must be defined formally to provide conditions for robust stability and performance compared with the $\mathcal{H}_\infty$.

The SSV can be used to quantify robustness margins for an LTI with linear fractional uncertainty, and not being necessarily a norm, since it does not satisfy the triangle inequality. Nevertheless, the SSV satisfies a scaling property, and so it is possible to define the μ–norm

$$\|\mu_{\Delta}[\mathbf{M}(s)]\|_\infty := \sup_{\omega \in \mathbb{R}} \mu_{\Delta}[\mathbf{M}[j\omega]] \tag{2.49}$$

Define $\mathrm{M}(\mathrm{X}_{\mathrm{M}})$ that denotes the set of all real-rational, proper, stable, block diagonal transfer matrices, with block structure like X_{M}:

$$\mathrm{M}(\mathrm{X}_{\mathrm{M}}) = \{\boldsymbol{\Delta} \in \mathcal{RH}_\infty : \boldsymbol{\Delta}(j\omega) \in \mathrm{X}_{\mathrm{M}} \text{ for all } \omega \in \mathbb{R}\} \tag{2.50}$$

The expression (2.50) is to cover dynamical systems due to the unmodeled dynamics in the uncertainty. The following theorems are based in equation (2.31), $\boldsymbol{\Delta} \in \mathcal{RH}_\infty$ partitioned and the main loop theorem.

Theorem 2.7 (Robust stability with μ) [12]. Suppose that $\mathbf{M}(s) \in \mathcal{RH}_\infty$ and $\beta \in \mathbb{R}$, $\beta > 0$. Then for all $\boldsymbol{\Delta}_1 = \mathrm{M}(\mathrm{X}_{\mathrm{M}_1})$ with $\|\boldsymbol{\Delta}_1\|_\infty \leq \beta$, the perturbed closed-loop system is well-posed and stable if and only if

$$\left\|\mu_{\boldsymbol{\Delta}_1}[\mathbf{M}_{11}(s)]\right\|_\infty := \sup_{\omega \in \mathbb{R}} \mu_{\mathrm{M}_{\boldsymbol{\Delta}_1}}[\mathbf{M}_{11}(j\omega)] < \frac{1}{\beta} \tag{2.51}$$

Note that if $\boldsymbol{\Delta}_1$ is normalized, that is $\|\boldsymbol{\Delta}_1\|_\infty \leq 1$ then

$$\left\|\mu_{\boldsymbol{\Delta}_1}[\mathbf{M}_{11}(s)]\right\|_\infty := \sup_{\omega \in \mathbb{R}} \mu_{\mathrm{M}_{\boldsymbol{\Delta}_1}}[\mathbf{M}_{11}(j\omega)] < 1 \tag{2.52}$$

Theorem 2.8 (Robust performance with μ) [12]. Assume that $\mathbf{M}(s) \in \mathcal{RH}_\infty$ and $\beta \in \mathbb{R}$, $\beta > 0$. Then for all $\boldsymbol{\Delta}_1 = \mathrm{M}(\mathrm{X}_{\mathrm{M}_1})$ with $\|\boldsymbol{\Delta}_1\|_\infty \leq \beta$, the perturbed closed-loop system is well-posed, stable and $\|F_u[\mathbf{M}(s), \boldsymbol{\Delta}_1(s)]\|_\infty := \sup_{\omega \in \mathbb{R}} \bar{\sigma}\left[F_u[\mathbf{M}(j\omega), \boldsymbol{\Delta}_1(j\omega)]\right] \leq \frac{1}{\beta}$ if and only if $\|\mu_{\mathrm{M}}[\mathbf{M}(s)]\|_\infty := \sup_{\omega \in \mathbb{R}} \mu_{\mathrm{M}}[\mathbf{M}(j\omega)] < \frac{1}{\beta}$.

Similar results can be derived for the last theorem if $\|\boldsymbol{\Delta}_1\|_\infty \leq 1$. The robust performance against robust stability with μ can be shown in Fig 2.13.

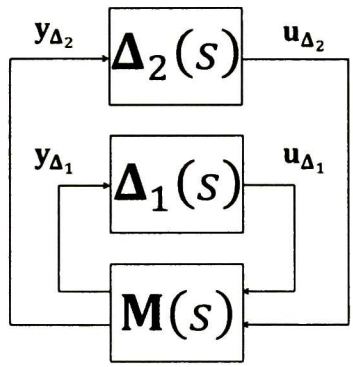

Figure 2.13. Robust performance against robust stability.

2.8 Model uncertainty representation in this dissertation

In this section, a general framework for power system robustness analysis is introduced that extends existing approaches to the study of mixed and complex uncertainty.

The analysis focuses on two main aspects:

1) Improving the discontinuity of the lower bound for the real SSV in large power systems by introducing small amounts of additional complex uncertainty.

2) Developing a general framework based on LFTs to represent the structured uncertainty of power systems for robust stability. This framework can be extended and generalized to design robust MIMO decentralized controllers.

2.8.1 Replacing real uncertainty with real+complex uncertainty

Much of the earlier numerical work with uncertain power system models has been based on the mixed structured singular value. The computation burden of the algorithms that compute μ, however, is an exponential function of the number of uncertainties thus limiting the size of the uncertainty matrix that can be analyzed. A usual solution is to compute lower and upper bounds on μ, assuming that little information is lost [12]. This is the approach adopted in this research.

In the case of purely real uncertainty problems, μ is not necessarily a continuous function [17-18]. These discontinuities can cause problems in the convergence of the lower bound mixed–μ algorithm. A practical method to avoid the discontinuity of $\mu[\mathbf{M}]$ is to add small amounts of complex uncertainty into the uncertainty model, in order to improve the convergence properties of the lower bound of μ [27]. This procedure is shown in Fig. 2.14 where α represents a scaling factor.

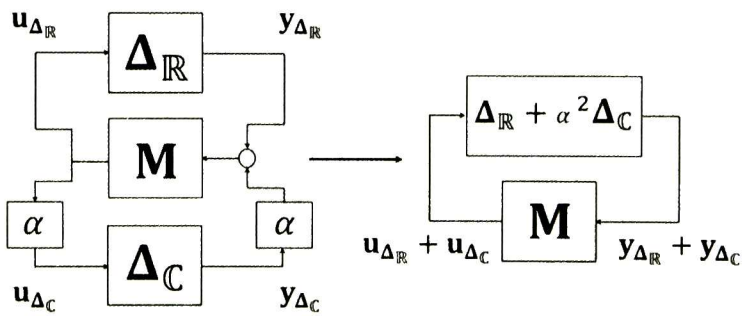

Figure 2.14. Replacing real uncertainty with real+complex uncertainty.

2.9 A general framework proposed for power systems to avoid the discontinuity of the lower upper bound of the SSV

The SSV is defined based on the structured uncertainty representation and is a generalization of the singular value and the spectral radius: full complex block and a single complex/real scalar block.

In general, the use of the SSV for power systems has focused in two categories: refining the bounds by reducing the gaps between the upper and

lower bounds to achieve high accuracy, and reducing the computational burden due to the number of uncertain parameters.

The use of the SSV for power systems was proposed in [20-21] to evaluate the robust stability; in general it was developed a general framework which takes into account non-linear parameter variations from a set of operating conditions. Based on the last references in [22-24] was proposed an extended framework for large power systems. In [25] a frequency sweep test to evaluate the real spectral radius was proposed. Furthermore, this method incorporated a skew μ problem for power systems.

Drawing on the above review, this dissertation proposes a new framework for power systems which takes into account a percent of complex uncertainty to avoid the discontinuity of the lower upper bound of the SSV

Consider, to introduce these ideas, a MIMO non-linear system in state form with the change in operating conditions. The dynamic equation for the linearized power system model is given by

$$\dot{\mathbf{x}}(t) = \mathbf{A}[\mathbf{p}]\mathbf{x}(t) \tag{2.53}$$

in which, the value of each varying element, $[\bar{a}'_{ij}]$, of the state representation (2.53) depends on a set of uncertain parameters $\mathbf{p} = [p_1, p_2, \dots, p_m]^T$ and can be expressed as $[\bar{a}'_{ij}] = f_{ij}[\mathbf{p}]$ where p_k takes values in a known range $p_k^{min} \leq p_k \leq p_k^{max}$ for $k = 1, \dots, m$. As shown in Refs. [20-24], each element $[\bar{a}'_{ij}]$ can be conveniently expressed in terms of the uncertain parameters, p_k, as:

$$[a'_{ij}][\mathbf{p}] = \begin{cases} [a'_{ij}]_0 + \sum_{k=1}^{S_r} [a'_{ij}]_k p_k + \sum_{k=1}^{S_r} [a'_{ij}]_{kk} p_k^2, & \text{if } S_r = 1 \\ [a'_{ij}]_0 + \sum_{k=1}^{S_r} [a'_{ij}]_k p_k + \sum_{k=1}^{S_r} [a'_{ij}]_{kk} p_k^2 + \sum_{k=1}^{S_r} \sum_{l=k+1}^{S_r} [a'_{ij}]_{kl} p_k p_l, & \text{if } S_r > 1 \end{cases} \tag{2.54}$$

In practice, it is desirable to normalize the range of the uncertain parameters such that the allowable range for each parameter lies in the interval $[-1, 1]$. This can be accomplished in the analysis framework as follows

$$p_k = a_k + b_k \delta_k^r = a_k[1 + r_k \delta_k^r], \; |\delta_k^r| \leq 1 \tag{2.55}$$

where $-1 \le \delta_k^r \le 1$, $a_k = \frac{1}{2}\left[p_k^{min} + p_k^{max}\right]$, $b_k = \frac{1}{2}\left[p_k^{max} - p_k^{min}\right]$ and $r_k = \frac{\left[p_k^{max} - p_k^{min}\right]}{\left[p_k^{max} + p_k^{min}\right]}$. Based on the above normalized parameters, the varying parameters, $[\bar{a}_{ij}][\boldsymbol{\Delta}]$, can be written as

$$[\bar{a}_{ij}][\boldsymbol{\Delta}] = \begin{cases} [\bar{a}_{ij}]_0 + \sum_{k=1}^{S_r} [\bar{a}_{ij}]_k \delta_k^r + \sum_{k=1}^{S_r} [\bar{a}_{ij}]_{kk} [\delta_k^r]^2, \text{if } S_r = 1 \\ [\bar{a}_{ij}]_0 + \sum_{k=1}^{S_r} [\bar{a}_{ij}]_k \delta_k^r + \sum_{k=1}^{S_r} [\bar{a}_{ij}]_{kk} [\delta_k^r]^2 + \sum_{k=1}^{S_r} \sum_{l=k+1}^{S_r} [\bar{a}_{ij}]_{kl} \delta_k^r \delta_l^r, \text{if } S_r > 1 \end{cases} \tag{2.56}$$

It may be noted finally that equation (2.56) can be rewritten in matrix form as:

$$\bar{\mathbf{A}}[\boldsymbol{\Delta}] = \begin{cases} \bar{\mathbf{A}}_0 + \sum_{k=1}^{S_r} \bar{\mathbf{A}}_k \delta_k^r + \sum_{k=1}^{S_r} \bar{\mathbf{A}}_{kk} [\delta_k^r]^2, \text{if } S_r = 1 \\ \bar{\mathbf{A}}_0 + \sum_{k=1}^{S_r} \bar{\mathbf{A}}_k \delta_k^r + \sum_{k=1}^{S_r} \bar{\mathbf{A}}_{kk} [\delta_k^r]^2 + \sum_{k=1}^{S_r} \sum_{l=k+1}^{S_r} \bar{\mathbf{A}}_{kl} \delta_k^r \delta_l^r, \text{if } S_r > 1 \end{cases} \tag{2.57}$$

where $\bar{\mathbf{A}}_0 = [\bar{a}_{ij}]_0, \bar{\mathbf{A}}_k = [\bar{a}_{ij}]_k, \bar{\mathbf{A}}_{kk} = [\bar{a}_{ij}]_{kk}$ and $\bar{\mathbf{A}}_{kl} = [\bar{a}_{ij}]_{kl}$. Then, in terms the singular value decomposition, which is a factorization of a real or complex matrix, (2.57) can be rewritten

$$\mathbf{A}[\boldsymbol{\Delta}] = \begin{cases} \mathbf{A}_0 + \mathbf{L}^T \left[\sum_{k=1}^{S_r} \mathbf{A}_k [\delta_k \mathbf{I}] + \sum_{k=1}^{S_r} \mathbf{A}_{kk} [\delta_k^r \mathbf{I}]^2 \right] \mathbf{R}, \text{if } S_r = 1 \\ \mathbf{A}_0 + \mathbf{L}^T \left[\sum_{k=1}^{S_r} \mathbf{A}_k [\delta_k \mathbf{I}] + \sum_{k=1}^{S_r} \mathbf{A}_{kk} [\delta_k^2 \mathbf{I}] + \sum_{k=1}^{S_r} \sum_{l=k+1}^{S_r} \mathbf{A}_{kl} [\delta_k^r \delta_l^r \mathbf{I}] \right] \mathbf{R}, \text{if } S_r > 1 \end{cases} \tag{2.58}$$

where $\mathbf{L}^T$ and $\mathbf{R}$ are matrices of 0's and 1's, respectively. In addition, $\mathbf{A}_0 = \bar{\mathbf{A}}_0$, $\bar{\mathbf{A}}_k = \mathbf{L}^T \mathbf{A}_k \mathbf{R}$, $\bar{\mathbf{A}}_{kk} = \mathbf{L}^T \mathbf{A}_{kk} \mathbf{R}$ and $\bar{\mathbf{A}}_{kl} = \mathbf{L}^T \mathbf{A}_{kl} \mathbf{R}$.

With this representation of $\mathbf{A}[\mathbf{p}]$, (2.53) can be defined in an LFT form for robust stability as shown in Fig. 2.15 for $S_r = 1$ and $S_r > 1$, respectively. Here, $\boldsymbol{\Xi}$ is given by

$$\Xi = \begin{bmatrix} \Xi_{11} & \Xi_{12} \\ \Xi_{21} & \Xi_{22} \end{bmatrix}$$

and represents the LFT for the matrix $\mathbf{A}[\Delta]$ with respect to $\Delta = \text{diag}[\delta_1, \ldots, \delta_{S_r}]$

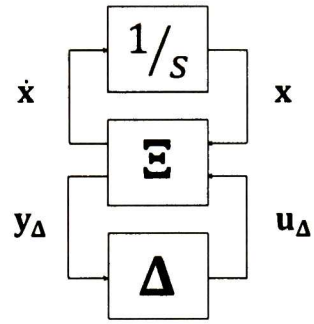

Figure 2.15. LFT form of $\dot{\mathbf{x}}(t) = \mathbf{A}[\Delta]\mathbf{x}(t)$.

It follows that the LFT form of $\dot{\mathbf{x}}(t) = \mathbf{A}[\Delta]\mathbf{x}(t)$ for $S_r = 1$ is given in Fig 2.16. A similar procedure can be used for $S_r > 1$. The details are omitted.

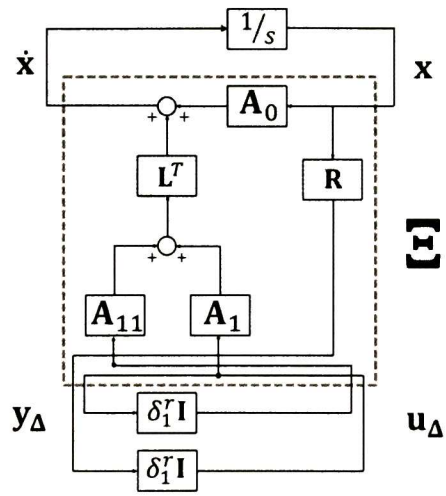

Fig. 2.16. LFT form of $\dot{\mathbf{x}}(t) = \mathbf{A}[\Delta]\mathbf{x}(t)$ for $S_r = 1$.

The key idea is to notice that the transfer matrix $\mathbf{M}(s)$ from $\boldsymbol{y}_\Delta$ to $\mathbf{u}_\Delta$ can be computed as:

$$\mathbf{M}(s) = \Xi_{22} + \Xi_{21}\frac{1}{s}\mathbf{I}\left[\mathbf{I} - \frac{1}{s}\Xi_{11}\right]^{-1}\Xi_{12} \tag{2.59}$$

and

$$\dot{\mathbf{x}} = \Xi_{11}\mathbf{x} + \Xi_{11}\mathbf{u}_\Delta$$
$$\mathbf{z} = \Xi_{21}\mathbf{x} + \Xi_{22}\mathbf{u}_\Delta \tag{2.60}$$

$$\mathbf{w} = \Delta\mathbf{z} \tag{2.61}$$

where

$$\Xi = \left[\begin{array}{c|cc} \mathbf{A}_0 & \mathbf{A}_1 & \mathbf{A}_{11} \\ \hline \mathbf{R} & \mathbf{0} & \mathbf{0} \\ \mathbf{0} & \mathbf{I} & \mathbf{0} \end{array}\right]$$

Now the $\mathbf{M}(s) - \boldsymbol{\Delta}(s)$ framework of $\dot{\mathbf{x}}(t) = \mathbf{A}[\boldsymbol{\Delta}]\mathbf{x}(t)$ for $S_r = 1$ have been prepared to introduce small levels of complex uncertainty into the uncertainty model. Fig. 2.14 represents this idea for power systems.

Assessment of robust stability is then straightforward:

1. For a set of independent parameters described by $\mathbf{p} = [p_1, p_2, \ldots, p_m]^T$ generate a range of operating scenarios. In general, $\mathbf{p}$ in power systems may describe uncertainty in a tie-line reactance, loads, etc. This means that for each operating condition of a power system, a load flow simulation must be computed and the associated linearized power system model represented by (2.53) must be obtained.

2. Compute coefficients of approximating polynomials for each varying element of (2.54), using the least square minimization technique.

3. Generate the $\mathbf{M}(s) - \boldsymbol{\Delta}(s)$ framework associated with the state representation $\dot{\mathbf{x}}(t) = \mathbf{A}[\boldsymbol{\Delta}]\mathbf{x}(t)$ for $S_r = 1$ or $S_r > 1$. Create matrices Ξ_{11}, Ξ_{12}, Ξ_{21}, and Ξ_{11} using equation (2.60).

4. Define a percent of complex uncertainty, α^2, into the $\mathbf{M}(s) - \boldsymbol{\Delta}(s)$ framework of $\dot{\mathbf{x}}(t) = \mathbf{A}[\boldsymbol{\Delta}]\mathbf{x}(t)$ for $S_r = 1$ or $S_r > 1$ as indicated in Fig. 2.14. A general representation can be described in Fig. 2.17 with a percent of complex uncertainty for $S_r = 1$.

5. Compute the SSV to determine the robust stability of power system.

2.10 Conclusions

The basic configuration of feedback systems with uncertainty considered in this chapter is a theory which leads to the concept of robust stability and robust performance. The small gain theorem plays an essential rule to derive these criterions. Nevertheless, the necessity of a formal mathematical

analysis to describe the differences between the complex and mixed SSV have been necessary to derive basic analytical limitations.

In this chapter has been shown how parametric uncertainties can be incorporated in a non-conservative uncertainty description. The main advantage of this approach is that not only stability but also performance can be guaranteed for the perturbed plant. In addition, a general framework based on the SSV which includes a percent of complex uncertainty have been proposed in this chapter to study the robust stability of large power systems.

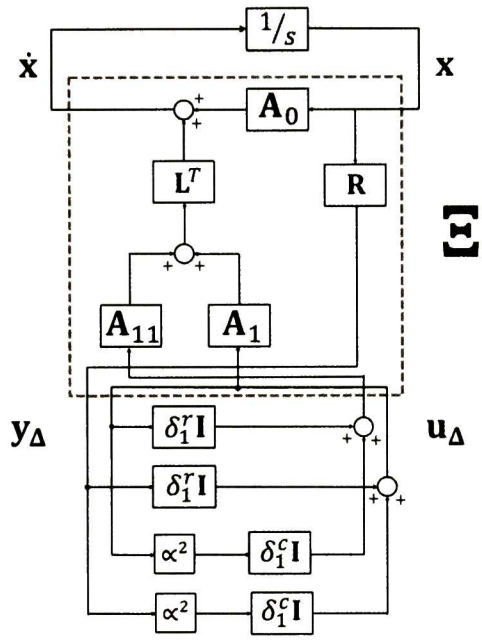

Fig. 2.17. LFT form of $\dot{\mathbf{x}}(t) = \mathbf{A}[\boldsymbol{\Delta}]\mathbf{x}(t)$ with a percent of complex uncertainty for $S_r = 1$.

2.11 References

[1] J. C. Doyle, and G. Stein, "Multivariable feedback design: concepts for a classical/Modern Synthesis," *IEEE Trans. Automat. Contr.*, vol. AC-26, pp. 4-16, Feb. 1981.

[2] B. A. Francis, *A course in H control theory*, Springer-Verlag, 1987, ISBN 0-387-170693.

[3] J. Doyle, "Analysis of feedback systems with structured uncertainties," *IEE Proc.*, vol. 129, Pt. D, pp. 242-250, Nov. 1982.

[4] P. Dorato, *Robust control*, IEEE Press, 1987, ISBN 0-87942-233-5.

[5] R. Lane Dailey, "A new algorithm for the structural singular value," *Proc. of the American Control Conference*, San Diego, CA, pp. 3036-3040, 1990.

[6] A. Packard, and J. C. Doyle, "The complex structured singular value,' *Automatica*, vol. 29, pp. 71-109, 1993.

[7] M. Morari, and E. Zafiriou, *Robust Process Control*, Prentice Hall, 1989, ISBN 0-13-782153-0.

[8] S. Skogestad, and I. Postlethwaite, *Multivariable feedback control: analysis and design*, John Wiley and Sons, 1996, ISBN 0-471-94277-4.

[9] K. Zhou, and J. C. Doyle, *Essentials of robust control*, Prentice Hall, 1998, ISBN 0-13-525833-2.

[10] M. K. H. Fan, and A. L. Tits, "Characterization and efficient computation of the structured singular value,' *IEEE Trans. Automat. Contr.*, Vol. AC-31, pp. 734-743, Aug. 1986.

[11] M. K. H. Fan, A. L. Tits, and J. C: Doyle, "Robustness in the presence of mixed parametric uncertainty and unmodeled dynamics, *IEEE Trans. Automat. Contr.*, vol. 36, pp. 25-38, 1991.

[12] P. Young, "Robustness with Parametric and Dynamic Uncertainty," PhD thesis, California Institute of Technology, 1993.

[13] P. M. Young, and J. C. Doyle, "Properties of the mixed μ problem and its bounds," *IEEE Trans. Automat. Contr.*, vol. 41, pp. 155-159, Jan. 1996.

[14] R.S. Sanchez Peña and A. Sideris, "A General program to compute the multivariable stability margin for systems with parametric uncertainty," *Proc. of the American Control Conference*, Atlanta, Georgia, pp. 317-322, 1988.

[15] R. R. E. De Gaston and M. G. Safonov, "Exact calculation of the multiloop stability margin" *IEEE Trans. Automat. Contr.*, vol. 33, pp. 156-171, Feb. 1988.

[16] M. G. Safonov, "Exact calculation of the multivariable structured singular value stability margin, in *Proc. 23th Conf. Decision and Contr.,* Los Angeles, Cal. pp. 1224-1225, Dec., 1984.

[17] G. J. Balas, J. C. Doyle, K. Glover, A. Packard, and R. Smith, *Mu Analysis and synthesis Toolbox User's Guide*, The Mathworks Inc.

[18] D.-W. Gu, P. Hr Petkov and M. M. Konstantinov, *Robust control design with Matlab*, Springer, 2005, ISB 1852339837.

[19] S. Toffner-Clausen, *System Identification and robust control: a synergistic approach*, 1996, Springer, ISBN 3540760873.

[20] M. Djukanovic, M. H. Khammash, and V Vittal, "Application of structured singular value theory for robust stability and control analysis in multimachine power systems part-I: Framework development," *IEEE Trans. Power Systems*, vol. 13, pp. 1311-1316, Nov. 1998.

[21] M. Djukanovic, M. H. Khammash, and V. Vittal, "Application of structured singular value theory for robust stability and control analysis in multimachine power systems part-II: Numerical simulations and results," *IEEE Trans. Power Systems*, vol. 13, pp. 1317-1322, Nov. 1998.

[22] R. Castellanos, A. R. Messina, and H. Sarmiento, "Robust stability analysis of large power systems using the structured singular value theory," *Electrical Power and Energy Systems*, vol. 27, pp. 389-397, Jun. 2005.

[23] R. Castellanos, A. R. Messina, and H. Sarmiento, "A μ-analysis approach to power systems stability robustness evaluation," *Electric Power Systems Research*, vol. 78, pp. 192-201, Feb. 2008.

[24] R. Castellanos, "Robust stability assessment of large power systems using the structured singular value theory," PhD thesis, CINVESTAV, 2006.

[25] C. Zhu, "Robustness analysis for power systems based on the structured singular value tools and the υ gap metric," PhD thesis, Iowa State University, 2001.

[26] X. Yu, "Robustness analysis and controller design for static var compensators in power systems," PhD thesis, Iowa State University, 2000.

[27] S. L. Gatley, D.G. Bates, M. J. Hayes, I. Postlethwaite, "Robustness analysis of an integrated flight and propulsion control system using μ and the υ-gap metric," *Control Eng. Practice*, vol. 10, 261-275, Mar. 2002.

Chapter 3

Interaction Measures for MIMO Decentralized and Hierarchical Control Configurations

This chapter examines the problem of loop interaction in decentralized MIMO control systems. Emphasis is placed upon the theory of interaction measures for decentralized controllers to quantify looop interaction in frequency domain as well as to select the most suitable input-output pairings while minimizing computational demand.

First, a review of scalar interaction measures is introduced and the concept of phase of the relative gain array for single-input single-output systems is proposed. Then, the concept of the block relative gain is introduced to determine the most suitable input-output pairings for block decentralized (wide-area) MIMO controllers to achieve good performance. In addition, the block relative gain for non-square block input-output pairings is defined to describe diferent types of power system control configurations. Unlike previous research, control structure is not limited to basic control control structures, namely fully decentralized or fully decentralized configurations.

In summary, the main contribution of this chapter is twofold: the use of the block relative gain array for power systems to select multiple-input multiple-output pairings for wide-area damping controllers and the development of new measures of interaction that account for more realistic operating conditions and control structures. Discussion is limited to linear time invariant and stable systems.

3.1 Introduction

Decentralized control systems are widely used in industrial plants and process industries for MIMO systems. It is well known that the interactions among loops can lead to tuning and stability problems. Furthermore, control system design involves input-output selection; that is, decisions on the number, and the placement of controllers.

Due to the combinatorial nature of the selection problem, several systematic methods have been proposed in the literature to satisfy requirements on the controlled variables. Essentially, the issue is to select suitable input variables to be manipulated by the controller and suitable output variables to be supplied to the controller.

The use of the RGA as interaction measure in frequency domain was developed to choose the selection of loop pairings in chemical processes to design decentralized controls, by assuming that the control has a PI feedback. The RGA, however, is a conservative and empirical method due to the fact that it uses knowledge of the steady-state process gain with integral feedback [1-4]. More recently, the DRGA was proposed to improve the pairing capabilities of the steady state RGA in cases where the RGA changes substantially with frequency [5].

In [6-7] the relative interaction array (RIA) was introduced, which defines the interaction on individual control loops. In a paralle effort, a new interaction measure was proposed using the concept of dynamic information and a complete configuration in the feedback to any control [8]. It was demonstrated that the GDRG includes the RGA as special case. In general, the RGA, and subsequent methodologies, are transfer functions and they provide similar empirical information [9-11].

In [12] a procedure for a new interaction measure and sensitivity of the process nodes was formulated. Then, the design procedure was developed on the dyadic expansion. Thus for instance, in [13] a graphical interpretation was proposed between the SVD and the RGA. However, it is necessary to analyze the singular vectors and their rotation matrices while the RGA is invariant of scaling; the issue of scaling is significant in determining the SVD of a matrix.

The non-diagonal elements of the transfer function were considered as complex uncertainties using the SSV in [14-17] to propose an interaction measure, but it is possible to modify this criterion using the skewed SSV. These methods express constraints on the closed loop transfer matrix and

sufficient stability conditions. Nevertheless, this tecnique quantifies the size of interaction measure and not internal loops.

The block relative gain (BRG) concept and its properties were originally proposed in [18] to extend criteria to determine of the most suitable input-output pairings from single-input single-output (SISO) to MIMO configurations. In addition in [19-21] a formal analysis of the BRG to avoid conjectures for pairing of variables was suggested. Finally, in [22-24] was proposed the dynamic BRG for control configurations under dynamic feedback control to avoid the concept of perfect control. In conclusion, this review emphasizes the importance of developing techniques to assess the potential for adverse interactions between control loops.

3.2 General linear representation

To introduce the proposed model, consider the linear multivariable system

$$\dot{\mathbf{x}}(t) = \mathbf{A}\mathbf{x}(t) + \mathbf{B}\mathbf{u}(t), \mathbf{x}(t_0) = \mathbf{x}_0 \tag{3.1}$$
$$\mathbf{y}(t) = \mathbf{C}\mathbf{x}(t) + \mathbf{D}\mathbf{u}(t)$$

where $\mathbf{x}(t) \in \mathbb{R}^n$ is the vector of system states, $\mathbf{x}(t_0)$ is the initial condition of the system, $\mathbf{u}(t) \in \mathbb{R}^{p_u}$ is the system input, and $\mathbf{y}(t) \in \mathbb{R}^{q_y}$ is the system output, $\mathbf{A} \in \mathbb{R}^{n\times n}$, $\mathbf{B} \in \mathbb{R}^{n\times p}$, $\mathbf{C} \in \mathbb{R}^{q\times n}$, $\mathbf{D} \in \mathbb{R}^{q\times p}$ are state, input, output matrices, respectively.

The corresponding frequency response $\mathbf{G}(j\omega) \in \mathbb{C}^{q\times p}$ of the transfer matrix from $\mathbf{u}(s)$ to $\mathbf{y}(s)$ is defined as

$$\mathbf{y}(s) = [\mathbf{C}(s\mathbf{I} - \mathbf{A})^{-1}\mathbf{B} + \mathbf{D}]\mathbf{u}(s) = \mathbf{G}(s)\mathbf{u}(s) \tag{3.2}$$

where $\mathbf{u}(s)$ and $\mathbf{y}(s)$ are in the frequency domain.

Assume in (3.2) that $\mathbf{G}(j\omega) \in \mathbb{C}^{q\times q}$, which makes the above expression a square transfer matrix function and can be written as:

$$\mathbf{y}(s) = \mathbf{G}(s)\mathbf{u}(s) = [g_{ij}(s)]\mathbf{u}(s)\ i,j = 1,\dots,q \tag{3.3}$$

where $g_{ij}(s)$ is the open loop gain from the j^{th} input to i^{th} output.

From the above equations, consider the $q \times q$ transfer function matrix $\mathbf{G}(s) = [g_{ij}(s)]$ and the corresponding $q \times q$ compensator matrix $\mathbf{K}(s) = [k_{ii}(s)]\ i = 1,\dots,q$ of a one-degree of freedom control configuration as shown in Fig. 3.1.

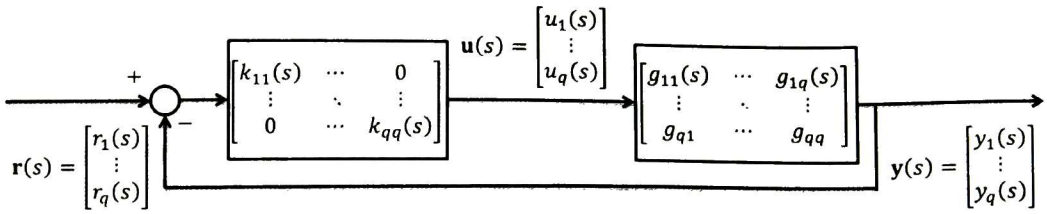

Figure 3.1. Feedback control configuration for SISO controllers.

Therefore, the closed-loop system function can be written as:

$$\mathbf{y}(s) = [[\mathbf{I} + \mathbf{G}(s)\mathbf{K}(s)]^{-1}\mathbf{G}(s)\mathbf{K}(s)]\mathbf{r}(s) = \mathbf{H}(s)\mathbf{r}(s) \tag{3.4}$$

where $\mathbf{H}(s) = [h_{ij}]\ i,j = 1,\dots,q$.

3.3 Interaction measures for SISO integral control configurations

Assume to introduce the more general ideas that follow, that $u_k = 0\ \forall\ k \neq j$, i.e. the loops are open and the effect of u_j on the i^{th} output y_i is considered. This gives the steady state gain between the j^{th} input to i^{th} output in the open loop, denoted by $g_{ij}(0)$. In an analogous manner, in the case of closed loop regulation let $y_k = 0\ \forall\ k \neq i$, i.e. all the outputs are constant except the i^{th} output, and assume perfect control in all other channels. This steady state gain is denoted by $\hat{g}_{ij}(0)$ and is the gain between the i^{th} output to the j^{th} input, where all the loops except the i^{th} output are under perfect control.

A perfect control in steady state means zero output offset and this is achieved with an stable integral feedback control evaluated at $s = 0$; this idea can be illustrated from equation (3.4) by noting that $[k_{ii}(s)] = diag\left[\frac{1}{s}\Big|_{s=0}\right]\ i = 1,\dots,q$, where $\frac{1}{s}\Big|_{s=0}$ denotes $\frac{1}{s}$ at $s = 0$. Then, the steady state diagonal controlled gain is

$$\mathbf{H}^i(0) = \left[\left[\mathbf{I} + \mathbf{G}(0)\mathbf{K}^i(0)\right]^{-1}\mathbf{G}(0)\mathbf{K}^i(0)\right] = \left[h_{ij}^i\right]\ i = 1,\dots,q \tag{3.5}$$

where $\mathbf{H}^i(0)$ denotes the closed-loop system function at $s = 0$ with the $y_i - u_i$ loop open and $\mathbf{K}^i(0)$ represents the diagonal matrix of controllers with $k_{ii}(s) = 0$. Hence, using (3.5), the controlled gain can be written as:

$$\hat{g}_{ii}(0) = h_{ii}^i(0) = \frac{h_{ii}(0)}{1 - h_{ii}(0)}\frac{1}{k_{ii}(0)} \tag{3.6}$$

Then, in general, the relative gain λ_{ij}, for a given input u_j and output y_i is defined as the ratio between the uncontrolled gain and the controlled gain as

$$\lambda_{ij}(0) = \frac{g_{ij}(0)}{\hat{g}_{ij}(0)} = g_{ij}(0)\hat{g}_{ij}^{-1}(0) \tag{3.7}$$

Extensions to the multivariate case are discussed below. Here after, the static gain, $\lambda_{ij}(0)$, is simply written as λ_{ij}.

Definition 3.1 [4]. The RGA $\mathbf{\Lambda}$ of an $q \times q$ matrix $\mathbf{G}$ is also a $q \times q$ matrix defined by:

$$\mathbf{\Lambda} := [\lambda_{ij}] = \mathbf{G} \odot [\mathbf{G}^{-1}]^T \tag{3.8}$$

where $\odot$ denotes element-by-element multiplication (the Schur product).

The following properties can be easily derived from the above definition:

1. The DRGA is independent of input and output scaling, i.e. $\mathbf{\Lambda}[\mathbf{DA}] = \mathbf{\Lambda}[\mathbf{A}]$ and $\mathbf{\Lambda}[\mathbf{AD}] = \mathbf{\Lambda}[\mathbf{A}]$.

2. A unity value $\lambda_{ij}(0) = 1$ implies that u_j affects y_i without interacting with other control loops, i.e. the system is completely decoupled.

3. The RGA can be used to measure diagonal dominance with the next intuitive quantity called the RGA-number

$$\mathrm{RGA_n} = \sum_{i=1}^{q} |\lambda_{ii}(0) - 1| + \sum_{\substack{j=1 \\ j \neq i}}^{q} |\lambda_{ij}(0)| \quad i = 1,2,\dots,q \tag{3.9}$$

4. $\mathbf{\Lambda}$ depends on plant model only and not on the controller, this is due to the static definition.
5. At least one eingenvalue and one singular value of the RGA is equal to 1.

6. In practical applications, it is recommended to avoid pairings with negative steady-state RGA elements to avoid significant degradation in performance. This means that if $\lambda_{ij}(0) < 0$ then $\hat{g}_{ij}(s)$ has an odd number of RHP-poles RHP and RHP-zeros [2].

For a set of SISO decentralized controllers it is desired that the pairing $y_i(0) - u_j(0)$ results in $\lambda_{ij}(0) = 1$, and that RGA-number is small or zero to avoid interactions. Thus, when the relative gain of a particular loop approaches to one, closing the other loops has no significant effect on the open loop gain of the aforementioned loop. Hence, the interaction among both loops will be less significant but it is very possible that the degradation in performance occurs. The steady state RGA can result in erroneous pairing assessments in the following cases:

1. The RGA changes substantially with frequency.

2. The RGA near the natural frequency of a loop differs substantially from the steady state RGA.

The above considerations lead to the DRGA, $\mathbf{\Lambda}(j\omega) \in \mathbb{C}^{q\times q}$ expressed as:

$$\mathbf{\Lambda}(s) = \mathbf{G}(s) \odot [\mathbf{G^{-1}}(s)]^T \tag{3.10}$$

By replacing $s = j\omega$ in equation (3.6), the elements of DRGA can be plotted versus frequency. The pairing should be such that, over the frequency range of interest, the magnitude of the diagonal elements is close to one and the magnitude of the off diagonal elements is small [5]. The DRGA of the uncontrolled gain is shown in Fig 3.2 that it is given by the elements of the MIMO system. Figure 3.3 shows a schematic diagram of the controlled gain and represents the elements of the inverse transpose matrix of the multivariable system.

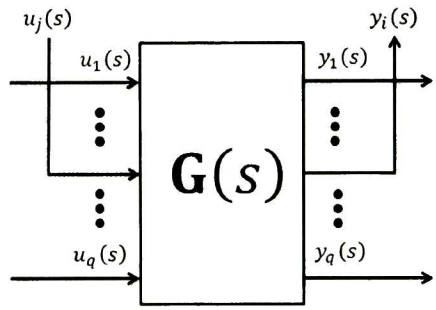

Figure 3.2. Uncontrolled gain, $g_{ij}(s)$, for $y_i(s) - u_j(s)$.

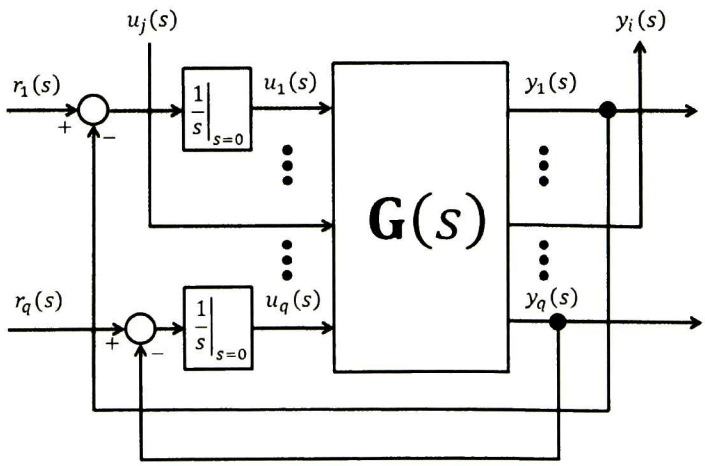

Figure 3.3. Controlled gain, $\hat{g}_{ij}(s)$, for $y_i(s) - u_j(s)$.

Insight into the nature of the proposed model can be obtained by rewriting (3.7) in the form

$$\left[\frac{\partial y_i(s)}{\partial u_j(s)}\right]_{u_k=0,k\neq j} = g_{ij}(s) \tag{3.11}$$

$$\left[\frac{\partial y_i(s)}{\partial u_j(s)}\right]_{y_k=0,k\neq i} = \hat{g}_{ij}(s) \tag{3.12}$$

from which it follows that

$$\lambda_{ij}(s) = \frac{\left[\frac{\partial y_i(s)}{\partial u_j(s)}\right]_{u_k=0,k\neq j}}{\left[\frac{\partial y_i(s)}{\partial u_j(s)}\right]_{y_k=0,k\neq i}} = \frac{g_{ij}(s)}{\hat{g}_{ij}(s)} \tag{3.13}$$

It should be emphasized that that equations (3.11) and (3.12) represent the uncontrolled gain and the controlled gain with integral feedback control evaluated at $s = 0$, respectively. Furthermore, (3.11) and (3.12) are functions in the frequency domain.

Based on Fig. 3.3 for an arbitrary pairing scheme with $k_{ii}(s)$ whithout perfect control, and focusing on the $y_i(s) - u_j(s)$ loop the next expression can be obtained

$$y_i(s) = g_{ij}(s)u_j(s) - \sum_{l=1,l\neq j}^{q} g_{il}(s)\, k_{ll}(s) y_l(s) \tag{3.14}$$

Succesively using equation (3.13) to express all the outputs in terms of u_j, the transmittance between the control action u_j and its own output can be written as

$$y_i(s) = [g_{ij}(s) + a_{ij}(s)]u_j(s) \tag{3.15}$$

from which, the perturbations caused by u_j on other loops is

$$y_k(s) = d_{kj}(s)u_j(s),\ \forall k \tag{3.16}$$

Structurally, $a_{ij}(s)$ represents the additional dynamics in the $y_i(s) - u_j(s)$ loop resulting from other control loops. $a_{ij}(s)$ can be defined as the absolute interaction. These concepts can be schematically illustrated in Fig. 3.4.

From the above analysis, a relative interaction can be defined as:

$$\phi_{ij}(s) = \frac{a_{ij}(s)}{g_{ij}(s)} \tag{3.17}$$

The above equation can be interpreted as the ratio of the absolute interaction and the uncontrolled gain. Iin literature the uncontrolled gain is often referred to, as *the interaction-free* gain [6-7].

When substituted back in equation (3.10), gives

$$y_i(s) = g_{ij}(s)[1 + \phi_{ij}(s)]u_j(s) \tag{3.18}$$

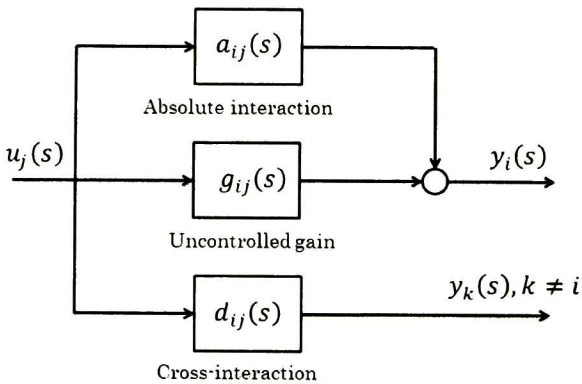

Fig. 3.4. Pairing scheme for $y_i(s) - u_j(s)$.

Using (3.17), with a perfect control described by $k_{ii}(s) = \frac{1}{s}\Big|_{s=0}$,results in

$$\phi_{ij}(s) = \frac{1}{\lambda_{ij}(s)} - 1 \tag{3.19}$$

where $\lambda_{ij}(s)$ is the element of the corresponding RGA and $\phi_{ij}(s)$ represents the RIA [6]. From the definition of RGA follows that

$$\mathbf{\Phi}_{\mathrm{RIA}}(s) = \frac{1}{\mathbf{G}(s) \otimes [\mathbf{G}^{-1}(s)]^T} - 1 \tag{3.20}$$

Notice that the division in (3.20) is defined element by element.

In this research, the following RIA-number of frequency domain is proposed

$$\mathrm{RIA_n} = \sum_{i=1}^{n} \left| \frac{1}{\lambda_{ii}(j\omega)} - 1 \right| \tag{3.21}$$

This approach is similar to the RGA-number in (3.9). However, the RGA-number takes into account non-diagonal elements of the RGA, but this is an unrealistic definition due the number of combinations of feedback decentralized controllers for the controlled gain [1]. For diagonal elements of the RGA are only necessary diagonal feedback controllers.

In order to illustrate the number of combinations of feedback decentralized controllers for the RGA consider a system described by $\mathbf{G}(s) \in \mathcal{RH}_{\infty}^{2\times 2}$ Clearly, only two possible combinations can be developed for the input-ouput pairings. This means that diagonal and non-diagonal elements of the controlled gains of RGA do not have relations and they are represented in Fig. 3.5 and Fig. 3.6, respectively. In addition, diagonal and non-diagonal controllers are defined as $\sum_{i=1}^{2} k_{ii} = \frac{1}{s}\Big|_{s=0}$ and $\sum_{\substack{j=1 \\ j\neq i}}^{2} k_{ji} = \frac{1}{s}\Big|_{s=0}$, respectively.

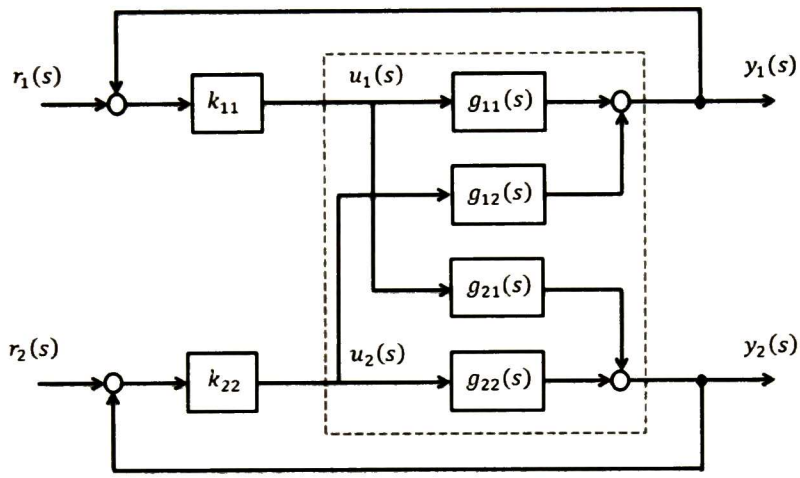

Fig. 3.5. Pairing scheme for $\lambda_{11}(s)$ and $\lambda_{22}(s)$.

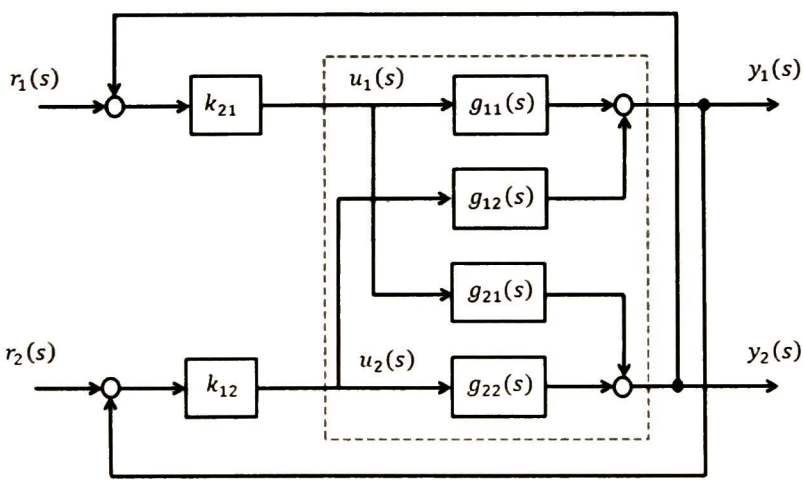

Fig. 3.6. Pairing scheme for $\lambda_{12}(s)$ and $\lambda_{21}(s)$.

To choose the best candidate of several pairing sets represented by η control alternatives with minimum interaction, the criteria is adopted

$$\min[[\mathrm{RIA_n}]^1,\ldots,[\mathrm{RIA_n}]^m]\ \eta = 1,\ldots,m \tag{3.22}$$

Compared to existing criteria, this last expression is an alternative to quantify the interaction of several sets of decentralized controllers.

3.4 Interaction measures for SISO general control configurations

At this point, the definitions of interaction measures have been expressed by feedback integral controllers at steady state. In the more general case, the transfer function from y_i to u_j in the ijth loop for the open-loop and closed-loop in frequency domain without assuming perfect control can be rewritten as

$$\tilde{\lambda}_{ij}(s) = \frac{\left[\frac{\partial y_i(s)}{\partial u_j(s)}\right]_{u_k=0,k\neq j}}{\left[\frac{\partial y_i(s)}{\partial u_j(s)}\right]_{y_k=0,k\neq i}} = \frac{g_{ij}(s)}{\tilde{g}_{ij}(s)} \tag{3.23}$$

Note that equation (3.23) describes the ratio of a SISO system. This expression is called GDRG and $\tilde{g}_{ij}(s)$ describes the diagonal and non-diagonal elements of a controlled gain without a perfect control [8]. Formally, the diagonal elements of GDRG can be expressed as

$$\tilde{\lambda}_{ii}(s) = \frac{g_{ii}(s)}{\tilde{g}_{ii}(s)} \tag{3.24}$$

where

$$\tilde{g}_{ii}(s) = \frac{h_{ii}(s)}{1-h_{ii}(s)}\frac{1}{k_{ii}(s)} \tag{3.25}$$

From the above equation, the controlled gain, $\tilde{g}_{ii}(s)$, can be represented in Fig 3.7. Note that $k_{ii}(s)$ is not a perfect control.

The next observations about GDRG, RGA and RIA can be made:

1. The overall interaction measure using the GDRG-number is described by

$$\mathrm{GDRG_n}(j\omega) = \sum_{i=1}^{q}\left|\frac{g_{ii}(j\omega)}{\tilde{v}_{ii}(j\omega)} - 1\right| \tag{3.26}$$

   Equation (3.26) was proposed originally in [27] and derived from equation (3.9) in the literature [2].

2. The GDRG is different for positive and negative feedback. However, the RGA and RIA are the same for negative and positive feedbacks.

3. Equation (3.25) is different for cascade SISO control configurations and was developed in [27].

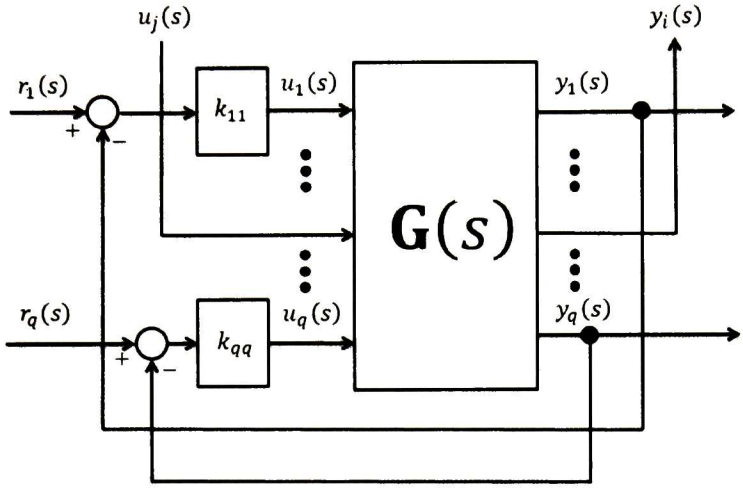

Fig 3.7. Controlled gain, $\tilde{g}_{ii}(s)$, for $y_i(s) - u_j(s)$.

Following these ideas, this section proposes to rewrite the expressions for the DRGA, RIA, and GDRG in a cartesian and polar form to describe the angle of each interaction measure. More formally, assume that

$$\lambda_{ij}(j\omega) = \mathrm{Re}[\lambda_{ij}(j\omega)] + j * \mathrm{Im}[\lambda_{ij}(j\omega)] = |\lambda_{ij}(j\omega)|e^{j\theta_{\lambda_{ij}}} \tag{3.27}$$

$$\phi_{ij}(j\omega) = \mathrm{Re}[\phi_{ij}(j\omega)] + j * \mathrm{Im}[\phi_{ij}(j\omega)] = |\phi_{ij}(j\omega)|e^{j\theta_{\phi_{ij}}} \tag{3.28}$$

$$\tilde{\lambda}_{ij}(j\omega) = \mathrm{Re}[\tilde{\lambda}_{ij}(j\omega)] + j * \mathrm{Im}[\tilde{\lambda}_{ij}(j\omega)] = |\tilde{\lambda}_{ij}(j\omega)|e^{j\theta_{\tilde{\lambda}_{ij}}} \tag{3.29}$$

where $\theta_{\lambda_{ij}} = \tan^{-1}\frac{\mathrm{Im}[\lambda_{ij}(j\omega)]}{\mathrm{Re}[\lambda_{ij}(j\omega)]}$, $\theta_{\phi_{ij}} = \tan^{-1}\frac{\mathrm{Im}[\phi_{ij}(j\omega)]}{\mathrm{Re}[\phi_{ij}(j\omega)]}$ and $\theta_{\tilde{\lambda}_{ij}} = \tan^{-1}\frac{\mathrm{Im}[\tilde{\lambda}_{ij}(j\omega)]}{\mathrm{Re}[\tilde{\lambda}_{ij}(j\omega)]}$ represent the angle of the RGA, RIA and GDRG, respectively. On the other hand, the modulus of equations (3.27), (3.28) and (3.29) are given by

$$|\lambda_{ij}(j\omega)| = \sqrt{\left(\mathrm{Re}[\lambda_{ij}(j\omega)]\right)^2 + \left(\mathrm{Im}[\lambda_{ij}(j\omega)]\right)^2}$$

$$|\phi_{ij}(j\omega)| = \sqrt{\left(\mathrm{Re}[\phi_{ij}(j\omega)]\right)^2 + \left(\mathrm{Im}[\phi_{ij}(j\omega)]\right)^2}$$

$$|\tilde{\lambda}_{ij}(j\omega)| = \sqrt{\left(\mathrm{Re}[\tilde{\lambda}_{ij}(j\omega)]\right)^2 + \left(\mathrm{Im}[\tilde{\lambda}_{ij}(j\omega)]\right)^2}$$

Expressions (3.27), (3.28) and (3.29) define the cartesian and polar form of the DRGA, RIA and GDRG. In general, it is possible to plot the magnitude and phase of the above expressions. Unfortunately, all these interaction measures are for SISO input-output pairings. This means that only SISO input-output pairings can be considered for decentralized controllers.

In the sections that follow, formal criteria to select the most suitable MIMO input-output pairings for WADCs or MIMO control devices in power systems are proposed and developed. This framework, based on the BRG, generalizes the concept of interaction to MIMO channels in frecuency domain. First, some background theory is introduced.

3.5 Definition of the BRG

Let the transfer function $\mathbf{G}(s) \in \mathcal{RH}_\infty^{q\times q}$ be partitioned as follows:

$$\begin{bmatrix}\mathbf{y}_1(s)\\ \mathbf{y}_2(s)\end{bmatrix} = \begin{bmatrix}\mathbf{G}_{11}(s) & \mathbf{G}_{12}(s)\\ \mathbf{G}_{21}(s) & \mathbf{G}_{22}(s)\end{bmatrix}\begin{bmatrix}\mathbf{u}_1(s)\\ \mathbf{u}_2(s)\end{bmatrix} \tag{3.30}$$

where $\mathbf{G}_{11}(s) \in \mathcal{RH}_\infty^{r_1\times r_1}$, $\mathbf{G}_{12}(s) \in \mathcal{RH}_\infty^{r_1\times(q-r_1)}$ $\mathbf{G}_{21}(s) \in \mathcal{RH}_\infty^{(q-r_1)\times r_1}$, $\mathbf{G}_{22}(s) \in \mathcal{RH}_\infty^{(q-r_1)\times(q-r_1)}$ and $\mathcal{RH}_\infty$ represents the real rational subspace of $\mathcal{H}_\infty$. Each block of transfer functions are described by

$$\begin{bmatrix}\mathbf{y}_1(s)\\ \bar{\mathbf{y}}_2(s)\\ \vdots\\ \bar{\mathbf{y}}_\mathbf{T}(s)\end{bmatrix} = \begin{bmatrix}\mathbf{G}_{11}(s) & \mathbf{G}_{12}(s)\\ \mathbf{G}_{21}(s) & \mathbf{G}_{22}(s)\end{bmatrix}\begin{bmatrix}\mathbf{u}_1(s)\\ \bar{\mathbf{u}}_2(s)\\ \vdots\\ \bar{\mathbf{u}}_\mathbf{T}(s)\end{bmatrix} = \begin{bmatrix}\mathbf{G}_{11}(s) & \bar{\mathbf{G}}_{12}(s)\cdots\bar{\mathbf{G}}_{1\mathbf{T}}(s)\\ \bar{\mathbf{G}}_{21}(s) & \bar{\mathbf{G}}_{22}(s)\cdots\bar{\mathbf{G}}_{2\mathbf{T}}(s)\\ \vdots & \vdots\ \ddots\ \vdots\\ \bar{\mathbf{G}}_{\mathbf{T}1}(s) & \bar{\mathbf{G}}_{\mathbf{T}2}(s)\cdots\bar{\mathbf{G}}_{\mathbf{TT}}(s)\end{bmatrix}\begin{bmatrix}\mathbf{u}_1(s)\\ \bar{\mathbf{u}}_2(s)\\ \vdots\\ \bar{\mathbf{u}}_\mathbf{T}(s)\end{bmatrix} \tag{3.31}$$

$$\mathbf{K}(s) = \begin{bmatrix}\mathbf{K}_{11}(s) & \mathbf{0} & \cdots & \mathbf{0}\\ \mathbf{0} & \bar{\mathbf{K}}_{22}(s)\cdots & & \mathbf{0}\\ \vdots & \vdots & \ddots & \vdots\\ \mathbf{0} & \mathbf{0} & \cdots & \bar{\mathbf{K}}_{\mathbf{TT}}(s)\end{bmatrix} = \begin{bmatrix}\mathbf{K}_{11}(s) & \mathbf{0}\\ \mathbf{0} & \mathbf{K}_{22}(s)\end{bmatrix} \tag{3.32}$$

where

$$\mathbf{G}_{12}(s) = [\ \bar{\mathbf{G}}_{12}(s)\cdots\bar{\mathbf{G}}_{1\mathbf{T}}(s)],\ \mathbf{G}_{21}(s) = \begin{bmatrix}\bar{\mathbf{G}}_{21}(s)\\ \vdots\\ \bar{\mathbf{G}}_{\mathbf{T}1}(s)\end{bmatrix},\ \mathbf{G}_{22}(s) = \begin{bmatrix}\bar{\mathbf{G}}_{22}(s) & \cdots & \bar{\mathbf{G}}_{2\mathbf{T}}(s)\\ \vdots & \ddots & \vdots\\ \bar{\mathbf{G}}_{\mathbf{T}2}(s) & \cdots & \bar{\mathbf{G}}_{\mathbf{TT}}(s)\end{bmatrix},$$

$$\mathbf{K}_{22}(s) = \begin{bmatrix}\bar{\mathbf{K}}_{22}(s) & \cdots & \mathbf{0}\\ \vdots & \ddots & \vdots\\ \mathbf{0} & \cdots & \bar{\mathbf{K}}_{\mathbf{TT}}(s)\end{bmatrix}$$

and, $\mathbf{T}$ represents a set of $\mathbf{T}$ non-overlapping square subsystems.

To introduce the proposed approach, consider a decentralized control structure in which the first r_1 outputs $\mathbf{y}_1(s)$ are interconnected with the first r_1 inputs $\mathbf{u}_1(s)$ and the last $(q-r_1)$ outputs $\mathbf{y}_2(s)$ are interconnected with the

last $(q - r_1)$ inputs to $\mathbf{u}_2(s)$. Figure 3.8 illustrated the corresponding block diagram representation.

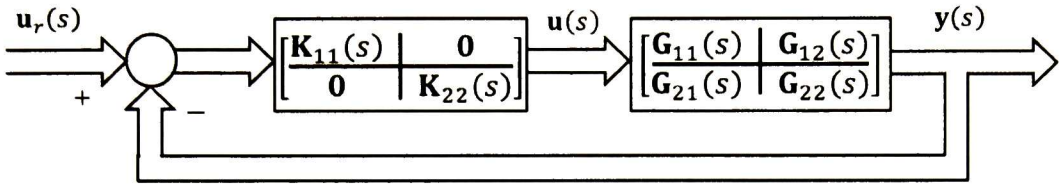

Figure. 3.8. General block decentralized configuration.

Based on this model, it is possible to represent various types of control strategies. These include as particular cases (Refer to Fig. 3.9):

- *Centralized control.* This type of design takes into accounts all the available (i. e. measured) power system signals (Fig. 3.10, with switches $u_{BD11}, \ldots, u_{BD1n}$ closed). In general, this configuration is unsuitable for power systems due to the cost of remote technologies. In the case of a failure of the central supervisor, control is lost over all areas.

- *Fully decentralized control.* This control structure takes into account local signals and uses SISO controllers for each loop of the transfer function (Fig. 3.10, with switches $u_{L1}, \ldots, u_{Lm}$ closed). In general this control strategy is widely used in most system controllers [26-29].

- *Quasi-decentralized control.* This representation uses a combination of local and remote signals (Fig. 3.10, with switches $u_{L1}, \ldots, u_{Lm}$ and u_{Q1} closed). The main characteristic can be a SISO configuration for each local control loop of the transfer function, but most signals used for control are collected and processed locally [30].

- *Block decentralized control structure.* This configuration considers a set of input and output signals from remote locations (SISO or MIMO configuration), in which each WADC is assigned to a specific area or areas (Fig. 3.10, with switches $u_{BD11}, \ldots, u_{BD1n}$ and $u_{BDm1}, \ldots, u_{BDmn}$ closed). A block decentralized control is a control structure that lies between a fully decentralized structure and a fully centralized one [31-35].

- *Hierarchical control.* This configuration consists of two or more levels [36-37, 42]. A two-level control scheme comprehends local

controllers in a first level and a central controller in a second level (Fig. 3.10, with switches $u_{L1}, \ldots, u_{Lm}$ and $u_{BD11}, \ldots, u_{BD1n}$ closed).

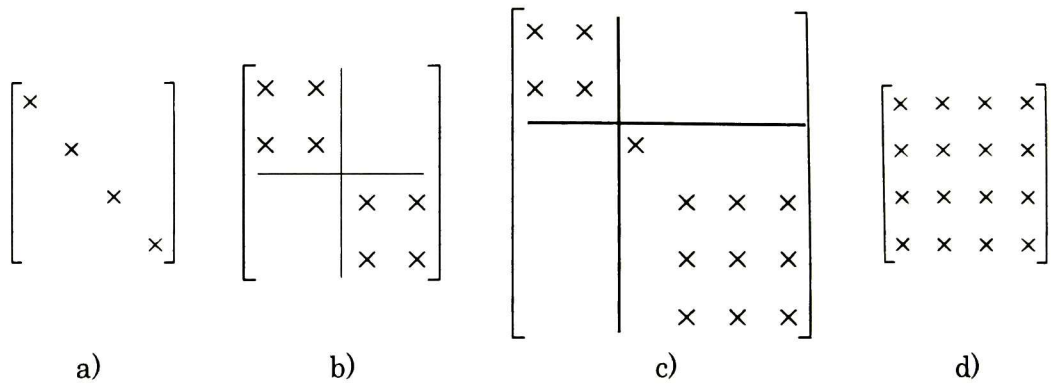

Figure. 3.9. Schematic illustration of control structures: a) fully decentralized control, b) and c) block decentralized control, c) centralized control.

The left-BRG array for the pairing $\mathbf{y}_1(s) - \mathbf{u}_1(s)$ is defined as the ratio of the open block gain to the apparent block gain in the same loop when all other control loops are closed [18],

$$[\boldsymbol{\lambda}(s)]_{11} = \left[\frac{\partial y_1(s)}{\partial u_1(s)}\Big|_{u_2=0}\right] \cdot \left[\frac{\partial y_1(s)}{\partial u_1(s)}\Big|_{y_2=0}\right]^{-1} = \mathbf{G}_{11}(s)[\mathbf{G}^{-1}(s)]_{11} \qquad (3.33)$$

where $\mathbf{y}_1(s) - \mathbf{u}_1(s)$ are related trough the Schur complement of $\mathbf{G}_{22}(s)$ in $\mathbf{G}(s)$,

$$[\mathbf{G}^{-1}(s)]_{11} = [\mathbf{G}_{11}(s) - \mathbf{G}_{12}(s)\mathbf{G}_{22}^{-1}(s)\mathbf{G}_{21}(s)]^{-1}$$

From the above equation, the uncontrolled block gain and the controlled block gain of the BRG for the pairing $\mathbf{y}_1(s) - \mathbf{u}_1(s)$ can be described in Fig. 3.11 and 3.12. Note that, in the proposed formulation, the input-output pairings are MIMO channels. This means that the BRG describes the interaction of a MIMO transfer function under a block perfect control in steady state.

It follows readily that the concept of a block perfect control in steady state can be defined by

$$[\mathbf{K}_{11}(s)] = diag\left(\frac{1}{s}\Big|_{s=0} * \begin{bmatrix} 1 & \cdots & 1 \\ \vdots & \cdot & \vdots \\ 1 & \cdots & 1 \end{bmatrix}\right) i = 1, \ldots, q. \qquad (3.34)$$

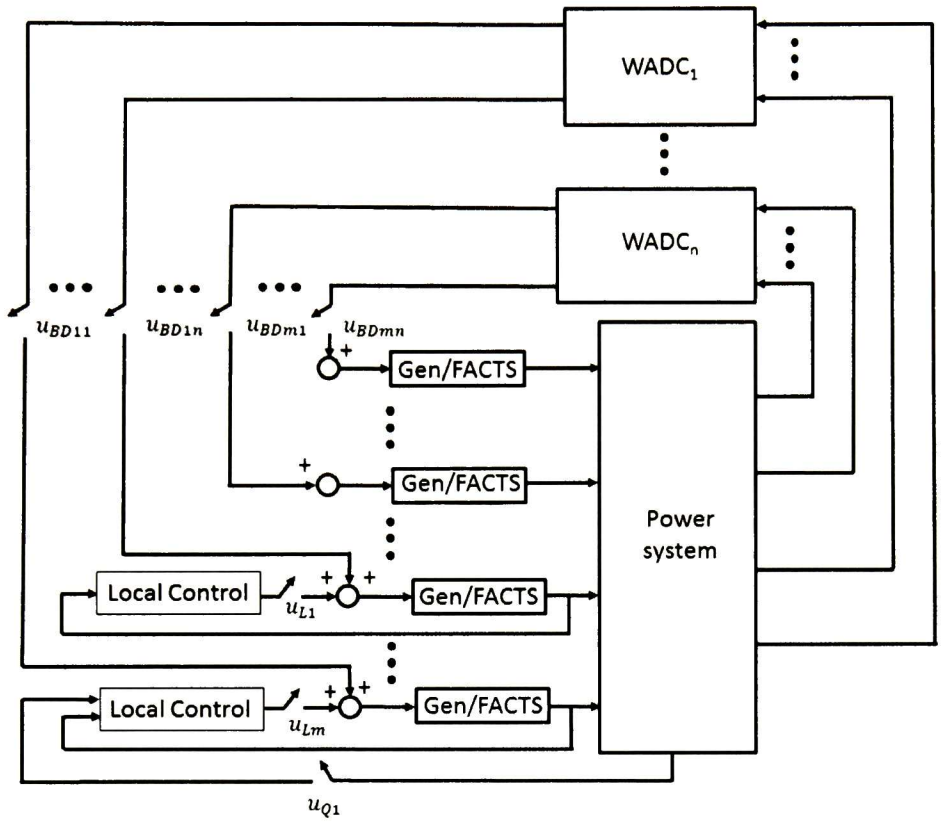

Figure. 3.10. General control structure for power systems.

In a similar manner, the right-BRG can be calculated as $[\boldsymbol{\lambda}(s)]_{11} = [\mathbf{G}^{-1}(s)]_{11}\mathbf{G}_{11}(s)$. Furthermore, $\mathbf{G}(s) \in \mathcal{RH}_\infty^{q\times q}$ can be partitioned into $\mathbf{T}$ diagonal blocks or a set of $\mathbf{T}$ non-overlapping square subsystems such that $\mathbf{G}_{ii}(s) \in \mathcal{RH}_\infty^{r_i\times r_i}, i = 1,2,\ldots,\mathbf{T}$ that gives $\sum_{i=1}^{\mathbf{T}} r_i = q$.

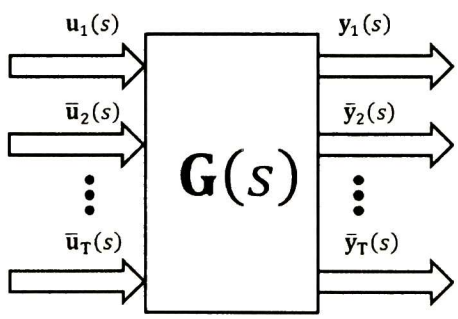

Figure 3.11. Uncontrolled block gain, $\mathbf{G}_{11}(s)$, for $\mathbf{y}_1(s) - \mathbf{u}_1(s)$.

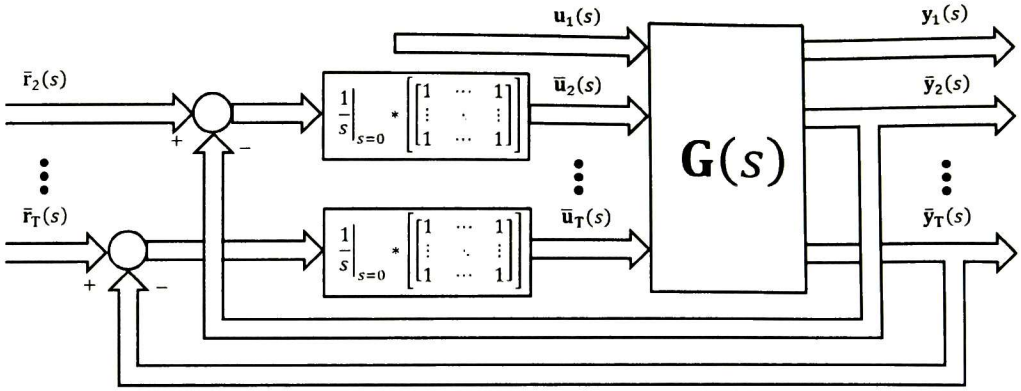

Figure 3.12. Controlled block gain, $[\mathbf{G}^{-1}(s)]_{11}$, for $\mathbf{y}_1(s) - \mathbf{u}_1(s)$.

In general, the transfer function evaluated at $s = j\omega$ is represented as $\mathbf{G}(j\omega)$ or simply $\mathbf{G} \in \mathbb{C}^{q\times q}$. The following properties of the proposed left and right-BRG can be easily verified:

- $[\boldsymbol{\lambda}]_{ii}$ is independent of scaling of $[\boldsymbol{\lambda}]_{jj}$, for all $i, j = 1,2,\ldots,\mathbf{T}, j \neq i$.
- The individual elements of the BRG are defined by β_{ii}. For diagonal elements of $[\boldsymbol{\lambda}]_{11}$, $\beta_{ii} = \sum_{k=1}^{r} \lambda_{ik}^2$. In addition, β_{ii} are independent of scaling.
- Consider the scaled matrix $\mathbf{G}^s = \mathbf{S}_1\mathbf{G}\mathbf{S}_2$, where $\mathbf{S}_1$ and $\mathbf{S}_2$ are real, diagonal input and output scaling matrices, respectively, and assume that they are partitioned as follows

$$\mathbf{S}_1 = \begin{bmatrix} \mathbf{S}_{11} & 0 \\ 0 & \mathbf{S}_{12} \end{bmatrix}, \mathbf{S}_2 = \begin{bmatrix} \mathbf{S}_{21} & 0 \\ 0 & \mathbf{S}_{22} \end{bmatrix}$$

  with $\mathbf{S}_{11}$, $\mathbf{S}_{21} \in \mathbb{C}^{r_1\times r_1}$ and $\mathbf{S}_{12}$, $\mathbf{S}_{22} \in \mathbb{C}^{(q-r_1)\times(q-r_1)}$. As a consequence, $[\boldsymbol{\lambda}^s]_{11} = \mathbf{S}_{11}[\boldsymbol{\lambda}]_{11}\mathbf{S}_{11}^{-1}$

- β_{ij}^s is independent of input scaling, but dependent on output scaling.
- If $\mathbf{G}$ is non-singular by assumption, $\mathbf{G}^{-1}$ and thus $[\mathbf{G}^{-1}]_{ii}$ exists. Thus, $[\boldsymbol{\lambda}]_{ii}$ exists, but is rank deficient due to rank deficiency of $\mathbf{G}_{ii}$.
- If $\mathbf{G}$ is block triangular implies that the corresponding $[\boldsymbol{\lambda}]_{ii} = \mathbf{I}_{r_i}$ for all $i = 1,2,\ldots,\mathbf{T}$.
- If $[\boldsymbol{\lambda}]_{ii} = \mathbf{I}_{r_i}$ for all $i = 1,2,\ldots,\mathbf{T}$ does not imply that $\mathbf{G}$ is block triangular.
- If one of the pairs, $\{\mathbf{G}_{12}, \mathbf{G}_{22}^{-1}\mathbf{G}_{21}\mathbf{G}_{11}^{-1}\}$ and $\{\mathbf{G}_{12}\mathbf{G}_{22}^{-1}, \mathbf{G}_{21}\mathbf{G}_{11}^{-1}\}$ lie in the null space of each other then $[\boldsymbol{\lambda}]_{11} = \mathbf{I}_{r_1}$. Similarly, if one of the pairs,

$\{\mathbf{G}_{21}, \mathbf{G}_{11}^{-1}\mathbf{G}_{12}\mathbf{G}_{22}^{-1}\}$ and $\{\mathbf{G}_{21}\mathbf{G}_{11}^{-1}, \mathbf{G}_{12}\mathbf{G}_{22}^{-1}\}$ lie in the null space of each other, $[\boldsymbol{\lambda}]_{22} = \mathbf{I}_{r_2}$.

It is well known that the gain of a multivariable system depends on the input direction. Then, the gain of $\mathbf{y}_1 - \mathbf{u}_1$ in the direction of $\mathbf{v}$ be $\|\mathbf{G}_{11}\mathbf{v}\|_2$, $\|\mathbf{v}\|_2 = 1$. Similarly, the gain of this loop in the direction of $\mathbf{w}$, when all other loops are closed be $\|[\mathbf{G}^{-1}]_{11}\mathbf{w}\|_2$, $\|\mathbf{w}\|_2 = 1$.

Proposition 3.1 [20]. The worst case gain mismatch between $\mathbf{G}_{11}$ and $[\mathbf{G}]_{11}$ is bounded as follows,

$$\bar{\sigma}[\boldsymbol{\lambda}]_{11} \leq \max_{\substack{\|\mathbf{v}\|_2=1 \\ \|\mathbf{w}\|_2=1}} \frac{\|\mathbf{G}_{11}\mathbf{v}\|_2}{\|[\mathbf{G}]_{11}\mathbf{w}\|_2} \tag{3.35}$$

$$\frac{1}{\underline{\sigma}[\boldsymbol{\lambda}]_{11}} \leq \max_{\substack{\|\mathbf{v}\|_2=1 \\ \|\mathbf{w}\|_2=1}} \frac{\|[\mathbf{G}]_{11}\mathbf{w}\|_2}{\|\mathbf{G}_{11}\mathbf{v}\|_2} \tag{3.36}$$

where $\bar{\sigma}$ and $\underline{\sigma}$ represent the largest and smallest singular value of $[\boldsymbol{\lambda}_B]_{11}$.

The above proposition means that if the conditions $\bar{\sigma}[\boldsymbol{\lambda}]_{11} \gg 1$ and $\underline{\sigma}[\boldsymbol{\lambda}]_{11} \ll 1$ are met, then the gain of $\mathbf{y}_1 - \mathbf{u}_1$ changes considerably due to the closure of all other loops. If $\bar{\sigma}[\boldsymbol{\lambda}]_{11} \approx 1$ and $\underline{\sigma}[\boldsymbol{\lambda}]_{11} \approx 1$, the change in gain may still be large. In general, if the largest singular value of BRG is far from the identity matrix, the system has large interactions, but the converse is not true. Note from Eq. (3.33) that if $[\boldsymbol{\lambda}]_{11} \in \mathbb{C}^{1\times 1}$ then the BRG is the scalar representation of the RGA.

The BRG analysis evidences the same limitations of closed-loop that the standard RGA analysis due to the perfect control [13]; these limitations make necessary to evaluate the interaction of the closed-loop transfer function using the information of each dynamic block decentralized controller as discussed below. In the literature the block GDRG is sometimes called *the dynamic BRG* [22-24]. Unfortunaly, this definition should be used for $[\boldsymbol{\lambda}(s)]_{11}$ at $s = j\omega$ due to the integral block feedback. In general, this dessertation proposes the use of the block GDRG to design WADCs in power systems.

3.6 Proposed block GDRG method for control configuration selection

Consider the input-ouput $\mathbf{y}_1(s) - \mathbf{u}_1(s)$ pair shown in Fig. 3.13. Then, from equation (3.5) with block controllers

$$\mathbf{H}^1(s) = [[\mathbf{I} + \mathbf{G}(s)\mathbf{K}^1(s)]^{-1}\mathbf{G}(s)\mathbf{K}^1(s)]$$

and using the Shur complement, the controlled block gain for $\mathbf{y}_1(s) - \mathbf{u}_1(s)$ is given by

$$\left[\widetilde{\mathbf{G}}(s)\right]_{11} = \mathbf{G}_{11}(s) - \mathbf{G}_{12}(s)\mathbf{K}_{22}(s)\left(\mathbf{I} + \mathbf{G}_{22}(s)\mathbf{K}_{22}(s)\right)^{-1}\mathbf{G}_{21}(s)$$

Hence, the right-block GDRG for $\mathbf{y}_1 - \mathbf{u}_1$ can be expressed as:

$$\left[\tilde{\boldsymbol{\lambda}}(s)\right]_{11} = \left[\left.\frac{\partial y_1(s)}{\partial u_1(s)}\right|_{u_2=0}\right]\left[\left.\frac{\partial y_1(s)}{\partial u_1(s)}\right|_{y_2=0}\right]^{-1} = \mathbf{G}_{11}(s)\left[\widetilde{\mathbf{G}}^{-1}(s)\right]_{11} \tag{3.37}$$

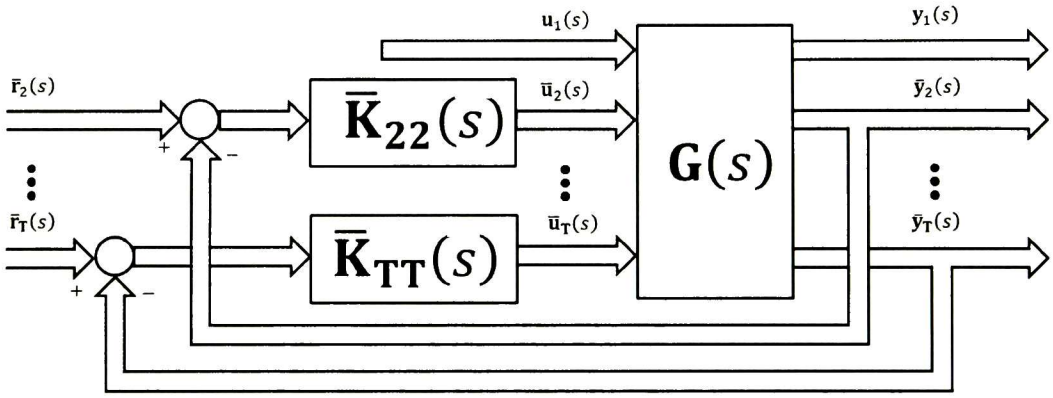

Figure 3.13. Controlled block gain, $\left[\widetilde{\mathbf{G}}(s)\right]_{11}$, for $\mathbf{y}_1(s) - \mathbf{u}_1(s)$.

Consider now the following proposition:

Proposition 3.2. The worst case gain mismatch between $\mathbf{G}_{11}$ and $\left[\widetilde{\mathbf{G}}\right]_{11}$ is bounded as follows,

$$\bar{\sigma}\left[\tilde{\boldsymbol{\lambda}}\right]_{11} \leq \max_{\substack{\|\mathbf{v}\|_2=1 \\ \|\mathbf{w}\|_2=1}} \frac{\|\mathbf{G}_{11}\mathbf{v}\|_2}{\left\|\left[\widetilde{\mathbf{G}}\right]_{11}\mathbf{w}\right\|_2} \tag{3.38}$$

$$\frac{1}{\underline{\sigma}\left[\tilde{\boldsymbol{\lambda}}\right]_{11}} \leq \max_{\substack{\|\mathbf{v}\|_2=1 \\ \|\mathbf{w}\|_2=1}} \frac{\left\|\left[\widetilde{\mathbf{G}}\right]_{11}\mathbf{w}\right\|_2}{\|\mathbf{G}_{11}\mathbf{v}\|_2} \tag{3.39}$$

Proof: From (3.38), using (3.39)

$$\max_{\substack{\|\mathbf{v}\|_2=1 \\ \|\mathbf{w}\|_2=1}} \frac{\|\mathbf{G}_{11}\mathbf{v}\|_2}{\left\|\left[\widetilde{\mathbf{G}}\right]_{11}\mathbf{w}\right\|_2} = \bar{\sigma}[\mathbf{G}_{11}]\bar{\sigma}\left[\left[\widetilde{\mathbf{G}}^{-1}(s)\right]_{11}\right] \geq \bar{\sigma}\left[\tilde{\boldsymbol{\lambda}}(s)\right]_{11}$$

It follows from the above proposition that the system is weakly interacting, if $\overline{\sigma}[\tilde{\boldsymbol{\lambda}}]_{11}$ and $\underline{\sigma}[\tilde{\boldsymbol{\lambda}}]_{11}$, are close to the identity matrix.

The use of the RGA analysis for power systems in previus researches have suggested that if the interaction among control loops is strong, the generators of the system would have a large participation in the overall process interaction. On the other hand, if the interaction is not different from the identity matrix, the feedback system could not guarantee a good performance [27, 43]. Similar conclusions can be made for the BRG and the block GDRG.

In what follows, the BRG is defined for non-square block decentralized controllers and its application to select the most suitable control configuration is discussed.

3.7 Interaction measures for non-square systems

For square systems, the closed-loop gain is defined as the gain between y_i and u_i when all other outputs are under perfect control, i.e. y_k are held constant for all $k \neq i$. Generally, it is not possible to keep all other outputs, y_k, under perfect control at all time if $\mathbf{G}(s)$ contains dead-time and/or RHP zeros. In addition, interaction measures applicable to non-square block decentralized controllers emerge as a necessity of geographic, physic and cost limitations of the power system. This section presents analysis tools to generalize the concept of interaction and computational algorithms for decentralized controllers.

Assume a non-square system with more outputs than inputs ($q > p$); as a result, it is not possible to keep all outputs at their set points. Therefore, the sense of perfect control in the definition of the closed-loop gain should be modified. A controller $\mathbf{K}$ is designed such that the steady-state offsets are minimized in the sense of least-square. In general, for a non-square system, $\mathbf{G}$, the non-square relative gain (NRG) is defined as [38]:

$$\lambda_{ij}^{N}(s) = \frac{\left[\frac{\partial y_i(s)}{\partial u_j(s)}\right]_{u_k, k\neq j}}{\left[\frac{\partial y_i(s)}{\partial u_j(s)}\right]_{y_k, k\neq i}} = g_{ij}(s)g_{ji}^{+}(s)$$

Thus, the non-square relative gain array at $s = j\omega$ is described as

$$\boldsymbol{\Lambda}^{N}(j\omega) = \mathbf{G}(j\omega) \odot [\mathbf{G}^{+}(j\omega)]^{*} \tag{3.40}$$

where + represents the Moore-Penrose pseudo-inverse and $*$ the Hermitian. The next theorem clarifies the use of these concepts.

Theorem 3.1 [39]. Let $\mathbf{A} \in \mathbb{C}^{m\times n}$

- If $\mathbf{A} \in \mathbb{C}_m^{m\times n}$, then $\mathbf{A}^+ = \mathbf{A}^H(\mathbf{A}\mathbf{A}^H)^{-1}$ and $\mathbf{A}\mathbf{A}^+ = \mathbf{I}$.
- If $\mathbf{A} \in \mathbb{C}_n^{m\times n}$, then $\mathbf{A}^+ = (\mathbf{A}\mathbf{A}^H)^{-1}\mathbf{A}^H$ and $\mathbf{A}^+\mathbf{A} = \mathbf{I}$.

The fundamental differences between the RGA and NRG are described by the next properties

- The sum of the elements in each column of the NRG is always equal to unity.
- The sum of the elements in each row of the NRG falls between zero and unity.

The above properties suggest that it is not possible to keep all outputs perfect for a non-square system, the row sum of the NRG being less than unity seems to indicate the deviation from perfect control for each output. In addition, similar to the RGA, the NRG is invariant under input scaling. Nevertheless, the NRG is variant under output scaling and it is important to express mathematically that if $\mathbf{G}(j\omega)$ is a square, then $\mathbf{\Lambda}^N(j\omega) = \mathbf{\Lambda}(j\omega)$.

Consider the open loop transfer function matrix of a non-square plant, $\mathbf{G}(s) \in \mathcal{RH}_\infty^{p\times q}$ with the partition developed in (3.29) and $\mathbf{G}_{11}(s) \in \mathcal{RH}_\infty^{p_1\times q_1}$ $\mathbf{G}_{12}(s) \in \mathcal{RH}_\infty^{p_1\times q_2}$, $\mathbf{G}_{21}(s) \in \mathcal{RH}_\infty^{p_2\times q_1}$ and $\mathbf{G}_{22}(s) \in \mathcal{RH}_\infty^{p_2\times p_2}$ This type of partition suggest two cases:

- If $\mathbf{G}(s)$ has more outputs than inputs, then its diagonal blocks must either be square or have more outputs than inputs.
- If $\mathbf{G}(s)$ has more inputs that outputs, its diagonal blocks must have the number of inputs greater than or equal to the number of outputs.

The following expression will be written to define a general equation of the BRG for non-squares systems [40]:

$$[\boldsymbol{\lambda}(s)]_{11} = \left[\frac{\partial y_1(s)}{\partial u_1(s)}\bigg|_{u_2=0}\right] \cdot \left[\frac{\partial y_1(s)}{\partial u_1(s)}\bigg|_{y_2=0}\right]^+ = \mathbf{G}_{11}(s)[\mathbf{G}^+(s)]_{11} \qquad (3.41)$$

where

$$\left[\left.\frac{\partial y_1(s)}{\partial u_1(s)}\right|_{u_2=0}\right] = \mathbf{G}_{11}(s)$$

$$\left[\left.\frac{\partial y_1(s)}{\partial u_1(s)}\right|_{y_2=0}\right]^{+} = [\mathbf{G}^{+}(s)]_{11} = [\mathbf{G}_{11}(s) - \mathbf{G}_{12}(s)[\mathbf{G}_{22}(s)]^{+}\mathbf{G}_{21}(s)]^{+}$$

Note that equation (3.41) reduces to (3.33) when the system is square. Therefore, for a system with more outputs than inputs $\mathbf{G}_{11} \in \mathbb{C}_{q_1}^{p_1 \times q_1}$ where q_1 denotes the rank of a complex matrix $p_1 \times q_1$, then $rank\ [\boldsymbol{\lambda}]_{11} = r$.

In general the following properties hold:

- The desired value for the BRG for non-square systems using the SVD will be 1.0 because the ideal BRG is the identity matrix. This can be expressed as $\bar{\sigma}[\boldsymbol{\lambda}]_{11} = 1$.
- The desired value for the diagonal elements and eigenvalues of the $[\boldsymbol{\lambda}^{-1}]_{11}$ for $\mathbf{G}_{11} \in \mathbb{C}_{p_1}^{p_1 \times q_1}$ will be 1.0 because the ideal $[\boldsymbol{\lambda}^{-1}]_{11} = \mathbf{I}$.
- For $\mathbf{G}_{11} \in \mathbb{C}_{q_1}^{p_1 \times q_1}$ the ideal $[\boldsymbol{\lambda}^{-1}]_{11}$ will be $\mathbf{G}_{11}(s)[\mathbf{G}^{+}(s)]_{11}$. Nevertheless the inverse BRG will always be singular. This means that $\mathbf{G}_{11}(s)[\mathbf{G}^{+}(s)]_{11}$ will only have eigenvalues of 0 and 1.0.

Finally, the block GDRG for non-square decentralized control structures is given by

$$\left[\tilde{\boldsymbol{\lambda}}(s)\right]_{11} = \left[\left.\frac{\partial y_1(s)}{\partial u_1(s)}\right|_{u_2=0}\right]\left[\left.\frac{\partial y_1(s)}{\partial u_1(s)}\right|_{y_2=0}\right]^{+} = \mathbf{G}_{11}(s)\left[\widetilde{\mathbf{G}}^{+}(s)\right]_{11} \tag{3.42}$$

where

$$\left[\widetilde{\mathbf{G}}^{+}(s)\right]_{11} = [\mathbf{H}^{1}(s)]^{+} = \left[\mathbf{G}_{11}(s) - \mathbf{G}_{12}(s)\mathbf{K}_{22}(s)\left(\mathbf{I} + \mathbf{G}_{22}(s)\mathbf{K}_{22}(s)\right)^{-1}\mathbf{G}_{21}(s)\right]^{+}$$

3.8 μ interaction measure

A key objective of an interaction measure should be to indicate under what conditions the stability of the diagonal blocks will guarantee that of the complete system [14]. Based on this idea, this section gives essential conditions to extend the μ interaction to the skewed μ interaction.

Consider the control system shown in Fig. 3.1 for the $q \times q$ plant, $\mathbf{G}(s)$, can be approximated by block-diagonal plant, $\widetilde{\mathbf{G}}(s)$, if the off-diagonal blocks are sufficiently small. Furthermore, it is that for sufficiently close plants, $\mathbf{G}(s)$

and $\tilde{\mathbf{G}}(s)$, a block-diagonal controller, $\mathbf{K}(s)$, can be designed to make the feedback loop around $\tilde{\mathbf{G}}(s)$ stable with the assurance that the feedback loop around $\mathbf{G}(s)$ will be stable as well. For this case, Fig. 3.14 represents the control system modified including $\tilde{\mathbf{G}}(s)$.

Then, the problem is to design a controller $\mathbf{K}(s)$, for the system $\tilde{\mathbf{G}}(s)$ such that the block-diagonal, the closed-loop system with the transfer matrix function

$$\tilde{\mathbf{H}}(s) = \left[\mathbf{I} + \tilde{\mathbf{G}}(s)\mathbf{K}(s)\right]^{-1}\tilde{\mathbf{G}}(s)\mathbf{K}(s) \tag{3.43}$$

is stable in $\xi = 0$. An interaction measure expresses the constraints imposed on the choice of the closed-loop transfer matrix, $\tilde{\mathbf{H}}(s)$, for the block-diagonal system which guarantees that the closed-loop system $\mathbf{H}(s)$ is stable in $\xi = 1$. It is necessary to define the following equation:

$$\mathbf{E}(s) = \left[\mathbf{G}(s) - \tilde{\mathbf{G}}(s)\right]\left[\tilde{\mathbf{G}}(s)\right]^{-1} \tag{3.44}$$

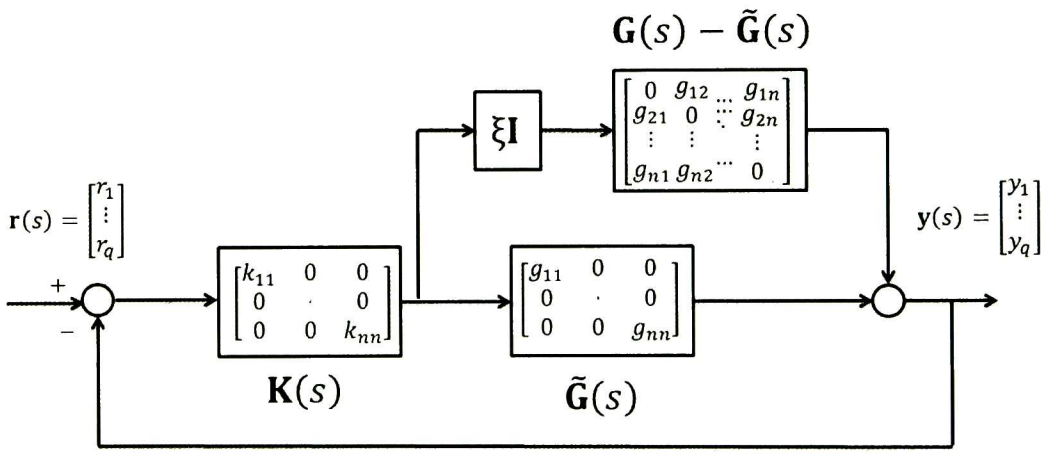

Fig. 3.14. Block representation of interactions as additive uncertainty.

Theorem 3.2 [15]. Assume that $\mathbf{G}(s)$ and $\tilde{\mathbf{H}}(s)$ are stable. Then the closed-loop system, $\mathbf{H}(s)$, is stable if and only if

$$N\left[0, \det\left[\mathbf{I} + \mathbf{E}(s)\tilde{\mathbf{H}}(s)\right]\right] = 0 \tag{3.45}$$

where $N[k, v(s)]$ denotes the net number of clockwise encirclements of the point $[k, 0]$ by the image of the Nyquist $\mathcal{D}$ contour under $v(s)$.

Equation (3.45) denotes the importance of the matrix $\mathbf{E}(s)$. This leads to next theorem that defines an interaction measure.

Theorem 3.3 [11]. Assume $\mathbf{G}(s)$ and $\widetilde{\mathbf{H}}(s)$ are stable. Then $\mathbf{H}(s)$ is stable if

$$\left\|\widetilde{\mathbf{H}}(j\omega)\right\| < \inf_{\mathbf{D}\in\mathbf{D}} \|\mathbf{D}\mathbf{E}(j\omega)\mathbf{D}^{-1}\| \,\forall\omega \tag{3.46}$$

The next expression is derived from theorem 3.3

$$\mu[\mathbf{E}(j\omega)] \leq \inf_{\mathbf{D}\in\mathbf{D}} \bar{\sigma}[\mathbf{D}\mathbf{E}(j\omega)\mathbf{D}^{-1}] \tag{3.47}$$

Note that μ is the complex structured singular value and $\mathbf{D} \in \mathrm{D}$ is the set of all regional matrices with same block-diagonal structure as $\widetilde{\mathbf{G}}(s)\widetilde{\mathbf{H}}(s)$. However, the limitation associated with the result of the last theorem is that μ gives equal preference to all the loops, but this can be modified using the skew SSV. Then, this dissertation proposes the use of the skew SSV to evaluate the interaction of the linear systems.

For a system **M**, with a set of perturbations, the definition of skew μ is the smallest SSV of a subset of perturbations that destabilizes the system **M** with the remainder of the perturbation being of fixed range [18-19].

Given a set of allowable perturbations,

$$\mathbf{Y}_{\mathbf{M}} = \left\{ \begin{matrix} \boldsymbol{\Delta}_v = diag\left[\delta_1^r \mathbf{I}_{k_1}, \ldots, \delta_{S_r}^r \mathbf{I}_{k_{S_r}}, \delta_1^c \mathbf{I}_{k_1}, \ldots, \delta_{S_c}^c \mathbf{I}_{r_{S_c}}, \boldsymbol{\Delta}_{m_1}^C, \ldots, \boldsymbol{\Delta}_{m_F}^C\right] \\ : \delta_i^r \in \mathbb{R}, \delta_j^c \in \mathbb{C}, \boldsymbol{\Delta}_{m_l}^C \in \mathbb{C}^{m_l \times m_l} \end{matrix} \right\} \tag{3.48}$$

and a secondary set of perturbations with structure **M** defined by

$$\mathbf{Z}_{\bar{\mathbf{M}}} = \left\{ \begin{matrix} \boldsymbol{\Delta}_f = diag\left[\delta_1^r \mathbf{I}_{k_1}, \ldots, \delta_{S_r}^r \mathbf{I}_{k_{S_r}}, \delta_1^c \mathbf{I}_{k_1}, \ldots, \delta_{S_c}^c \mathbf{I}_{r_{S_c}}, \boldsymbol{\Delta}_{m_1}^C, \ldots, \boldsymbol{\Delta}_{m_F}^C\right] \\ : \delta_i^r \in \mathbb{R}, \delta_j^c \in \mathbb{C}, \boldsymbol{\Delta}_{m_l}^C \in \mathbb{C}^{m_l \times m_l} \end{matrix} \right\} \tag{3.49}$$

where $\mathbf{Z}_{\bar{\mathbf{M}}}$ is restricted to the unit ball

$$B\mathbf{Z}_{\bar{\mathbf{M}}} = \{\boldsymbol{\Delta}_f \in \mathbf{Z}_{\bar{\mathbf{M}}} : \bar{\sigma}[\boldsymbol{\Delta}_f \leq 1]\}$$

The composite perturbations are defined as

$$\mathbf{W}_{\mathbf{M},\bar{\mathbf{M}}} = \{\boldsymbol{\Delta} = diag[\boldsymbol{\Delta}_f, \boldsymbol{\Delta}_v]\}$$

or

$$\boldsymbol{\Delta} = \begin{bmatrix} \boldsymbol{\Delta}_f & \mathbf{0} \\ \mathbf{0} & \boldsymbol{\Delta}_v \end{bmatrix}$$

Note that $\mathbf{Y_M}$ and $\mathbf{Z_{\bar{M}}}$ define a mixed uncertainty. Furthermore, the last specifications allow the skewed SSV definition:

Definition 3.2 [39]. The skewed SSV $\mu_s[\mathbf{M}]$ of a matrix $\mathbf{M} \in \mathbb{C}^{n\times n}$ with respect to a block structure $\boldsymbol{\Delta} \in \mathbf{W_{M,\bar{M}}}$ is defined as:

$$\mu_s[\mathbf{M}] = \frac{1}{\min\limits_{\boldsymbol{\Delta}\in\mathbf{W_{M,\bar{M}}}} \{\bar{\sigma}\,[\boldsymbol{\Delta}_v] \,|\, \det[\mathbf{I}+\mathbf{M}\boldsymbol{\Delta}]=0\}} \tag{3.50}$$

with $\mu_s[\mathbf{M}] = 0$ if no $\boldsymbol{\Delta} \in \mathbf{W_{M,\bar{M}}}$ solves $\det[\mathbf{I} + \mathbf{M}\boldsymbol{\Delta}] = 0$.

Details of the interaction measure based on the skewed SSV are ommited, but it is only necessary to change $\mathbf{E}(s)$ into a set fixed range of perturbations described by equations (3.48) and (3.49).

3.9 Geometric measures of modal controllability and observability

From equation (3.1), let the eigenvalues of the matrix $\mathbf{A}$ $(i = 1, \ldots, n)$ be distinct and let the corresponding matrices of the right and the left eigenvectors be written as $\mathbf{E} = [\mathbf{e}_1, \ldots, \mathbf{e}_n]$ and $\mathbf{F} = [\mathbf{f}_1, \ldots, \mathbf{f}_n]$, respectively; the eigenvectors $\mathbf{e}_i$ and $\mathbf{f}_i$ are assumed to be normalized and orthogonal.

Geometric measures of controllability, m_{ci}, and observability, m_{oi}, associated with the i-mode are defined as [44]:

$$m_{ci}(k) = \cos\left(\alpha(\mathbf{f}_i, \mathbf{b}_k)\right) = \frac{|\mathbf{b}_k^T \mathbf{f}_i|}{\|\mathbf{f}_i\|\|\mathbf{b}_k\|} \tag{3.51}$$

$$m_{oi}(l) = \cos\left(\theta(\mathbf{c}_l^T, \mathbf{e}_i)\right) = \frac{|\mathbf{c}_l \mathbf{e}_i|}{\|\mathbf{e}_i\|\|\mathbf{c}_l\|} \tag{3.52}$$

where $\mathbf{b}_k$ and $\mathbf{c}_l^T$ represent the kth column of $\mathbf{B}$ and the lth row of $\mathbf{C}$, respectively. $|\mathbf{z}|$ and $\|\mathbf{z}\|$ are the modulus and Euclidean norm of $\mathbf{z}$. Finally, $\alpha(\mathbf{f}_i, \mathbf{b}_k)$ and $\theta(\mathbf{c}_l^T, \mathbf{e}_i)$ represent the geometrical angle between the input vector i and the kth left eigenvector, and the geometrical angle between the output vector j and the kth right eigenvector, respectively. These expressions lead to the joint controllability/observability measures

$$m_{coi}(k, l) = m_{ci}(k) m_{oi}(l) \tag{3.53}$$

3.10 Selection of the most suitable input-output pairings for MIMO systems

The notion of interaction measures has been used for some time in designing and locating power system controllers [43, 45]. In [27], a decentralized method to mitigate adverse interaction between controllers and electromechanical oscillations based on the notion of a dynamic RGA was proposed. More recently, the RGA in [28, 29] was used to evaluate the capability, control structure and the bifurcation subsystems of a μ-synthesis power system stabilizer design. References [31, 32] examine the use of various analytical methods to select signals for FACTS devices and locate controllers.

A more recent and interesting development, has the use of DRGA-based techniques to obtain suitable inputs for FACTS and high-voltage direct current (HVDC) devices in wide-area control schemes [33]. In most cases, the selection of the input-output variables for the design of WADCs has been based on single-input single-output models.

Unfortunaly, all these methods only have described SISO configurations of the supplementary devices in power systems. Nevertheless, WAMS technology gives the opportunity to design WADCs which could have MIMO signals. Then, this section concludes with an original method to select the most suitable input-output pairings for MIMO control configurations in power systems. This method can be described as follows:

1. On the basis of small-signal stability analysis identify suitable input-output signals pairings using the geometric measures of controllability m_{ci} and observability m_{oi} associated with the mode "i" described by (3.51) and (3.52). For the purposes tie-line currents, I_{i-j}, and the speed deviations of generators, ω_i, can be selected, but it is possible to include other type of signals as active power, voltage angle difference, etc.

2. Based on the candidate sets information in 1, compute the largest singular value of $[\lambda(s)]_{ii}$ using Eq. (3.41) for the selected input-output pairing sets of WADCs. This ensures a better coordination among controllers. To obtain a good performance among controls, select the last two set of controllers that exhibit maximum interaction using the properties of the BRG. It should be emphasized, however, that the BRG does not represent the true interaction and it is necessary to compute and compare the closed loop interaction using the block GDRG described in equations (3.37) and (3.42).

3. Design a supplementary MIMO controller to compute the block GDRG and evaluate the closed-loop interaction of the two selected candidate sets of controllers using (14); choose the candidate set with maximum interaction since this results in good performance. If it is necessary to add another set of controllers, then, absorb each designed set into the nominal linear system to avoid re-tuning of controllers. In general, it is necessary to return to step-1.

3.11 Conclusions

In this chapter, the theory of interaction measures to choose input-output pairings in frequency domain for large power systems has been introduced. Extensions and generalizations to the existing theory to design WADCs in power systems based on the notion of the BRG have been proposed and proved to be more efficient than current design methodologies. Following these ideas, a rigorous review of interaction measures that leads to new concepts that still remain to be analyzed in a deeper way in power systems has been presented.

Of note, the issue of control desing was omitted. This stage is crucial to compute the block GDRG. The following chapter examines the use of control techiques in the context of power system applications.

3.12 References

[1] E. H. Bristol, "On a new measure of interaction for multivariable process control," *IEEE Trans. Automat. Contr.*, vol. 11, pp. 133-134, Jan. 1966.

[2] S. Skogestad, and I. Postlethwaite, *Multivariable feedback control: analysis and design*, John Wiley and Sons, 1996, ISBN 0-471-94277-4.

[3] S. Skogestad, and M. Morari, "Implications of large RGA elements on control performance, *Ind. Eng. Chem. Res.*, vol. 26, pp. 2323-2330, Nov. 1987.

[4] P. J. Campo, and M. Morari, "Achievable closed-loop properties of systems under decentralized control: Conditions involving the steady state gain," *IEEE Trans. Automatic Control*, vol. 39, no. 5, pp. 932-943, 1994.

[5] E. H. Bristol, "RGA 1977: Dynamic effects of interaction," *in Proc. 16th Conf. Decision and Contr.*, New Orleans, Louisiana, pp. 1096-1100, Dec. 1977.

[6] Z-X. Zhu, "Variable pairing selection based on individual and overall interaction measures," *Ind. Eng. Chem. Res.*, vol. 35, pp. 4091-4099, 1996.

[7] Z-X Zhu, "Structural analysis and stability conditions of decentralized control systems, *Ind. Eng. Chem. Res.*, vol. 35, pp. 736-745., 1996.

[8] H.-P. Huang, M. Ohshima and L. Hashimoto, "Dynamic interaction and multiloop control system design," *J. Proc. Cont.*, vol. 4, pp. 15-27, 1994.

[9] M. Van de Wal, and B. De Jaber, "A review of methods for input/ouput selection," *Automatica,* vol. 37, pp. 487-510, Abr. 2001.

[10] A. Khali-Sedigh, and B. Moaveni, *Control configuration selection for multivariable plants*, Springer-Verlag Berlin Heidelberg, 2009, ISBN 978-3-642-03193-9.

[11] M. Morari, and E. Zafiriou, *Robust Process Control*, Prentice Hall, 1989, ISBN 0-13-782153-0.

[12] H. Lau, J. Alvarez, and K. F. Jensen, "Synthesis of control structures by singular value analysis: Dynamic measure of sensitivity and interaction," *AIChe J.*, vol. 31, pp. 427-439, Mar. 1985.

[13] R. Piette, T. J. Harris, and P. J. Mclellan, "Graphical interpretations of steady-state interaction measures,' *Ind. Eng. Chem. Res.*, vol. 34, pp. 4436-4450, Dec. 1995.

[14] P Grosdidier, and M. Morari, "The μ interaction measure, *Ind. Eng. Chem. Res.*, vol. 26, pp. 1193-1202, Jun. 1987.

[15] P Grosdidier, and M. Morari, "Interaction measures for systems under decentralized control," *Automatica*, vol. 22, pp. 309-319, May. 1986.

[16] G. Ferreres, *A practical approach to robustness analysis with aeronautical applications*, Kluwer Academic Publishers, 1999, ISBN 0-306-46973-1.

[17] G. Ferreres, and V Fromion, "Computation of the robustness margin with the skewed μ tool," Systems and Control Letters, vol. 32, pp. 193-202, Dec. 1997.

[18] V Manousiouthakis, R. Savage, and Y. Arkun, "Synthesis of decentralized process control structures using the concept of block relative gain," *AIChe J.*, vol. 32, pp. 991-1003, Jun. 1986.

[19] C. N. Nett, and V. Manousiouthakis, "Euclidian condition and block relative gain: connections, conjectures, and clarifications,' *IEEE Trans. Autom. Control*, vol. 32, pp. 405-407, May. 1987.

[20] V Kariwala, J. F. Forbes, and E. S. Meadows, "Block relative gain: properties and pairing rules, *Ind. Eng. Chem. Res.*, vol. 42, pp. 4564-4574, Jul. 2003.

[21] J. Chen, "Relations between block relative and euclidian condition number," *IEEE Trans. Autom. Control*, vol. 37, pp. 127-129, Jan. 1992.

[22] A. Yaman, "Dynamic block relative gain and its connection with the performance and stability of decentralized control structures," *Int. J. Control*, vol. 46, pp. 1187-1193, Nov. 1987.

[23] A. Yaman, and V Manousiouthakis, "The dynamic block relative gain and its role in the desing of robust decentralized control, *American control conference*, Seatle, WA, USA, pp. 11-16, Jun. 1986.

[24] A. Yaman, "New concepts in the synthesis of decentralized control structures: block relative gain (BRG), Dynamic block relative gain (DBRG) and relative sensitivity," *American control conference*, Minneapolis, MN, USA, pp. 1331-1336, Jun. 1987.

[25] R. A. Horn, and C. R. Johnson, *Matrix analysis*, Cambridge University Press, 1985, ISBN 0-521-30586-1.

[26] M. Djuvanovic, M. Khammash, and V Vittal, "Sequential synthesis of structured singular value based decentralized controllers, *IEEE Trans. Power Syst.*, vol. 14, pp. 635-641, May. 1999.

[27] A. R. Messina, O. Begovich, J. H. López, E. N. Reyes, "Design of multiple facts controllers for damping inter-area oscillations: a decentralized control approach,' *Electric Power and Energy Systems*, vol. 26, pp. 19-29, Jan. 2004.

[28] M. Yue, and R. A. Schlueter, "μ-synthesis power system stabilizer design using a bifurcation subsystem based methodology," *IEEE Trans. Power Syst.*, vol. 18, pp. 1497-1506, Nov. 2003.

[29] M. Yue, and R. A. Schlueter, "Robust control designs for multiple bifurcations," *IEEE Trans. Power Syst.*, vol. 20, pp. 301-311, Feb. 2005.

[30] B. Chaudhuri, R. Majumder, and B. C. Pal, "Robust damping of multiple swing modes employing global stabilizing signals with a TCSC," *IEEE Trans. Power Syst.*, vol. 19, pp. 499-506, Feb. 2004.

[31] M. M. Farsangi, Y. H. Song, and Kwang Y. Lee, "Choice of FACTS device control inputs for damping interarea oscillations, *IEEE Trans. Power Syst.*, vol. 19, pp. 1135-1143, May. 2004.

[32] M. M. Farsangi, H. Nezamabadi-pour, Y. H. Song, and K. Y. Lee, "Placement of SVCs and selection of stabilizing signals in power systems," *IEEE Trans. Power Syst.*, vol. 22, pp. 1061-1071, Aug. 2007.

[33] Y. Li, C. Rehtanz, S. R. L. Luo, and Y. Cao, "Assessment and choice of input signals for multiple HVDC and FACTS wide-area damping controllers," *IEEE Trans. Power Syst.,* vol. 27, pp. 1969-1977, Nov. 2012.

[34] W. Yao, L. Jiang, J. Wen, Q. H. Wu, and S. Cheng, "Wide-area damping controllers of FACTS devices for inter-area oscillations considering communications time delays," *IEEE Trans. Power Syst.*, vol. 29, pp. 318-329, Jan. 2014.

[35] Y. Zhang, and A. Bose, "Design of wide-area damping controllers for inter-area oscillations," *IEEE Trans. Power Syst.*, vol. 23, pp. 1136-1143, Aug. 2008.

[36] I. Kamwa, R. Grondin, and Y. Hébert, "Wide-area measurements based stabilizing control of large power systems –A decentralized/hierarchical approach," *IEEE Trans. Power Syst.*, vol. 16, pp. 136-153, Feb. 2001.

[37] F. Okuo, L. A. Dessaint, and O. Akhrig, "Power systems stability enhancement using a wide-area signals based hierarchical controller," *IEEE Trans. Power Syst.*, vol. 20, pp. 1465-1477, Aug. 2005.

[38] J. W. Chang, and C. Yu, "The relative gain for non-square multivariable systems," Chemical Eng. Science, vol 45, pp. 1309-1323, 1990.

[39] F. A. Graybill, *Introduction to matrices with applications in statics*, Wadsworth Publishing Co Inc., 1969, ISBN-10 0534367003.

[40] D. E. Reeves, and Y. Arkun, "Interaction measures for Nonsquare decentralized control structure," *AIChE Journal*, vol. 35, pp. 603-613, Apr. 1989.

[41] D. Dotta, A. S. Silva, and I. C. Decker, "Wide-area measurements-based two-level control design considering signal transmission delay," *IEEE Trans. Power Syst.*, vol. 24, pp. 208-216, Feb. 2009.

[42] M. Halton, M. J. Hayes and P Iardanov, "State-space μ-analysis for an experimental drive-by-wire vehicle," *in Proc. 44th Conf. Decision and Contr., and the European Control Conference*, Seville, Spain, pp. 7912-7917, Dec. 2005.

[43] J. V Milanovic, and A. C. S. Duque, "Identification of electromechanical modes and placement of PSSs using relative gain array," *IEEE Trans. Power Syst.*, vol. 19, pp. 410-417, Feb. 2004.

[44] A. Heniche, and I. Kamwa, "Control loops selection to damp inter-area oscillations of electrical networks," *IEEE Trans. Power Syst.*, vol. 17, pp. 378-384, May. 2002.

[45] P. Zhang, A. R. Messina, A. Coonick and B. J. Cory, "Selection of locations and input signals for multiple SVC damping controllers in large power systems," presented at the Proc. 1998 IEEE/Power Eng. Soc. Winter Meeting, Paper IEEE-0-7803-4403-0, pp. 667-670.

Chapter 4
Synthesis of Robust Linear Controllers

This chapter examines the problem of synthesis of robust linear controllers for uncertain MIMO systems. The different synthesis techniques are critically compared in terms of accuracy, applicability to realistic power system models, and computational cost.

The chapter begins with $\mathcal{H}_\infty$ control and mixed $\mathcal{H}_2$ /$\mathcal{H}_\infty$ theory using classic methods and linear matrix inequality (LMI) techniques. Then, the D-K and D-G-K iteration for complex and real uncertainty are introduced and compared. Advantages and limitations are pointed out in the context of this dissertation.

Based on these ideas, a basic control structure to study the effects of latency in power systems is introduced. Finally, a general method to design wide-area damping controller devices and hierarchical control configurations in large power systems is suggested.

4.1 Introduction

The use of the maximum singular value as a norm on unstructured uncertainty overcomes the limitations of classical gain and phase margins in MIMO systems. Oftentimes uncertainty may be highly structured in real systems. Neglecting this effect may lead to very conservative results [1]. Furthermore, the uncertainty can be expressed as complex uncertainty and real uncertainty.

The SSV was introduced to study structured and unstructured uncertainty [2-4]. Complex perturbations are used to represent uncertainties associated with unmodeled dynamics and parametric uncertainties. These representations, however, can be conservative due to the influence of real parametric perturbations and scaling matrices to approximate the complex SSV.

The use of the D-K iteration has been considered and implemented in several researches in recent years to design robust controllers for complex uncertainties [5-9]. In addition, the complex uncertainty in D-K iteration is taken as complex uncertainty, even with real parametric uncertainties, rendering the standard complex D-K synthesis technique inadequate. This approach, referred to as μ-synthesis with D-K iteration attempts to find a μ-optimal controller, but during the synthesis process it is possible that some requirements as $\mathcal{H}_\infty$ are not met, and the method may not be convergent due to real parametric uncertainties.

For models which incorporate real parametric uncertainties the D-G-K iteration was developed as a consequence of the mixed SSV [10-11]. Unfortunately, the computational burden is increased and analytical expressions are more complex. The similarities between D-K and D-G-K iteration are obvious. However, there is one notable difference: the determination of scaling matrices; in particular the fitting of scaling matrices that forces to fit the phase and magnitude. Furthermore, the D-G-K iteration needs inner-outer and spectral factorizations [12-13].

Some researchers have also considered rearranging the D-G-K iteration; the method proposed was the μ-K iteration, which lost some of the guaranteed convergence properties of D-G-K iteration, but with good results [14-16]. Essentially, the μ-K iteration only requires that scaling matrices are fitted in magnitude and uses a scalar transfer function to compensate the real uncertainty which is not considered in the D-K iteration. An alternative methodology to design controllers is the use of LMI techniques [20]. These techniques may be difficult to analyze, in particular when incorporated into larger feedback systems where the computational burden is limited due to LMI expressions.

Experience shows that it is most suitable to design WADCs using the mixed $\mathcal{H}_2/\mathcal{H}_\infty$ which mitigate inter-area oscillations with a good performance and incorporate MIMO control configurations [18-19]. In addition, the use of the SSV in power system has been proposed in recent work for the design of robust controllers, but using only the D-K iteration [24-28].

4.2 Control synthesis on $\mathcal{H}_\infty$ and $\mathcal{H}_2/\mathcal{H}_\infty$

The $\mathcal{H}_\infty$ technique based on Ricatti equations to design supplementary controllers in power systems was introduced. This type of method, despite unstructured uncertainty in some plants, can guarantee robust performance and robust stability. The applications of $\mathcal{H}_\infty$ based on Ricatti equations to complex power system models from various limitations resulting from pole-zero cancelations of the plant and the controller. A mixed sensitivity formulation, such as Fig. 4.1, fails to provide a solution when the augmented plant has invariant zeros either at infinity or on the imaginary axes.

In Fig. 4.1, $\mathbf{W}_1(s)$, and $\mathbf{W}_2(s)$ represent weighting functions. Of relevance, some basic specifications in time domain, such as settling time, peak overshoot cannot be formulated in a Ricatti based design.

In general, the standard $\mathcal{H}_\infty$ problem is described as follows. Given a real rational transfer matrix $\mathbf{J}(s)$, called the plant, and a space $\mathcal{K}_s$ of real rational transfer matrices $\mathbf{K}(s)$, called the controller space, characterize and compute an optimal solution $\mathbf{K}(s) \in \mathcal{K}_s$ to the following optimization

$$\begin{gathered} \min \|F_l[\mathbf{J}(s), \mathbf{K}(s)]\|_\infty \\ \text{subject to } \mathbf{K}(s) \text{ stabilizes } \mathbf{J}(s) \text{ internally} \\ \mathbf{K}(s) \in \mathcal{K}_s \end{gathered} \tag{4.1}$$

The objective function is the $\mathcal{H}_\infty$-norm of the closed loop performances channel described in Fig. 4.2 and the plant $\mathbf{J}(s)$ has a state-space representation of the form

$$\begin{bmatrix} \dot{\mathbf{x}}(t) \\ \mathbf{z}(t) \\ \mathbf{y}(t) \end{bmatrix} = \begin{bmatrix} \mathbf{A} & \mathbf{B}_1 & \mathbf{B}_2 \\ \mathbf{C}_1 & \mathbf{D}_{11} & \mathbf{D}_{12} \\ \mathbf{C}_2 & \mathbf{D}_{21} & \mathbf{D}_{22} \end{bmatrix} \begin{bmatrix} \mathbf{x}(t) \\ \mathbf{w}(t) \\ \mathbf{u}(t) \end{bmatrix} \tag{4.2}$$

This can be written by

$$\mathbf{J}(s): \left[\begin{array}{c|cc} \mathbf{A} & \mathbf{B}_1 & \mathbf{B}_2 \\ \hline \mathbf{C}_1 & \mathbf{D}_{11} & \mathbf{D}_{12} \\ \mathbf{C}_2 & \mathbf{D}_{21} & \mathbf{D}_{22} \end{array}\right] \tag{4.3}$$

where $\mathbf{x}(t_0) = \mathbf{x}_0$, $\mathbf{x}(t) \in \mathbb{R}^n$ is the state, $\mathbf{u}(t) \in \mathbb{R}^{p_u}$ the control, $\mathbf{y}(t) \in \mathbb{R}^{q_y}$ the measured output, $\mathbf{w}(t) \in \mathbb{R}^{r_w}$ the exogenous input, $\mathbf{z}(t) \in \mathbb{R}^{s_z}$ the regulated output and the matrix $\mathbf{A}$ is stable. Similarly, $\mathbf{K}(s)$ has a state-space representation given by:

$$\begin{bmatrix} \dot{\mathbf{x}}_\mathbf{K}(t) \\ \mathbf{u}(t) \end{bmatrix} = \begin{bmatrix} \mathbf{A}_\mathbf{K} & \mathbf{B}_\mathbf{K} \\ \mathbf{C}_\mathbf{K} & \mathbf{D}_\mathbf{K} \end{bmatrix} \begin{bmatrix} \mathbf{x}_\mathbf{K}(t) \\ \mathbf{y}(t) \end{bmatrix} \tag{4.4}$$

$$\mathbf{K}(s): \left[\begin{array}{c|c} \mathbf{A}_\mathbf{K} & \mathbf{B}_\mathbf{K} \\ \hline \mathbf{C}_\mathbf{K} & \mathbf{D}_\mathbf{K} \end{array}\right] \tag{4.5}$$

where $\mathbf{x}_\mathbf{K}(t) \in \mathbb{R}^k$.

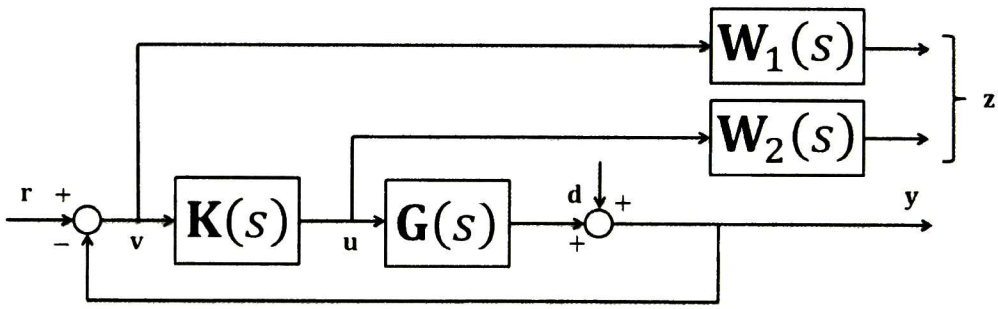

Fig. 4.1. Standard mixed sensitivity feedback configuration.

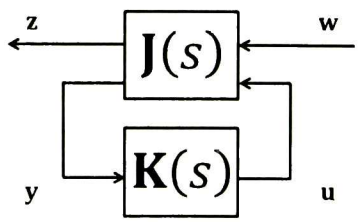

Figure 4.2. Synthesis framework.

The solution of the optimization problem (4.1) is not unique except in the scalar case [17]. Generally speaking, there are no analytic solution formulae for the solutions. In practical design, it is usually sufficient to find a stabilizing controller $\mathbf{K}(s)$ such that the $\mathcal{H}_\infty$-norm of the closed-loop transfer function is less than a given positive number

$$\begin{gathered} \min \|F_l[\mathbf{J}(s), \mathbf{K}(s)]\|_\infty < \gamma \\ \text{subject to } \mathbf{K}(s) \text{ stabilizes } \mathbf{J}(s) \text{ internally} \\ \mathbf{K}(s) \in \mathcal{K}_s \end{gathered} \tag{4.6}$$

where $\gamma > \gamma_0$. This is called the $\mathcal{H}_\infty$ suboptimal problem.

The value of γ starts from a relatively large number to ensure the existence of a suboptimal solution based on Ricatti equations, but γ may approach an optimal solution. It should, however, be pointed out here that when γ is approaching its minimum value γ_0, the problem would become more and more ill-conditioned numerically.

The following assumptions are necessary for the $\mathcal{H}_\infty$ synthesis process.

A.1 $(\mathbf{A}, \mathbf{B}_1)$ is controllable and $(\mathbf{A}, \mathbf{B}_1)$ is observable;

A.2 $(\mathbf{A}, \mathbf{B}_2)$ is stabilizable and $(\mathbf{A}, \mathbf{B}_2)$ is detectable;

A.3 $\mathbf{D}_{12} = \begin{bmatrix} \mathbf{0} \\ \mathbf{I} \end{bmatrix}$ and $\mathbf{D}_{12} = [\mathbf{0} \quad \mathbf{I}]$;

A.4 $\begin{bmatrix} \mathbf{A} - \mathrm{j}\omega\mathbf{I} & \mathbf{B}_2 \\ \mathbf{C}_1 & \mathbf{D}_{12} \end{bmatrix}$ has full column rank for all ω;

A.5 $\begin{bmatrix} \mathbf{A} - \mathrm{j}\omega\mathbf{I} & \mathbf{B}_1 \\ \mathbf{C}_2 & \mathbf{D}_{21} \end{bmatrix}$ has full column rank for all ω.

Some remarks are in order here:

Remark 1. A.1 and A.2 are required for the existence of a stabilizing $\mathbf{K}(s)$.

Remark 2. A.2 assumes that the matrices $\mathbf{D}_{12}$ and $\mathbf{D}_{21}$ are in normalized forms and the system $\mathbf{J}(s)$ is thus so called a normalized system. The case in which those two matrices are of full rank but no necessarily in the normalized forms is discussed in [13].

The $\mathcal{H}_\infty$ synthesis can be formulated as a convex optimization problem involving LMIs as a counterpart of the usual $\mathcal{H}_\infty$ Ricatti equations. One way of simultaneously tuning the $\mathcal{H}_\infty$-performance and transient behavior is to combine the $\mathcal{H}_\infty$ and pole-placement objectives. For example, the step response of a second-order system with poles $\lambda = \zeta\omega_n \pm j\omega_d$ is fully characterized in terms of the undamped natural frequency $\omega_n = |\lambda|$, the damping ratio ζ, and the damped natural frequency ω_d. This means that satisfactory time response and closed-loop damping can be achieved by forcing the closed-loop poles into a suitable subregion of the left-half plane as shown in Fig. 4.3. In addition, it is desirable to obtain a controller on $\mathcal{H}_2/\mathcal{H}_\infty$ specifications and suitable subregion of the left-half plane [20].

In general, $\mathcal{H}_2/\mathcal{H}_\infty$ control design has three objectives: the $\mathcal{H}_\infty$ performance, the $\mathcal{H}_2$ norm, and the closed-loop poles into a suitable region. Then, the configuration of multiobjective damping controller for power systems can be described in a block diagram as shown in Fig. 4.4.

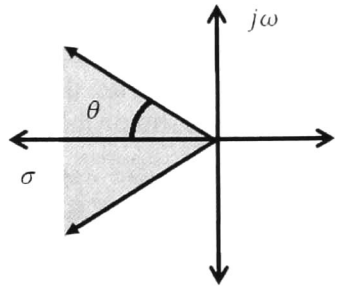

Figure 4.3. Region for the closed-loop poles into suitable subregion.

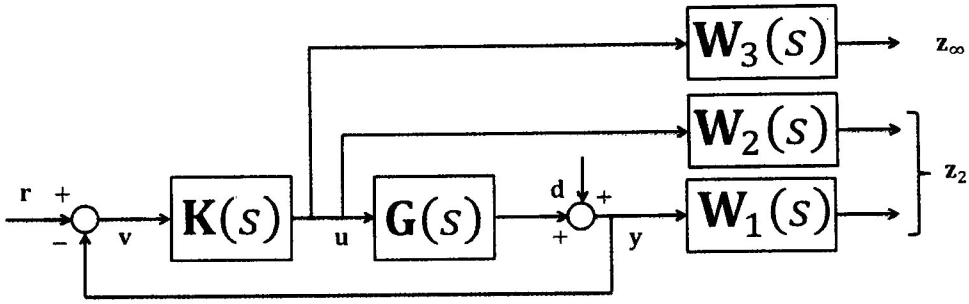

Figure 4.4. Multiobjective damping controller block diagram.

Assume a general control structure as that described in Fig. 4.5. The output channel $\mathbf{z}_\infty \in \mathbb{R}^{s_{z\infty}}$ is associated with the performance while the channel $\mathbf{z}_2(t) \in \mathbb{R}^{s_{z2}}$ is associated with the linear quadratic Gaussian (LQG) aspects ($\mathcal{H}_2$ performance).

Consider the linear dynamic system,

$$\begin{bmatrix} \dot{\mathbf{x}}(t) \\ \mathbf{z}_\infty(t) \\ \mathbf{z}_2(t) \\ \mathbf{y}(t) \end{bmatrix} = \begin{bmatrix} \mathbf{A} & \mathbf{B}_1 & \mathbf{B}_2 \\ \mathbf{C}_1 & \mathbf{D}_{11} & \mathbf{D}_{12} \\ \mathbf{C}_2 & \mathbf{D}_{21} & \mathbf{D}_{22} \\ \mathbf{C}_3 & \mathbf{D}_{31} & \mathbf{D}_{32} \end{bmatrix} \begin{bmatrix} \mathbf{x}(t) \\ \mathbf{w}(t) \\ \mathbf{u}(t) \end{bmatrix} \tag{4.7}$$

This can be written by

$$\mathbf{J}(s): \left[\begin{array}{c|cc} \mathbf{A} & \mathbf{B}_1 & \mathbf{B}_2 \\ \hline \mathbf{C}_1 & \mathbf{D}_{11} & \mathbf{D}_{12} \\ \mathbf{C}_2 & \mathbf{D}_{21} & \mathbf{D}_{22} \\ \mathbf{C}_3 & \mathbf{D}_{31} & \mathbf{D}_{32} \end{array}\right] \tag{4.8}$$

where $\mathbf{K}(s)$ has a representation given by Eq. (4.4).

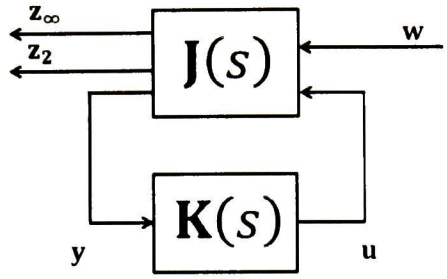

Figure 4.5. Synthesis framework on $\mathcal{H}_2/\mathcal{H}_\infty$.

Let

$$\begin{bmatrix} \dot{\mathbf{x}}_{cl}(t) \\ \mathbf{z}_\infty(t) \\ \mathbf{z}_2(t) \end{bmatrix} = \begin{bmatrix} \mathbf{A}_{cl} & \mathbf{B}_{cl} \\ \mathbf{C}_{cl1} & \mathbf{D}_{cl1} \\ \mathbf{C}_{cl2} & \mathbf{D}_{cl2} \end{bmatrix} \begin{bmatrix} \mathbf{x}_{cl}(t) \\ \mathbf{w}(t) \end{bmatrix}$$

be the corresponding closed-loop state-space equations. Then, the three design objectives can be expressed as follows:

- $\mathcal{H}_\infty$ performance: the closed-loop RMS gain from $\mathbf{w}(s)$ to $\mathbf{z}_\infty(s)$ does not exceed γ if and only if there exist a positive definitive symmetric matrix $\mathbf{X}_\infty$ such that

$$\begin{bmatrix} \mathbf{A}_{cl}\mathbf{X}_\infty + \mathbf{X}_\infty\mathbf{A}_{cl}^T & \mathbf{B}_{cl} & \mathbf{X}_\infty\mathbf{C}_{cl1}^T \\ \mathbf{B}_{cl}^T & -\mathbf{I} & \mathbf{D}_{cl1}^T \\ \mathbf{C}_{cl1}\mathbf{X}_\infty & \mathbf{D}_{cl1} & -\gamma^2\mathbf{I} \end{bmatrix} < 0$$

- $\mathcal{H}_2$ performance: the $\mathcal{H}_2$ norm of the closed-loop transfer function from $\mathbf{w}(s)$ to $\mathbf{z}_2(s)$ does not exceed ν if and only if $\mathbf{D}_{cl2} = 0$ and there exist two symmetric matrices $\mathbf{X}_2$ and $\mathbf{Q}$ such that

$$\begin{bmatrix} \mathbf{A}_{cl}\mathbf{X}_2 + \mathbf{X}_2\mathbf{A}_{cl}^T & \mathbf{B}_{cl} \\ \mathbf{B}_{cl}^T & -\mathbf{I} \end{bmatrix} < 0$$

$$\begin{bmatrix} \mathbf{Q} & \mathbf{C}_{cl2}\mathbf{X}_2 \\ \mathbf{X}_2\mathbf{C}_{cl2}^T & \mathbf{X}_2 \end{bmatrix} > 0$$

$$\text{Trace}[\mathbf{Q}] < \nu^2$$

- Pole placement: the closed-loop poles lie in the LMI region

$$\mathcal{D} = \{\mathbf{z} \in \mathbb{C}: \mathbf{L} + \mathbf{M}\mathbf{z} + \mathbf{M}^T\bar{\mathbf{z}}\} < 0$$

where $\mathbf{M}$ and $\mathbf{L} = \mathbf{L}^T$ are fixed real matrices. The matrix-value function $f_{\mathcal{D}}(\mathbf{z}) = \mathbf{L} + \mathbf{M}\mathbf{z} + \mathbf{M}^T\bar{\mathbf{z}}$ is called the characteristic function of the region $\mathcal{D}$. In the above equation $\mathbf{L} = \mathbf{L}^T = [\mathfrak{L}_{ij}]$ and $\mathbf{M} = [\mathfrak{M}_{ij}]$ if and only if there exists a positive definite symmetric matrix $\mathbf{X}_{pol}$ satisfying

$$[\mathfrak{L}_{ij}\mathbf{X}_{pol} + \mathfrak{M}_{ij}\mathbf{A}_{cl}\mathbf{X}_{pol} + \mathfrak{M}_{ij}\mathbf{X}_{pol}\mathbf{A}_{cl}^T] < 0$$

These three sets of conditions add up to a nonconvex optimization problem with variables $\mathbf{Q}$, $\mathbf{K}$, $\mathbf{X}_\infty$, $\mathbf{X}_2$ and $\mathbf{X}_{pol}$. For tractability in the LMI framework, it is necessary a single Lyapunov matrix with $\mathbf{X} = \mathbf{X}_\infty = \mathbf{X}_2 = \mathbf{X}_{pol}$ that enforces all three objectives. Find matrices $\mathbf{M}$, $\mathbf{N}$, $\mathbf{R} = \mathbf{R}^T$ and $\mathbf{S} = \mathbf{S}^T$ to factorize $\mathbf{X}$ as

$$\mathbf{X} = \mathbf{X}_1\mathbf{X}_2^{-1},\ \mathbf{X}_1 = \begin{bmatrix} \mathbf{R} & \mathbf{I} \\ \mathbf{M}^T & \mathbf{0} \end{bmatrix},\ \mathbf{X}_2 = \begin{bmatrix} \mathbf{0} & \mathbf{S} \\ \mathbf{I} & \mathbf{N}^T \end{bmatrix}$$

and introducing the change of controller variables:

$$\mathfrak{A}_\mathbf{K} = \mathbf{N}\mathbf{A}_\mathbf{K}\mathbf{M}^T + \mathbf{N}\mathbf{B}_\mathbf{K}\mathbf{C}_3\mathbf{R} + \mathbf{S}\mathbf{B}_2\mathbf{C}_\mathbf{K}\mathbf{M}^T + \mathbf{S}[\mathbf{A} + \mathbf{B}_2\mathbf{D}_\mathbf{K}\mathbf{C}_3]\mathbf{R}$$

$$\mathfrak{B}_\mathbf{K} = \mathbf{N}\mathbf{B}_\mathbf{K} + \mathbf{S}\mathbf{B}_2\mathbf{D}_\mathbf{K}$$

$$\mathfrak{C}_\mathbf{K} = \mathbf{C}_\mathbf{K}\mathbf{M}^T + \mathbf{D}_\mathbf{K}\mathbf{C}_3\mathbf{R}$$

the inequality constraints on $\mathbf{X}$ are readily turned into LMI constraints in the variables $\mathbf{R}$, $\mathbf{S}$, $\mathbf{Q}$, $\mathfrak{A}_\mathbf{K}$, $\mathfrak{B}_\mathbf{K}$, $\mathfrak{C}_\mathbf{K}$ and $\mathbf{D}_\mathbf{K}$. In general, the following suboptimal LMI formulation of multi-objective synthesis problem can be expressed as

minimize $\propto \gamma^2 + \beta Trace[\mathbf{Q}]$ over $\mathbf{R}, \mathbf{S}, \mathbf{Q}, \mathfrak{A}_\mathbf{K}, \mathfrak{B}_\mathbf{K}, \mathfrak{C}_\mathbf{K}, \mathbf{D}_\mathbf{K}$ and γ^2 satisfying:

$$\begin{bmatrix} \mathbf{A}\mathbf{R} + \mathbf{R}\mathbf{A}^T + \mathbf{B}_2\mathfrak{C}_\mathbf{K} + \mathfrak{C}_\mathbf{K}^T\mathbf{B}_2^T & \mathfrak{A}_\mathbf{K}^T + \mathbf{A} + \mathbf{B}_2\mathbf{D}_\mathbf{K}\mathbf{C}_3 & \mathbf{B}_1 + \mathbf{B}_2\mathbf{D}_\mathbf{K}\mathbf{D}_{31} & [\mathbf{C}_1\mathbf{R} + \mathbf{D}_{12}\mathbf{C}_\mathbf{K}]^T \\ \mathfrak{A}_\mathbf{K} + [\mathbf{A} + \mathbf{B}_2\mathbf{D}_\mathbf{K}\mathbf{C}_3]^T & \mathbf{A}^T\mathbf{S} + \mathbf{S}\mathbf{A} + \mathfrak{B}_\mathbf{K}\mathbf{C}_3 + \mathbf{C}_3^T\mathfrak{B}_\mathbf{K}^T & \mathbf{S}\mathbf{B}_1 + \mathfrak{B}_\mathbf{K}\mathbf{D}_{31} & \mathbf{C}_1^T + \mathbf{C}_3^T\mathbf{D}_\mathbf{K}^T\mathbf{D}_{12}^T \\ [\mathbf{B}_1 + \mathbf{B}_2\mathbf{D}_\mathbf{K}\mathbf{D}_{31}]^T & [\mathbf{S}\mathbf{B}_1 + \mathbf{B}_\mathbf{K}\mathbf{D}_{31}]^T & -\mathbf{I} & [\mathbf{D}_{11} + \mathbf{D}_{12}\mathbf{D}_\mathbf{K}\mathbf{D}_{31}]^T \\ \mathbf{C}_1\mathbf{R} + \mathbf{D}_{12}\mathfrak{C}_\mathbf{K} & \mathbf{C}_1 + \mathbf{D}_{12}\mathbf{D}_\mathbf{K}\mathbf{C}_3 & \mathbf{D}_{11} + \mathbf{D}_{12}\mathbf{D}_\mathbf{K}\mathbf{D}_{31} & -\gamma^2\mathbf{I} \end{bmatrix} < 0 \tag{4.9}$$

$$\begin{bmatrix} \mathbf{Q} & \mathbf{C}_2\mathbf{R} + \mathbf{D}_{22}\mathfrak{C}_\mathbf{K} & \mathbf{C}_2 + \mathbf{D}_{22}\mathbf{D}_\mathbf{K}\mathbf{C}_3 \\ [\mathbf{C}_2\mathbf{R} + \mathbf{D}_{22}\mathfrak{C}_\mathbf{K}]^T & \mathbf{R} & \mathbf{I} \\ [\mathbf{C}_2 + \mathbf{D}_{22}\mathbf{D}_\mathbf{K}\mathbf{C}_3]^T & \mathbf{I} & \mathbf{S} \end{bmatrix} > 0 \tag{4.10}$$

$$\left[\mathfrak{L}_{ij} \begin{bmatrix} \mathbf{R} & \mathbf{I} \\ \mathbf{I} & \mathbf{S} \end{bmatrix} + \mathfrak{M}_{ij} \begin{bmatrix} \mathbf{A}\mathbf{R} + \mathbf{B}_2\mathfrak{C}_\mathbf{K} & \mathbf{A} + \mathbf{B}_2\mathbf{D}_\mathbf{K}\mathbf{C}_2 \\ \mathfrak{A}_\mathbf{K} & \mathbf{S}\mathbf{A} + \mathfrak{B}_\mathbf{K}\mathbf{C}_2 \end{bmatrix} + \right.$$
$$\left. \mathfrak{M}_{ij} \begin{bmatrix} \mathbf{R}\mathbf{A}^T + [\mathbf{B}_2\mathfrak{C}_\mathbf{K}]^T & \mathfrak{A}_\mathbf{K}^T \\ [\mathbf{A} + \mathbf{B}_2\mathbf{D}_\mathbf{K}\mathbf{C}_2]^T & [\mathbf{S}\mathbf{A} + \mathfrak{B}_\mathbf{K}\mathbf{C}_2]^T \end{bmatrix} \right] < 0 \tag{4.11}$$

$$\text{Trace}[\mathbf{Q}] < v_0^2 \tag{4.12}$$

$$\gamma^2 < \gamma_0^2 \tag{4.13}$$

$$\mathbf{D}_{21} + \mathbf{D}_{22}\mathbf{D}_K\mathbf{D}_{31} = 0 \tag{4.14}$$

Given optimal solutions of this LMI problem, the closed-loop $\mathcal{H}_\infty$ and $\mathcal{H}_2$ performances are bounded by

$$\|\mathbf{T}_\infty\|_\infty \leq \gamma^* \tag{4.15}$$

$$\|\mathbf{T}_2\|_2 \leq \sqrt{\text{Trace}[\mathbf{Q}^*]} \tag{4.16}$$

where $\mathbf{T}_\infty$ and $\mathbf{T}_2$ denote the closed-loop transfer functions from $\mathbf{w}$ to $\mathbf{z}_\infty$ and $\mathbf{z}_2$, respectively.

Fig. 4.6 gives a conceptual overview of $\mathcal{H}_2/\mathcal{H}_\infty$ of a multimachine power system in which generator j has a local controller that is to be designed, $\mathbf{K}(s)$. Here, $\mathbf{G}_j$, $\mathbf{Exc}_j$, $\Delta\omega_j$, ΔV_{ref_j} and ΔV_{n_j} represent the *jth* generator, the *jth* exciter, the *jth* relative rotor speed, the *jth* voltage reference and the *jth* noise signal to satisfy necessary conditions for $\mathcal{H}_\infty$ controller synthesis, respectively. Note that the subscript Δ represents the incremental variables of the linearized model.

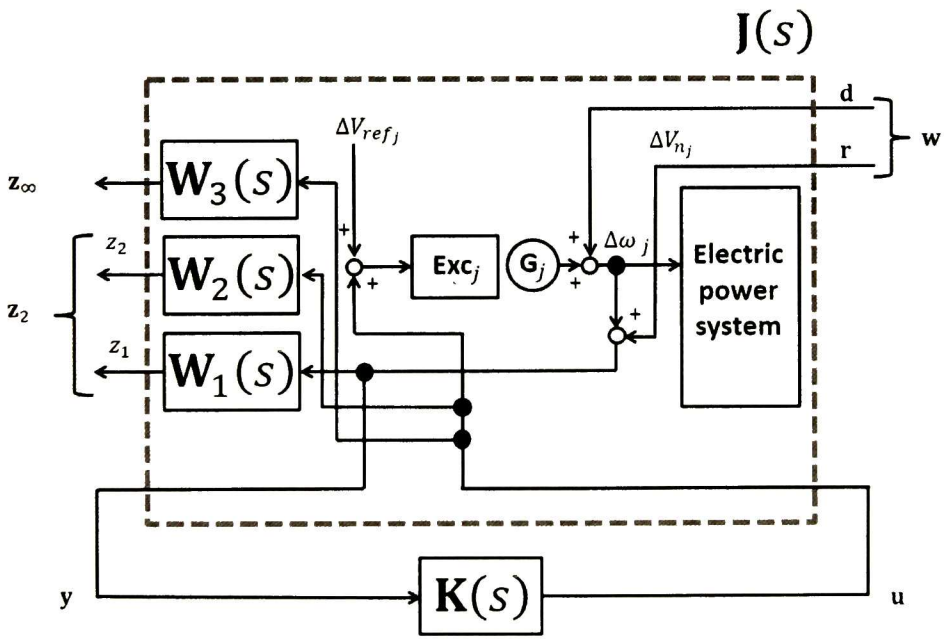

Figure 4.6. Schematic synthesis framework on $\mathcal{H}_2/\mathcal{H}_\infty$ of a multimachine power system for the jth generator.

Practical application of the $\mathcal{H}_2/\mathcal{H}_\infty$ technique in large power systems requires a reduced-order model of the nominal model due to high number of generators and the LMI formulation. In general, this method achieves good results for SISO and MIMO controllers which can be WADCs and local supplementary controllers [18-19]. Furthermore, it is easy to include unstructured uncertainty to describe unmodelled dynamics. Although, this usually leads to conservativeness of the control design.

4.3 μ-synthesis

A controller based on $\mathcal{H}_2/\mathcal{H}_\infty$ specifications can have analytical limitations to represent structured uncertainty. Nevertheless with the use of SSV, where the uncertainty can be represented with complex or real parameters, it is possible to extend this type of representation to obtain a robust controller. In addition, this controller can have robust properties but the computational burden is increased due to scaling matrices of the SSV In general, the synthesis of controllers which are optimal with respect to a performance criterion expressed in terms of a SSV is called μ-synthesis [12-13].

Let a finite dimensional LTI dynamical system described by the following state space representation:

$$\begin{bmatrix} \dot{\mathbf{x}}(t) \\ \mathbf{y}_\Delta(t) \\ \mathbf{z}(t) \\ \mathbf{y}(t) \end{bmatrix} = \begin{bmatrix} \mathbf{A} & \mathbf{B}_1 & \mathbf{B}_2 & \mathbf{B}_3 \\ \mathbf{C}_1 & \mathbf{D}_{11} & \mathbf{D}_{12} & \mathbf{D}_{13} \\ \mathbf{C}_2 & \mathbf{D}_{21} & \mathbf{D}_{22} & \mathbf{D}_{23} \\ \mathbf{C}_3 & \mathbf{D}_{31} & \mathbf{D}_{32} & \mathbf{D}_{33} \end{bmatrix} \begin{bmatrix} \mathbf{x}(t) \\ \mathbf{u}_\Delta(t) \\ \mathbf{w}(t) \\ \mathbf{u}(t) \end{bmatrix} \tag{4.17}$$

and

$$\mathbf{P}(s): \left[\begin{array}{c|ccc} \mathbf{A} & \mathbf{B}_1 & \mathbf{B}_2 & \mathbf{B}_3 \\ \hline \mathbf{C}_1 & \mathbf{D}_{11} & \mathbf{D}_{12} & \mathbf{D}_{13} \\ \mathbf{C}_2 & \mathbf{D}_{21} & \mathbf{D}_{22} & \mathbf{D}_{23} \\ \mathbf{C}_3 & \mathbf{D}_{31} & \mathbf{D}_{32} & \mathbf{D}_{33} \end{array}\right] \tag{4.18}$$

where $\mathbf{x}(t_0) = \mathbf{x}_0$, $\mathbf{x}(t) \in \mathbb{R}^n$ is the state, $\mathbf{u}(t) \in \mathbb{R}^{p_u}$ the control input, $\mathbf{y}(t) \in \mathbb{R}^{q_y}$ the control output, $\mathbf{w}(t) \in \mathbb{R}^{r_w}$ the exogenous input, $\mathbf{z}(t) \in \mathbb{R}^{s_z}$ the regulated output, $\mathbf{u}_\Delta(t) \in \mathbb{C}^{d_{u\Delta}}$ the uncertainty input, and $\mathbf{y}_\Delta(t) \in \mathbb{R}^{e_{y\Delta}}$ the uncertainty output. Assume that the matrix $\mathbf{A}$ is stable, and the input $\mathbf{u}_\Delta(t)$ is described as

$$\mathbf{u}_\Delta(t) = \boldsymbol{\Delta}\mathbf{y}_\Delta(t) \tag{4.19}$$

The representation given in (4.17) is defined for the open-loop system augmented by weighting functions for performance and controllers. The open-loop system in frequency domain can be described in Fig. 4.7 with a LFT, and

the uncertainty $\boldsymbol{\Delta}$ can be absorbed to derive the synthesis framework represented in Fig. 4.2.

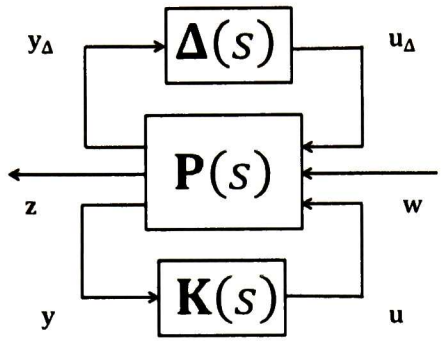

Figure 4.7. Open-loop system.

Reordering equation (4.18) can be expressed as

$$\mathbf{P}(s) = \left[\begin{array}{c|cc} \mathbf{A} & \mathbf{B} & \mathbf{B_3} \\ \hline \mathbf{C} & \bar{\mathbf{D}}_{11} & \bar{\mathbf{D}}_{12} \\ \mathbf{C_3} & \bar{\mathbf{D}}_{21} & \bar{\mathbf{D}}_{22} \end{array}\right] \tag{4.20}$$

where

$$\mathbf{B} = [\mathbf{B_1} \quad \mathbf{B_2}]; \ \mathbf{C} = \begin{bmatrix} \mathbf{C_1} \\ \mathbf{C_2} \end{bmatrix}; \ \bar{\mathbf{D}}_{11} = \begin{bmatrix} \mathbf{D}_{11} & \mathbf{D}_{12} \\ \mathbf{D}_{21} & \mathbf{D}_{22} \end{bmatrix}; \ \bar{\mathbf{D}}_{12} = \begin{bmatrix} \mathbf{D}_{13} \\ \mathbf{D}_{23} \end{bmatrix};$$

$$\bar{\mathbf{D}}_{21} = [\mathbf{D}_{31} \quad \mathbf{D}_{32}]; \ \bar{\mathbf{D}}_{22} = \mathbf{D}_{33}$$

In particular, the representation in (4.20) expresses a general form to the control synthesis problem. Then to ensure robust stability and robust performance a stabilizing controller $\mathbf{K}(s)$ is required, such that

$$\sup_{\omega \in \mathbb{R}} \mu_{\boldsymbol{\Delta}}\left[F_l[\mathbf{P}(j\omega), \mathbf{K}(j\omega)]\right] < 1 \tag{4.21}$$

That is, the design objective is to find a stabilizing controller $\mathbf{K}(s)$, such that for all perturbation $\|\boldsymbol{\Delta}\|_\infty \leq 1$, the closed-loop system will be stable and then will satisfy

$$\|F_u[F_l[\mathbf{P}(s), \mathbf{K}(s)], \boldsymbol{\Delta}]\|_\infty \leq 1 \tag{4.22}$$

This is shown in Fig. 4.8 and formally can be expressed as:

$$\min_{\mathbf{K}(s) \in \mathcal{K}_s} \sup_{\omega \in \mathbb{R}} \mu_{\boldsymbol{\Delta}}\left[F_l[\mathbf{P}(j\omega), \mathbf{K}(j\omega)]\right] < 1 \tag{4.23}$$

The problem proposed in (4.23) is not yet fully solved and it is shown in Fig. 3.8. However, a reasonable approach is to use the upper bound of SSV obtained by scaling and applying $\mathcal{H}_\infty$. Finally, the condition in (4.21) is subject to the internal stability of the nominal system.

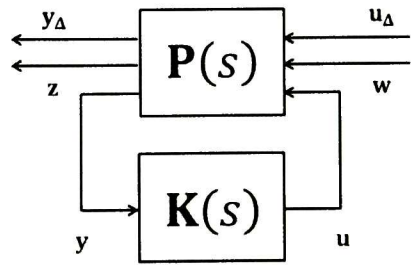

Figure 4.8. General framework for μ-synthesis.

Fig. 4.9 shows a schematic diagram on μ-synthesis framework for a supplementary local controller of a multimachine power system for the jth generator. Note that the structured uncertainty, $\mathbf{\Delta}$, is taken into account.

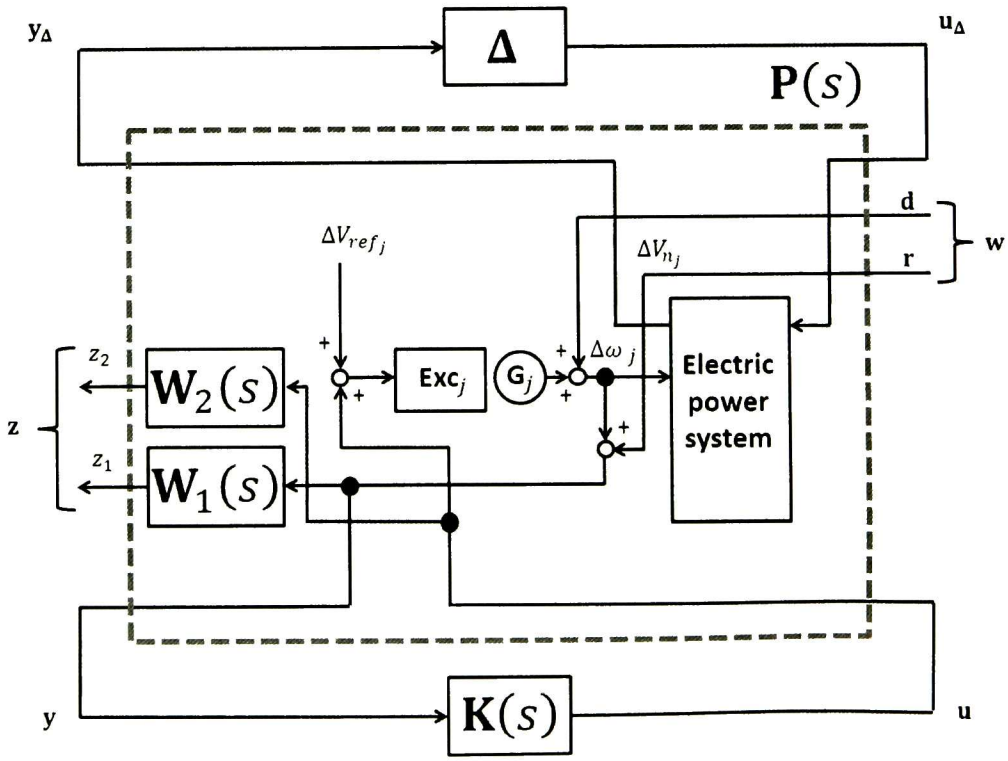

Figure 4.9. μ-synthesis framework for a supplementary local controller.

Generally, three algorithms to obtain a solution to the problem of μ-synthesis have been developed and tested in the literature [5-16]: the D-K iteration for complex structured uncertainties, the D-G-K iteration for mixed structured uncertainties and the μ-K iteration, which uses a scalar approximation to compensate the real uncertainty which is not considered in the D-K iteration. These algorithms are briefly summarized in the next subsections.

4.3.1 Complex μ design

In this subsection, the D-K iteration is presented in order to solve the problem of synthesis to achieve the best robust performance with complex structured uncertainty [12-13]. In the literature, sometimes the D-K iteration is called *the standard μ-synthesis framework* [2, 7].It is assumed that transfer functions have perfect state space minimal realization [12-13].

The approach to design μ optimal controller corresponding to (4.21) is derived as:

$$\mathbf{K}(s) = \arg \min_{\mathbf{K}(s)\in\mathcal{K}_s} \sup_{\omega\in\mathbb{R}} \mu_{\Delta}\left[F_l[\mathbf{P}(j\omega), \mathbf{K}(j\omega)]\right] \tag{4.24}$$

Note that (4.24) uses the complex SSV. Unfortunately, the above equation is not tractable since μ cannot be directly computed. Hence, using the upper bound of the complex SSV is possible to express

$$\mathbf{K}(s) = \arg \min_{\mathbf{K}(s)\in\mathcal{K}_s} \sup_{\omega\in\mathbb{R}} \inf_{\mathbf{D}(\omega)\in\mathrm{D}} \left[\bar{\sigma}[\mathbf{D}(\omega)F_l[\mathbf{P}(j\omega), \mathbf{K}(j\omega)]\mathbf{D}^{-1}(\omega)]\right] \tag{4.25}$$

One approach is alternatively minimize (4.25). That is, $\mathbf{K}(s)$ or $\mathbf{D}(\omega)$ are held constant while one of them is calculated. This can be expressed as

a. For a fixed scaling transfer function $\mathbf{D}(s)$, $\mathbf{K}(s) = \arg \min_{\mathbf{K}(s)\in\mathcal{K}_s} \left\|F_l[\mathbf{D}(s)\mathbf{P}(s)\mathbf{D}^{-1}(s), \mathbf{K}(s)]\right\|_{\infty}$ represents a standard $\mathcal{H}_{\infty}$ control.

b. For a fixed $\mathbf{K}(s)$, $\mathbf{D}(\omega) = \arg \min_{\mathbf{D}(\omega)\in\mathrm{D}} \{\bar{\sigma}[\mathbf{D}(\omega)F_l[\mathbf{P}(j\omega), \mathbf{K}(j\omega)]\mathbf{D}^{-1}(\omega)]\}$ can be minimized at each frequency as a convex optimization problem.

The resulting $\mathbf{D}(\omega)$ can be fit with a stable minimum phase, rational transfer function with stable inverse, such that

$$\mathbf{D}(s)\mathbf{\Delta}(s) = \mathbf{\Delta}(s)\mathbf{D}(s) \tag{4.26}$$

It follows from the above considerations a process optimization by an iterative approach, referred as D-K iteration and shown in Fig. 4.10 and 4.11. Details of this process are summarized in the following steps:

1. Given a system $\mathbf{P}(s)$, let $i = 1$, $\mathbf{D}_i(\omega) = \mathbf{I}$, $\forall\omega$.

2. Fit a stable minimum phase transfer function matrix $\mathbf{D}_i(s)$ to the pointwise scaling $\mathbf{D}_i(\omega)$.

3. Construct a state space model for the described system in Fig. 4.4:

$$\widehat{\mathbf{P}}_i(s) = \begin{bmatrix} \mathbf{D}_i(s) & \mathbf{0} \\ \mathbf{0} & \mathbf{I} \end{bmatrix} \mathbf{P}(s) \begin{bmatrix} \mathbf{D}_i^{-1}(s) & \mathbf{0} \\ \mathbf{0} & \mathbf{I} \end{bmatrix} \tag{4.27}$$

4. Solve an $\mathcal{H}_\infty$ to minimize

$$\mathbf{K}_i(s) = \arg\min_{\mathbf{K}(s)\in\mathcal{K}_s} \left\| F_l\left[\widehat{\mathbf{P}}_i(s), \mathbf{K}_i(s)\right] \right\|_\infty \tag{4.28}$$

5. Compute the new scalings $\mathbf{D}_{i+1}(\omega)$ from the complex μ upper bound problem

$$\mathbf{D}_{i+1}(\omega) = \arg\min_{\mathbf{D}_{i+1}(\omega)\in\mathbf{D}} \{\bar{\sigma}[\mathbf{D}_{i+1}(\omega) F_l[\mathbf{P}(j\omega), \mathbf{K}_i(j\omega)] \mathbf{D}_{i+1}^{-1}(\omega)]\} \tag{4.29}$$

   pointwise across frequency ω.

6. Compare $\mathbf{D}_i(\omega)$ with the previous $\mathbf{D}_{i+1}(\omega)$. Stop if they are close. Otherwise let $i = i + 1$ and repeat from 2.

Notice that the D-K iteration may not converge in some cases, but many designs have shown that this approach works very well. The result controller can be very conservative due to the complex uncertainties. However, the elements of D can be allowed to take any nonzero complex values and do not change the value of the upper bound, $\min_{\mathbf{D}(\omega)\in\mathbf{D}} \{\bar{\sigma}[\mathbf{D}(\omega) F_l[\mathbf{P}(j\omega), \mathbf{K}_i(j\omega)] \mathbf{D}^{-1}(\omega)]\}$, that is, the phase is freedom.

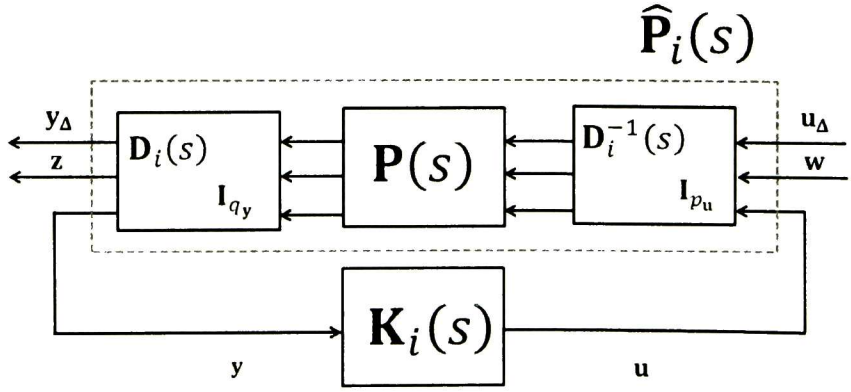

Figure 4.10. $\mathbf{K}_i(s)$-step in D-K iteration.

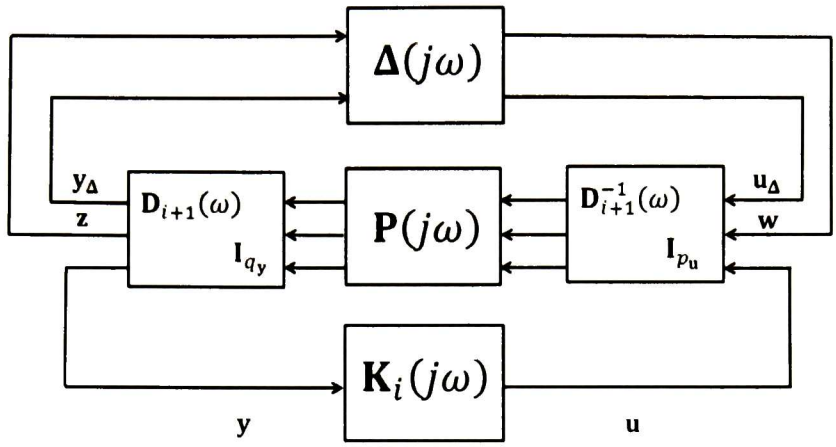

Figure 4.11. $\mathbf{D}_{i+1}(\omega)$-step in D-K iteration.

The design of supplementary controllers based on μ-synthesis has been discussed in recent work to design local supplementary controllers in power systems, but only using the D-K iteration [24-27]. In [28] was implemented a centralized controller for a 7-bus, 5 machine system. Note that these implementations have been based on polynomial framework described in [21-23].

4.3.2 Mixed μ synthesis

For the design problems which arise with real and complex perturbations, there is a corresponding D-G-K iteration procedure proposed in [2]. Using this approach, the mixed upper bound can be written as

$$\mu_{\mathbf{M}}[\mathbf{M}] \leq \inf_{\mathbf{D}\in\mathbf{D},\mathbf{G}\in\mathbf{G}_{\mathbf{M}}} \min_{0\leq\beta\in\mathbb{R}} \{\beta: \mathbf{M}^{*}\mathbf{D}\mathbf{M} + j[\mathbf{G}\mathbf{M} - \mathbf{M}^{*}\mathbf{G}] - \beta^{2}\mathbf{D} \leq 0\}$$

The above expression can be rewritten for the controller synthesis problem as

$$\mathbf{K}(s) = \arg\min_{\mathbf{K}(s)\in\mathcal{K}_s} \sup_{\omega\in\mathbb{R}} \inf_{\mathbf{D}(\omega)\in\mathbf{D},\mathbf{G}(\omega)\in\mathbf{G}_{\mathbf{M}}} \inf_{0\leq\beta(\omega)\in\mathbb{R}} \{\beta(\omega): \boldsymbol{\Gamma}(\omega) \leq 1\} \qquad (4.30)$$

where

$$\boldsymbol{\Gamma}(\omega) = \bar{\sigma}\left[\left(\frac{\mathbf{D}(\omega)F_l[\mathbf{P}(j\omega),\mathbf{K}(j\omega)]\mathbf{D}^{-1}(\omega)}{\beta(\omega)} - j\mathbf{G}(\omega)\right)[\mathbf{I} + \mathbf{G}^{2}(\omega)]^{-\frac{1}{2}}\right]$$

For fixed $\mathbf{K}(s)$ the problem of finding $\mathbf{D}(\omega)$, $\mathbf{G}(\omega)$ and $\beta(\omega)$ is the mixed μ upper bound problem across frequency. For fixed $\mathbf{D}(s)$, $\mathbf{G}(s)$ and $\beta(s)$ transfer matrices then the problem of finding $\mathbf{K}(s)$ will be reduced to a standard $\mathcal{H}_{\infty}$ problem. The last analysis leads to the D-G-K iteration for mixed μ. In general, this method is summarized in the following steps:

1. Given a system $\mathbf{P}(s)$, let $i = 1$, $\mathbf{D}_i(\omega) = \mathbf{I}$, $\mathbf{G}_i(\omega) = \mathbf{0}$ and $\beta_i^* = 1, \forall\omega$.

2. Fit transfer function matrices $\mathbf{D}_i(s)$ and $\mathbf{G}_i(s)$ to the pointwise scalings $\mathbf{D}_i(\omega)$ and $j\mathbf{G}_i(\omega)$, so that $\mathbf{D}_i(j\omega)$ approximates $\mathbf{D}_i(\omega)$ and $\mathbf{G}_i(j\omega)$ approximates $j\mathbf{G}_i(\omega)$. Replace $\mathbf{D}_i(s)$ and $\mathbf{G}_i(s)$ with appropriate factors so that $\mathbf{D}_i(s)$, $\mathbf{D}_i^{-1}(s)$, $\mathbf{G}_{h_i}(s)$ and $\mathbf{G}_i(s)\mathbf{G}_{h_i}(s)$ are all stable, where $\mathbf{G}_{h_i}(s)$ is a spectral factor satisfying $[\mathbf{I} + \mathbf{G}_i(s)\mathbf{G}_i^T(-s)]^{-1} = \mathbf{G}_{h_i}(s)\mathbf{G}_{h_i}^T(-s)$. Augment $\mathbf{D}_i(s)$ and $\mathbf{G}_{h_i}(s)$ with identity matrices, and $\mathbf{G}_i(s)$ with a zero matrix, of appropriate dimensions so that $\mathbf{D}_i(s)$, $\mathbf{G}_i(s)$, $\mathbf{G}_{h_i}(s)$ are compatible with $\mathbf{P}(s)$. Form the state space system

$$\mathbf{P}_{\mathbf{DG}_i}(s) = [\mathbf{D}_i(s)\mathbf{P}(s)\mathbf{D}_i^{-1}(s) - \beta_i^*\mathbf{G}_i(s)]\mathbf{G}_{h_i}(s) \tag{4.31}$$

3. Find the $\mathcal{H}_\infty$ optimal controller $\mathbf{K}_i(s)$:

$$\mathbf{K}_i(s) = \arg \min_{\mathbf{K}_i(s)\in\mathcal{K}_s} \left\| F_l\left[\mathbf{P}_{\mathbf{DG}_i}(s), \mathbf{K}_i(s)\right]\right\|_\infty \tag{4.32}$$

4. Compute the maximum upper bound β_{i+1}^* as

$$\beta_{i+1}^* = \sup_{\omega\in\mathbb{R}} \inf_{\mathbf{D}(\omega)\in\mathbf{D},\mathbf{G}(\omega)\in\mathbf{G}_\mathbf{M}} \inf_{0\le\beta(\omega)\in\mathbb{R}} \{\beta(\omega): \mathbf{\Gamma}(\omega) \le 1\} \tag{4.33}$$

where $\mathbf{\Gamma}(\omega)$ is given by

$$\mathbf{\Gamma}(\omega) = \bar{\sigma}\left[\left(\frac{\mathbf{D}(\omega)F_l[\mathbf{P}(j\omega),\mathbf{K}_i(j\omega)]\mathbf{D}^{-1}(\omega)}{\beta(\omega)} - j\mathbf{G}(\omega)\right)[\mathbf{I} + \mathbf{G}^2(\omega)]^{-\frac{1}{2}}\right] \tag{4.34}$$

5. Calculate the new scalings $\mathbf{D}_{i+1}(\omega)$ and $\mathbf{G}_{i+1}(j\omega)$ solving the minimization problem

$$\mathbf{D}_{i+1}(\omega), \mathbf{G}_{i+1}(\omega) = \arg \inf_{\mathbf{D}_{i+1}(\omega)\in\mathbf{D},\mathbf{G}_{i+1}(\omega)\in\mathbf{G}_\mathbf{M}} \bar{\sigma}\left[\left(\frac{\mathbf{D}_{i+1}(\omega)F_l[\mathbf{P}(j\omega),\mathbf{K}_i(j\omega)]\mathbf{D}_{i+1}^{-1}(\omega)}{\beta_{i+1}^*} - j\mathbf{G}_{i+1}(\omega)\right)[\mathbf{I} + \mathbf{G}_{i+1}^2(\omega)]^{-\frac{1}{2}}\right] \tag{4.35}$$

pointwise across frequency.

6. Compare $\mathbf{D}_{i+1}(\omega)$ and $\mathbf{G}_{i+1}(\omega)$ with the previous estimates $\mathbf{D}_i(\omega)$ and $\mathbf{G}_i(\omega)$. Stop if they are close. Otherwise let $i = i + 1$, and repeat from 2.

Some remarks are necessary about the D-G-K iteration

- It is necessary a spectral factor in step 2 which implies that $[\mathbf{I} + \mathbf{G}_i(s)\mathbf{G}_i^T(-s)]^{-1} = \mathbf{G}_{h_i}(s)\mathbf{G}_{h_i}^T(-s)$.

- The determination of scaling matrices in step 5, $\mathbf{D}_{i+1}(\omega)$ and $\mathbf{G}_{i+1}(\omega)$ are not the scaling matrices from the μ_k in step 4.

- It must be fitted the phase and magnitude in scaling matrices.

In general, the principal stages of D-G-K iteration can be shown in Fig. 4.12 and 4.13.

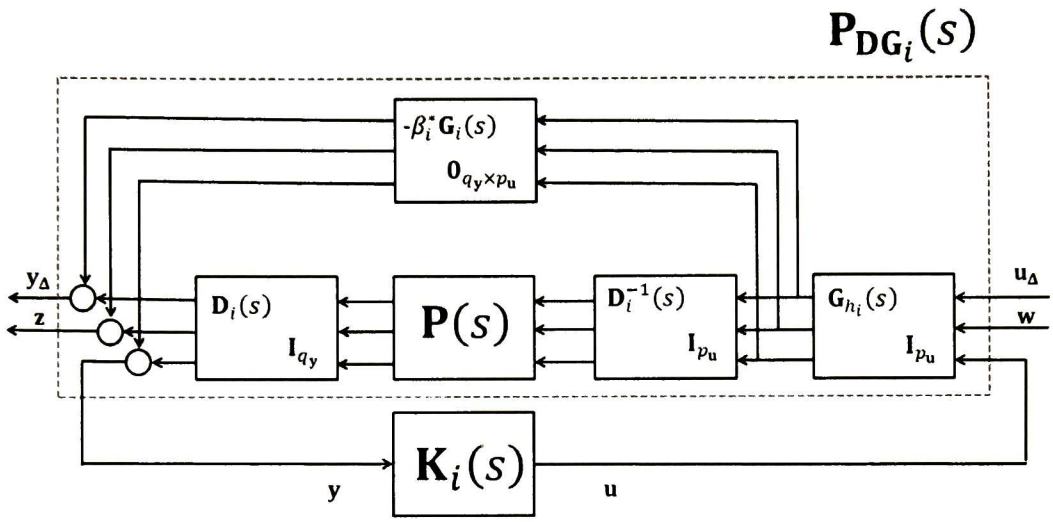

Fig. 4.12. $\mathbf{K}_i(s)$-step in D-G-K iteration.

The D-G-K iteration for controller synthesis with mixed perturbation sets $\mathbf{\Delta}$ provides a method which it is better that the D-K iteration. However, the D-G-K iteration is more complicated that the corresponding D-K iteration for complex perturbations. In essential, the fitting of scaling matrices are more complex due to the fact that the phase and magnitude must be fitted.

For large power systems the D-G-K iteration is impractical, even for small systems, since the iterations may converge slowly. This is an open problem that warrants further investigation,

In [14], the μ-K iteration was proposed as an alternative between mixed and complex μ iteration. Whereas the D-G-K iteration is a direct upper bound minimization, the μ-K iteration is an indirect upper bound. That is, the μ-K iteration does not have the structure of the SSV upper bound described by $[\mathbf{I} + \mathbf{G}_i(s)\mathbf{G}_i^T(-s)]^{-1} = \mathbf{G}_{h_i}(s)\mathbf{G}_{h_i}^T(-s))$. The structured of the μ-K iteration is constructed by applying two scaling to the original system (s), that is, it will be constructed a system $\mathbf{P}_{\mathbf{D}\Gamma}(s)$ with a $\mathbf{D}(s)$ scaling such that $\bar{\sigma}[F_l[\mathbf{P}_{\mathbf{D}\Gamma}(j\omega), \mathbf{K}(j\omega)]]$ approximates the complex μ upper bound and a $\mathbf{\Gamma}(s)$ scaling to shift from complex to mixed μ.

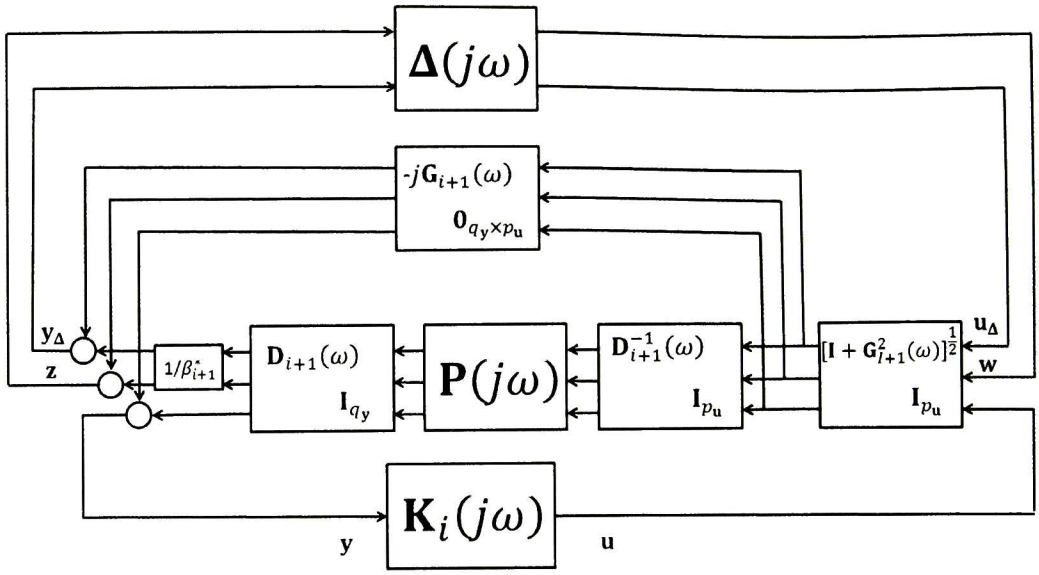

Fig. 4.13. $\mathbf{D}_{i+1}(\omega), \mathbf{G}_{i+1}(\omega)$ step in D-G-K iteration.

The μ -K iteration procedure can be summarized as follows:

1. Given the augmented system $\mathbf{P}(s)$, let $\gamma_0(s) = \mathbf{1}$, $\mathbf{D}_0(s) = \mathbf{I}$, express $\mathbf{P}_{\mathbf{D}\Gamma_0}(s)$ in the form

$$\mathbf{P}_{\mathbf{D}\Gamma_0}(s) = \begin{bmatrix} \gamma_0(s)\mathbf{I}_{y_\Delta} & \mathbf{0} \\ \mathbf{0} & \mathbf{I}_{p_y} \end{bmatrix} \mathbf{D}_0(s)\mathbf{P}(s)\mathbf{D}_0^{-1}(s) = \boldsymbol{\Gamma}_0(s)\mathbf{D}_0(s)\mathbf{P}(s)\mathbf{D}_0^{-1}(s) \tag{4.36}$$

$$\boldsymbol{\Gamma}_0(s)\mathbf{D}_0(s)\mathbf{P}(s)\mathbf{D}_0^{-1}(s) = \mathbf{P}(s)$$

2. Compute the $\mathcal{H}_\infty$ optimal controller $\mathbf{K}_0(s) = \mathbf{K}_1(s)$ a, nd $i = 1$.

$$\mathbf{K}_i(s) = \arg \min_{\mathbf{K}_i(s) \in \mathcal{K}_s} \|F_l[\mathbf{P}(s), \mathbf{K}_i(s)]\|_\infty \tag{4.37}$$

3. Compute the mixed and complex μ upper bounds $\mu_{\mathrm{C}}[F_l[\mathbf{P}(j\omega), \mathbf{K}_i(j\omega)]]$, $\mu_{\mathrm{M}}[F_l[\mathbf{P}(j\omega), \mathbf{K}_i(j\omega)]]$ where the scaling matrices $\mathbf{D}_i(\omega)$ are found solving the minimizations

$$\mathbf{D}_i(\omega) = \arg \min_{\mathbf{D}_i(\omega) \in \mathsf{D}} \{\bar{\sigma}[\mathbf{D}_i(\omega)F_l[\mathbf{P}(j\omega), \mathbf{K}_i(j\omega)]\mathbf{D}_i^{-1}(\omega)]\}, \forall\omega > 0 \tag{4.38}$$

4. Compute $\beta_i(\omega)$ given by:

$$\beta_i(\omega) = \frac{\mu_M[F_l[\mathbf{P}(j\omega),\mathbf{K}_i(j\omega)]]}{\mu_C[F_l[\mathbf{P}(j\omega),\mathbf{K}_i(j\omega)]]}\frac{1}{\gamma_{i-1}(j\omega)} - 1 \tag{4.39}$$

5. Fit, in magnitude, a stable minimum phase transfer function matrix $\mathbf{D}_i(s)$ to $\mathbf{D}_i(\omega)$ so that $\mathbf{D}_i(j\omega)$ approximates $\mathbf{D}_i(\omega)$ across frequency ω. Augmented $\mathbf{D}_i(s)$ with a unity matrix of appropriate size such that $\mathbf{D}_i(s)$ is compatible with $\mathbf{P}(s)$.

6. Determine an upper bound for the constant $\alpha_i \in [0;1]$ according to

$$\bar{\alpha}_i(\omega) = \begin{cases} \min\{1, \xi_i(\omega)\}, & if\ \beta_i(\omega) > 0 \\ 1, & if\ \beta_i(\omega) \leq 0 \end{cases} \tag{4.40}$$

where $\xi_i(\omega)$ is given by

$$\xi_i(\omega) = \left(\frac{\left\|F_l\left[\mathbf{P}_{\mathbf{D}\Gamma_{i-1}}(s),\mathbf{K}_{i-1}(j\omega)\right]\right\|_\infty}{\bar{\sigma}\left[F_l[\mathbf{D}_i(j\omega)\mathbf{P}(j\omega)\mathbf{D}_i^{-1}(j\omega),\mathbf{K}_i(j\omega)]\right]|\gamma_{i-1}(j\omega)|} - 1\right)\frac{1}{\beta_i(\omega)} \tag{4.41}$$

7. Choose a constant $\alpha_i = \kappa \inf_\omega \bar{\alpha}_i(\omega)$ where $\kappa \in [0;1]$ and compute for all ω:

$$\gamma_i(\omega) = (1-\alpha_i)|\gamma_{i-1}(j\omega)| + \alpha_i \frac{\mu_M[F_l[\mathbf{P}(j\omega),\mathbf{K}_i(j\omega)]]}{\mu_C[F_l[\mathbf{P}(j\omega),\mathbf{K}_i(j\omega)]]} \tag{4.42}$$

8. Construct

$$\mathbf{P}_{\mathbf{D}\Gamma_i}(s) = \begin{bmatrix} \gamma_i(s)\mathbf{I}_{y_\Delta} & \mathbf{0} \\ \mathbf{0} & \mathbf{I}_{p_y} \end{bmatrix} \mathbf{D}_i(s)\mathbf{P}(s)\mathbf{D}_i^{-1}(s) = \mathbf{\Gamma}_i(s)\mathbf{D}_i(s)\mathbf{P}(s)\mathbf{D}_i^{-1}(s) \tag{4.43}$$

9. Compute the $\mathcal{H}_\infty$ optimal controller:

$$\mathbf{K}_{i+1}(s) = \arg \min_{\mathbf{K}_{i+1}(s)\in\mathcal{K}_s} \|F_l[\mathbf{P}(s), \mathbf{K}_{i+1}(s)]\|_\infty \tag{4.44}$$

10. Compute the mixed and complex μ upper bounds $\mu_C[F_l[\mathbf{P}(j\omega), \mathbf{K}_{i+1}(j\omega)]]$, $\mu_M[F_l[\mathbf{P}(j\omega), \mathbf{K}_{i+1}(j\omega)]]$ where the scaling matrices $\mathbf{D}_{i+1}(\omega)$ are found solving the minimizations

$$\mathbf{D}_{i+1}(\omega) = \arg \min_{\mathbf{D}_i(\omega)\in\mathsf{D}} \{\bar{\sigma}[\mathbf{D}_{i+1}(\omega)F_l[\mathbf{P}(j\omega), \mathbf{K}_i(j\omega)]\mathbf{D}_{i+1}^{-1}(\omega)]\}, \forall\omega > 0 \tag{4.45}$$

11. Compute $\beta_{i+1}(\omega)$ given by:

$$\beta_{i+1}(\omega) = \frac{\mu_M[F_l[\mathbf{P}(j\omega),\mathbf{K}_{i+1}(j\omega)]]}{\mu_C[F_l[\mathbf{P}(j\omega),\mathbf{K}_{i+1}(j\omega)]]}\frac{1}{\gamma_i(j\omega)} - 1 \tag{4.46}$$

12. If $\sup_\omega|\beta_{i+1}(\omega)| > \sup_\omega|\beta_i(\omega)|$ return to 7 and reduce κ. Otherwise let $i = i + 1$.

13. Compare $\mathbf{D}_{i+1}(s)$ and $\gamma_i(s)$ with the previous scalings $\mathbf{D}_i(s)$ and $\gamma_{i-1}(s)$. Stop if they are close and $\sup_\omega|\beta_{i+1}(\omega)| \approx 0$. Otherwise repeat from step 5.

The $\mathbf{K}_i(s)$ and $\mathbf{D}_{i+1}(\omega), \gamma_i(\omega)$–step of μ-K iteration can be shown in Fig. 4.14 and 4.15.

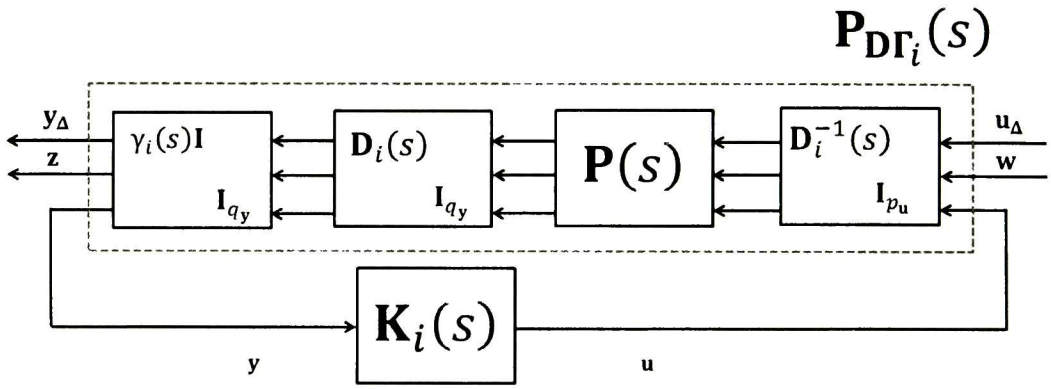

Fig. 4.14. $\mathbf{K}_i(s)$-step in μ-K iteration.

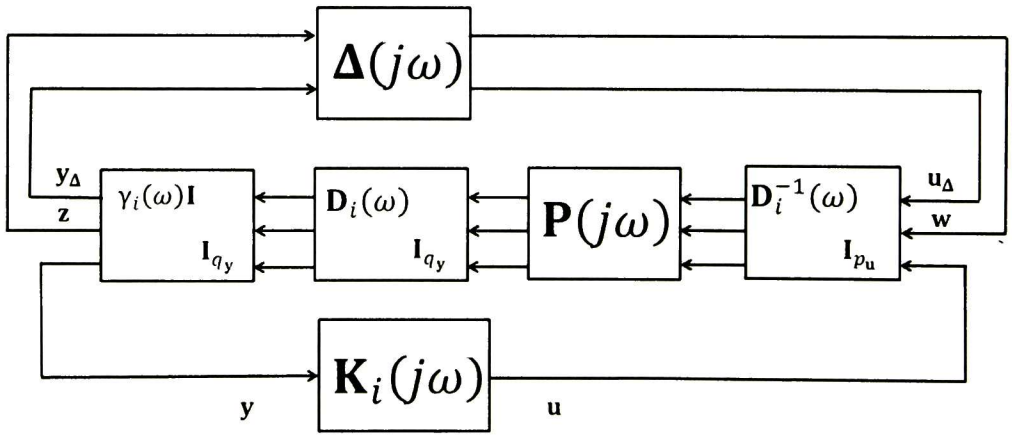

Fig. 4.15. $\mathbf{D}_{i+1}(\omega), \gamma_i(\omega)$-step in μ-K iteration.

An adverse limitation of a synthetized μ controller is its high-order obtained due to the interpolation theory in each element during the synthesis process; hence it is necessary to find a reduced-order controller. It is well known the notion of balanced realization and balanced truncation model reduction to obtain a low-order controller, in general, these topics can be seen in [12].

Another limitation is the lack of global convergence, but the synthesis process generally works well.

4.4 Comparison of synthesis techniques

Table 4.1 compares the main characteristics of the synthesis techniques described in this chapter in terms of the uncertainty model adopted, the computational implementation and the resulting reduced-order model. In general, $\mathcal{H}_\infty$ and $\mathcal{H}_2/\mathcal{H}_\infty$ can have unstructured uncertainty in some plants. On the other hand, μ-synthesis can have unstructured and structured uncertainty.

The third column describes the implementation of each technique for large power systems. It should be emphasized that the D-G-K iteration method is impractical for large power systems, even with a single perturbation parameter due to the number of generators in some networks. Finally, the fourth column gives a short description of each necessary reduced-order model for the nominal model and the obtained controller after synthesis process. Of particular interest, there does not exist a reduced-order model in literature of power systems, for the μ-synthesis framework, which takes into account the real perturbation. The D-K iteration has been implemented, but a reduced-order model with uncertainty may reduce computational costs.

Table 4.1.

Comparison of the synthesis techniques

Technique	Uncertainty model	Computational implementation	Reduced-order model
$\mathcal{H}_\infty$ based on Riccati equations	*Unstructured uncertainty*	*For large power systems*	*For the obtained controller*
$\mathcal{H}_\infty$ based on LMI technique	*Unstructured uncertainty*	*For large power systems 1*	*For the nominal model and the obtained controller*
$\mathcal{H}_2/\mathcal{H}_\infty$ based on LMI technique	*Unstructured uncertainty*	*For large power systems*	*For the nominal model and the obtained controller*
μ-synthesis based on D-K iteration	*Unstructured and structured uncertainty*	*For large power systems with one parameter*	*For the obtained controller*
μ-synthesis based on D-G-K iteration	*Unstructured and structured uncertainty*	*Impractical for large power systems*	*For the obtained controller*
μ-synthesis based on μ -K iteration	*Unstructured and structured uncertainty*	*Practical for large power systems*	*For the obtained controller*

In summary, the above table open new topics that must be resolved for large power systems with structured uncertainty. A model reduction with structured uncertainty could provide a framework in large power systems to use the D-G-K, the μ-K. On the other hand, a model reduction also may be interpreted as state order reduction for multi-dimensional systems.

4.5 Effect of communication time-delays

This section gives an introduction to investigate the feasibility of WADCs under the communication time-delays. Long time-delay may be a detriment to wide area damping stability, and such time-delays may degrade system robustness [29].

Time-delays are caused by the following factors [30]:

- Transducer delays
- Window size of the discrete Fourier transform (DFT)
- Processing time of PMU
- Data size of the PMU output
- Multiplexing and transitions
- Communication link involved
- Data processing and synchronizations

The total time-delays for different communications link, from the instant of data measured by the PMUs to the instant that the control signals arrive at control locations, are shown in Table 4.2 [31].

Time-delays are usually modeled by a first-order Padé approximation [32]. This approximation gives good phase approximation, but the time response presents a response at $t = 0$. A strictly proper second order approximation presented a slightly better approximation for larger time-delays in tests carried out in [33].

The transfer function is given by

$$e^{-sT} \approx g_d(s) = \frac{6-2Ts}{6+4Ts+(sT)^2} \tag{4.47}$$

where T is the time-delay.

From (4.47) the state-space representation is

$$\begin{bmatrix}\dot{\mathbf{x}}_d(t)\\ \mathbf{y}_d(t)\end{bmatrix} = \begin{bmatrix}\mathbf{A}_d & \mathbf{B}_d\\ \mathbf{C}_d & \mathbf{D}_d\end{bmatrix}\begin{bmatrix}\mathbf{x}_d(t)\\ \mathbf{u}_d(t)\end{bmatrix};$$

$$g_d(s): \left[\begin{array}{c|c}\mathbf{A}_d & \mathbf{B}_d\\ \hline \mathbf{C}_d & \mathbf{D}_d\end{array}\right]$$

where $\mathbf{x}_d(t)$, $\mathbf{u}_d(t)$ and $\mathbf{y}_d(t)$ represent the delay state vector, the input vector and the output vector, respectively.

Fig 4.16 represents the effect of the time-delays for a WADC, where u_{d_1} and y_{d_q} are the inputs and outputs of equation (4.47). Furthermore, T_{out_p} represents the time used for control signal calculations and transmission from the controller to control sites, and T_{inp_q} the time used for measurement processing, synchronization and transmission from PMUs to the centralized controller.

Table 4.2.

Time-delays for different communications links

Communication link	Associated delay (milliseconds)
Fiber-optic cables	1-10
Microwave links	100-150
Power line (PLC)	150-350
Telephone lines	200-300
Satellite link	10-100
Internet	100-1000

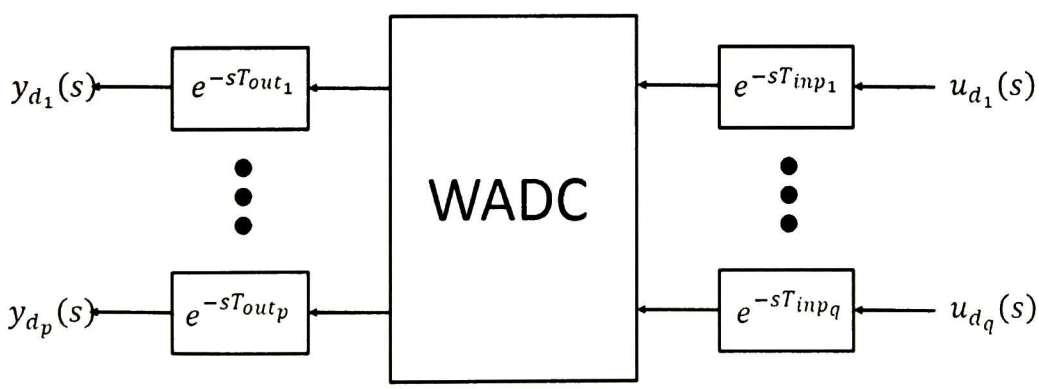

Fig 4.16. WADC with time-delays.

4.6 A general method to design wide-area damping controllers

In this section a general method is proposed to design WADC devices and hierarchical control configurations in large power systems based on analytical experience in Table 4.1. In light of the above discussion, the $\mathcal{H}_2$ /$\mathcal{H}_\infty$ technique to design MIMO controllers has been adopted. The analysis method includes five main steps:

Step-1) Small-signal analysis. In this step, modal analyses are conducted to determine the frequencies and damping ratios of all low-frequency electromechanical oscillations as well as to identify the critical inter-area modes.

Step-2) Robust stability analysis using the complex and mixed SSV. Obtain the framework to compute the SSV and check the robust stability of power system [3-5]. In this step, it is possible to include into the real parameter uncertainty a percent of complex uncertainty. In general, the expressions of sections 2.8 and 2.9 are used to study robust stability.

Step-3) Input-output pairings for MIMO and hierarchical control configurations. From small-signal stability analysis identify the most suitable input-output signals pairings using the method described in section 3.10. It should be emphasized that it is necessary to compute the closed loop interaction using the block GDRG. Then, a MIMO or SISO control device must be designed to evaluate the closed-loop interaction.

Step-4) Design of a WADC or block decentralized controller. Design a supplementary MIMO controller with the $\mathcal{H}_2$ /$\mathcal{H}_\infty$ technique using the tie-line currents, ΔI_{i-j}, and the speed deviations of generators, $\Delta\omega_i$. Fig. 4.17 represents this idea for a multimachine power system. If it is necessary to add another controller, then, absorb each designed control into the nominal linear system to avoid re-retuning of controllers. In general, it is necessary to return to step-1.

Step-5) Evaluate control performance under transient conditions. To verify the effect of controllers on the power system, perform non-linear time simulations under different scenarios.

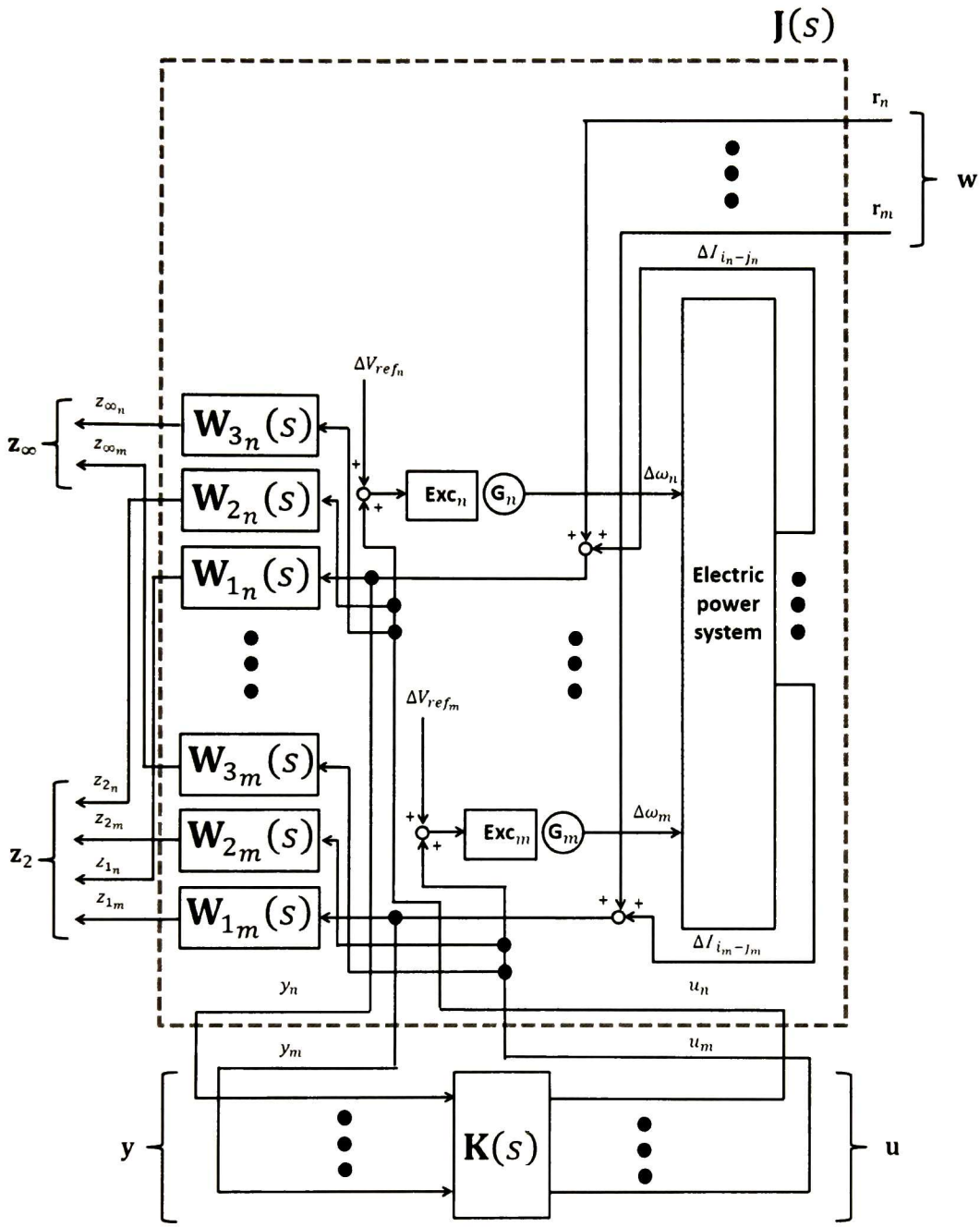

Fig. 4.17. General framework of a supplementary MIMO controller using line currents and speed deviations of generators.

4.7 Conclusions

In this chapter, a rigorously analytical approach to design WADCs with hierarchical control configurations has been proposed. First, the theory of synthesis of controllers to design robust controllers in power systems has been reviewed. Generally, the μ-K iteration and the D-K iteration can be viewed like a first synthesis approximation where parametric uncertainties have been taken account to solve the problem of μ-synthesis. Unfortunately, the problem is very complex for large power systems due to the scaling matrices. In addition, the size of power system lead to numerical limitations that are necessary to research in a deeper way.

Nevertheless, even with these limitations it is possible to design robust MIMO decentralized controllers using LMI techniques to damp electromechanical oscillations. In general, the proposed method provides the possibility to design different types of control configurations.

4.8 References

[1] P. Dorato, *Robust control*, IEEE Press, 1987, ISBN 0-87942-233-5.

[2] P. Young, "Robustness with Parametric and Dynamic Uncertainty," PhD thesis, California Institute of Technology, 1993.

[3] P. M. Young, and J. C. Doyle, "Properties of the mixed μ problem and its bounds," *IEEE Trans. Automat. Contr.*, vol. 41, pp. 155-159, Jan. 1996.

[4] M. K. H. Fan, A. L. Tits, and J. C. Doyle, "Robustness in the presence of mixed parametric uncertainty and unmodeled dynamics," *IEEE Trans. Automat. Contr.*, vol. 36, pp. 25-38, Jan. 1991.

[5] M. Morari, and E. Zafiriou, *Robust Process Control*, Prentice Hall, 1989, ISBN 0-13-782153-0.

[6] S. Buso, "Design of a robust voltage controller for a buck-boost converter using μ synthesis," *IEEE Trans. Control Systems Technology*, vol. 7, Mar. 1999.

[7] D.-W. Gu, P Hr Petkov and M. M. Konstantinov, *Robust control Design with Matlab*, Springer, 2005, ISB 1852339837.

[8] M. Fujita, T. Namerikawa, F. Matsumura, and K. Uchida, "μ synthesis of an electromagnetic suspension system, *IEEE Trans. Automat. Contr.*, vol. 40, pp. 530-536, Mar. 1995.

[9] P. M. Young and B. Bienkiewicz, "Robust controller design for the active mass driver benchmark problem,' in *Proc. 36th Conf. Decision and Control*, San Diego, Cal., Dec. 1997, pp. 2696-2701.

[10] P.M. Young, "Controller design with mixed uncertainties," in *Proc. American Control Conference*, Baltimore, Jun. 1994, pp. 2333-2337.

[11] R. P. Braatz, P. M. Young, J. C. Doyle, and M. Morari, "Computational complexity of μ calculation,' *IEEE Trans. Automat. Contr.*, vol. 39, pp.1000-1002, May. 1994.

[12] K. Zhou, and J. C. Doyle, *Essentials of Robust Control*, Prentice Hall, 1998, ISBN 0-13-525833-2.

[13] K. Zhou, J. C. Doyle. and K. Glover, *Robust and Optimal Control*, 1996, Prentice Hall, ISB 0134565673.

[14] S. Toffner-Clausen, "System identification and Robust Control: A synergistic Approach" PhD. Thesis, Aalborg University, 1995.

[15] H. H. Niemann, J. Stoustrup, S. Toffner-Clausen and P. Andersen, "μ synthesis for the coupled mass benchmark problem," in *Proc. American Control Conference*, Baltimore, Jun. 1997, pp. 2611-2615.

[16] S. Toffner-Clausen, *System Identification and Robust Control: A Synergistic Approach*, 1996, Springer, ISBN 3540760873.

[17] K. Glover and J.C. Doyle, "State-space formulae for all stabilizing controllers that satisfy an $\mathcal{H}_\infty$ norm bound and relations to risk sensitivity," *Systems and Control Letters*, vol. 11, pp. 167-172, Sep. 1988.

[18] B. Pal, and B. Chaudhuri, *Robust control in power systems*, Springer, 2005, ISNB 0-387-25949-X.

[19] Y. Zhang, and A. Bose, "Design of wide-area damping controllers for inter-area oscillations," *IEEE Trans. Power Syst.*, vol. 23, pp. 1136-1143, Aug. 2008.

[20] M. Chilali and P. Gahinet, "$\mathcal{H}_\infty$ design with pole placement constraints: an LMI approach,' *IEEE Trans. Automat. Contr.*, vol. 41, pp. 358-367, Mar. 1996.

[21] M. Djukanovic, M. H. Khammash, and V Vittal, "Application of structured singular value theory for robust stability and control analysis in multimachine power systems part-I: Framework development," *IEEE Trans. Power Systems*, vol. 13, pp. 1311-1316, Nov. 1998.

[22] M. Djukanovic, M. H. Khammash, and V. Vittal, "Application of structured singular value theory for robust stability and control analysis in multimachine power systems part-II: Numerical simulations and results," *IEEE Trans. Power Systems*, vol. 13, pp. 1317-1322, Nov. 1998.

[23] R. Castellanos, A. R. Messina, and H. Sarmiento, "Robust stability analysis of large power systems using the structured singular value theory," *Electric Power and Energy Systems*, vol. 27, pp. 389-397, Jun. 2005.

[24] M. Djukanovic, M. Khammash, and V. Vittal, "Sequential synthesis of structured singular value based decentralized controllers in power systems, *IEEE Trans. Power Systems*, vol. 14, pp. 635-641, May. 1999.

[25] X. Yu, and M. Khammash, and V. Vittal, "Robust design of a damping controller for static var compensators in power systems,' *IEEE Trans. Power Systems*, vol. 16, pp. 456-462, Aug. 2001.

[26] M. Yue, and R. A. Schlueter, "μ-synthesis power system stabilizer design using a bifurcation subsystem based methodology," *IEEE Trans. Power Systems*, vol. 18, pp. 1497-1506, Nov. 2003.

[27] M. Yue, and R. A. Schlueter, "Robust control designs for multiple bifurcations,' *IEEE Trans. Power Systems*, vol. 20, pp. 301-311, Feb. 2005.

[28] G. E. Boukarim, S. Wang, J. H. Chow, G. N. Taranto, and N. Martins, "A comparison of classical, robust and decentralized control design for multiple power system stabilizers," *IEEE Trans. Power Systems*, vol. 15, pp. 1287-1292, Nov. 2000.

[29] B. Chaudhuri, R. Majumder, and B. C. Pal, "Wide-Area measurement-based stabilizing control of power system considering signal transmission delay," *IEEE Trans. Power Syst.*, vol. 19, pp. 1971-1979, Nov. 2004.

[30] K. E. Holbert, G. T. Heydt, and H. Ni, "Use of satellite technologies for power system measurements, command, and control," Proceedings of the IEEE, vol. 93, pp. 947-955, May 2005.

[31] Y. Zhang, "Design of wide-area damping control systems for power system low-frequency inter-area oscillations," PhD thesis, Washington State University, 2007.

[32] J. H. Chow, J. J. Sanchez-Gazca, R. Haoxing, and S. Wang, "Power system damping controller design using multiple input signals, *IEEE Control Syst. Mag.*, vol. 20, no. 4, pp. 82–90, Aug. 2000.

[33] D. Dotta, A. S. Silva, and I. C. Decker, "Wide-area measurements-based two-level control design considering signal transmission delay" *IEEE Trans. Power Syst.*, vol. 24, pp. 208-216, Feb. 2009.

Chapter 5
Applications

This chapter examines the application of the general method proposed in chapter 4 to damp electromechanical oscillations: the robustness analysis and the input-output pairings to design block decentralized and a hierarchical control configurations. These original contributions for power systems are evaluated in the Mexican interconnected system.

First, eigenanalys is performed to identify the critical system modes. Then, the robust analysis framework is used to compute the SSV A block relative gain approach is utilized to determine the best input-output pairing for MIMO system control. LMI techniques are finally employed to design WADCs. In general, this systematic method allows better coordination of control capabilities, and the use of interaction measures allows to help in the choice of control location and structure.

Two basic control structures are investigated and used to benchmark the proposed control structure: a block decentralized control structure, and a hierarchical control structure.

Application studies on a realistic test power system show that hierarchical and block decentralized control structures using remote measurements from phasor measurement units are very effective to damp both, local and inter-area modes.

The effects of latency, uncertainty in system behavior, and interactions among controllers are investigated in detail. Detailed nonlinear time simulations are conducted to verify the efficiency of the proposed design methodologies.

5.1 Application to a large test system

A 5-area, 189-bus model of the Mexican interconnected system (MIS) is used to illustrate the proposed general method. A simplified schematic diagram of this system illustrating the location of geographical areas representing regional systems and major interfaces of concern is shown in Fig. 5.1. System studies are based on a system model that includes representations of the northern, northeastern, western, central, southeastern and peninsular areas of the system.

The basic characteristics of this system are described in previous work [1, 2].

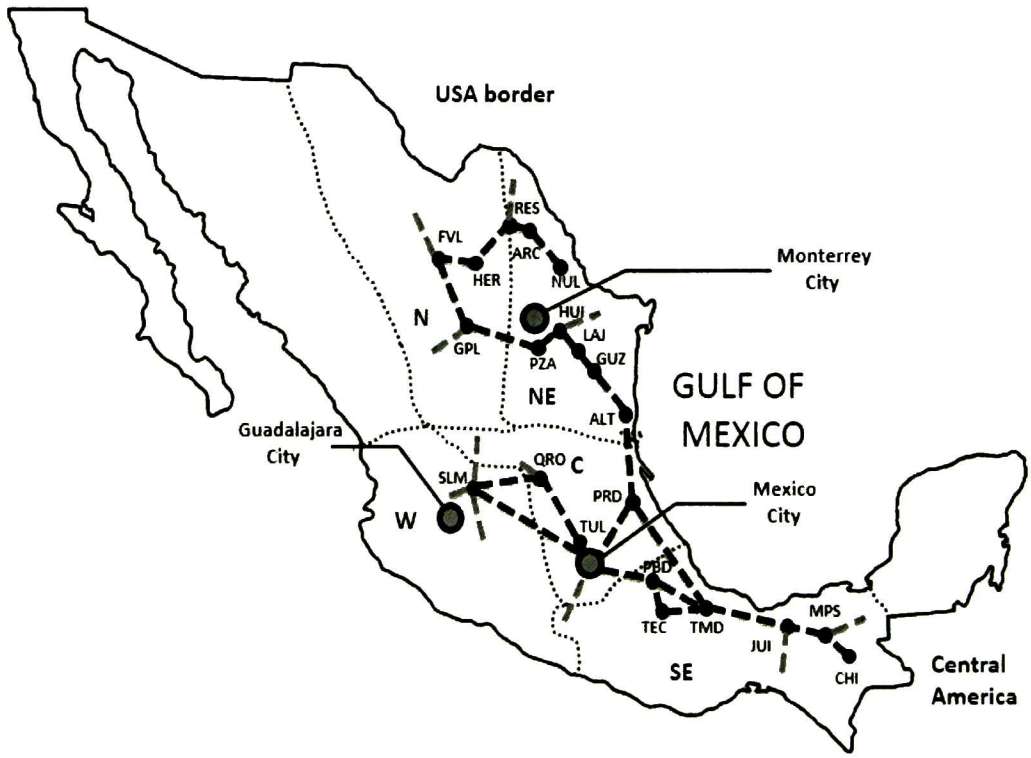

Fig. 5.1. Simplified geographical representation of the MIS showing the location of major generators and transmission paths.

5.2 Modeling considerations

The base case scenario for the MIS includes two Static VAR Compensators (SVCs) at the 400 kV substations TMD and GUZ. These locations provide ideal voltage regulation which are the primary function of the SVCs. For the

purposes of this study, the loads are represented by constant impedance. Each generator is represented by a fourth-order model equipped with a static exciter. The linearized state-space model of the power system representation has 249 states.

In order to compute the $\mathbf{M}(s) - \mathbf{\Delta}(s)$ framework described in Chapter 2 for the evaluation of the robust stability without controllers, loads at buses GUZ-400 and MTY-115 are considered as uncertain parameters and varied from 10 MW and 300 MW to 400 MW and 600 MW, respectively. At this operating change, the system is dominated by the plant modes.

As the operating conditions change, the state space matrices of the linearized power system also change. The peak of μ^{-1} provides assessment of the maximum allowable value of all varying parameters, which are simultaneously increased form their mid-point values. As discussed before, the robustness of a power system will not be robustly stable for a given operating range if $\mu > 1$. From the robustness analysis described by μ, two control schemes are proposed and compared in this work to damp electromechanical oscillations for the MIS.

Case study 1: Block decentralized control.

From the nominal model and its eigenvalue analysis, a pair of block decentralized controllers is proposed as a first control alternative following the approach in Chapter 3. Then, the peak of the BRG is evaluated, which is represented by $\|[\boldsymbol{\lambda}(s)]_{ii}\|_{\infty}$, to describe interactions among control loops. If block pairings have strong interaction in a specific range of frequency each control cannot be designed independently. For this option it was enough to design two WADCs based on LMI techniques without hierarchical configuration for electromechanical modes. Finally, the performance of controllers were evaluated by time domain simulation in order to verify the design effectiveness in the non-linear system.

Case study 2: Hierarchical control configuration.

This control configuration takes into account the same nominal model described for the Case 1. This case implements a hierarchical control configuration with a previous study of block pairings for non-square MIMO controllers to damp inter-area modes. For local modes PSSs are designed. Detailed non-linear time simulations are computed to verify the design effectiveness.

Finally, in order to compare Cases 1 and 2, small signal analyses, non-linear time simulations, the SSV and latency analyses are computed to compare the improved damping of modes with WADCs.

5.3 Case 1: Design of block decentralized controllers

5.3.1 Small-signal analysis

Conventional eigenanalysis was first performed on the linear system representation in order to precisely identify the nature of oscillatory behavior. Once the estimated stability was computed, uncertainty analysis was used to estimate robust stability as well as to design system controllers.

The 5-area test system exhibits three major inter-area modes. In addition, three local modes of interest to damp with local controllers, but for this case the main purpose will be to damp inter-area modes. Table 5.1 summarizes the main characteristics of these modes. Based on system-wide information, the use of WADCs at critical machines is investigated.

Table 5.1.

Slowest inter-area electromechanical modes of the MIS. Base case with no controllers

Mode	Eigenvalue	Freq. (Hz)	Damp. Factor	Swing pattern
Inter-area mode 1	-.0769 ±j2.6975	0.42	0.028	Northeastern system vs southeastern system
Inter-area mode 2	-.1916 ±j3.6439	0.58	0.052	Northern system vs. Northeastern system
Inter-area mode 3	-.1338 ±j4.8535	0.77	0.027	Western system and southeastern system
Local mode 4	-.1926 ±j6.4254	1.02	0.030	Southeastern system
Local mode 5	-.2636 ±j7.0585	1.12	0.037	Southeastern system
Local mode 6	-.2536 ±j7.7506	1.23	0.032	Northeastern system

5.3.2 Robust stability analysis using the complex and mixed SSV

As indicated previously, a case with two parameter variation, in which load at buses GUZ-400 [0.1-4 p. u.], and MTY-115 [3-6 p. u.] are allowed to vary simultaneously is chosen to illustrate the robust design techniques. This case is chosen to illustrate worst-case parameter combinations or uncertainties occurring simultaneously at different locations in the system.

The upper bound of the complex and mixed SSV are plotted in Fig. 5.2 as a function of frequency, for the frequency range associated with the inter-area modes of concern. The lower bound of the mixed SSV is zero, which is associated with pure real uncertainties. Note that the proximity of the lower bound and upper bound of the complex SSV implies that the calculation of μ

is very accurate in this case. In addition, the peaks for the complex and mixed case are 2.7766 at frequency 0.4341 and 1.3813 at frequency 0.4501, respectively. This means that there are two types of perturbation matrices $\mathbf{\Delta}$ such that $\|\mathbf{\Delta}\|_\infty = \frac{1}{2.7766}$ for the complex case and $\|\mathbf{\Delta}\|_\infty = \frac{1}{1.3813}$ for the real pure case, which can be constructed to destabilize the system, due to fact that $\mu > 1$. Robust stability analysis results three dominant modes of oscillation at 0.42 Hz, 0.58 Hz, 0.77 Hz, and 1.23 Hz associated with major inter-area and local modes.

Of note, simulation results in Fig. 5.2 shows that the system does not have robust stability with complex (dotted line) and mixed SSV (solid line). The dimensions of the perturbations matrices are:

$$\mathbf{\Delta} := \{\text{diag}[\delta_1^c \mathbf{I}_{417\times417}, \delta_2^c \mathbf{I}_{278\times278}]: \delta_1^c,\ \delta_1^c \in \mathbb{C}\}$$

$$\mathbf{\Delta} := \{\text{diag}[\delta_1^r \mathbf{I}_{417\times417}, \delta_2^r \mathbf{I}_{278\times278}]: \delta_1^r,\ \delta_2^r \in \mathbb{R}\}$$

for the complex and real case, respectively. In addition, Fig. 5.3 represents the LFT form of $\dot{\mathbf{x}}(t) = \mathbf{A}[\mathbf{\Delta}]\mathbf{x}(t)$.

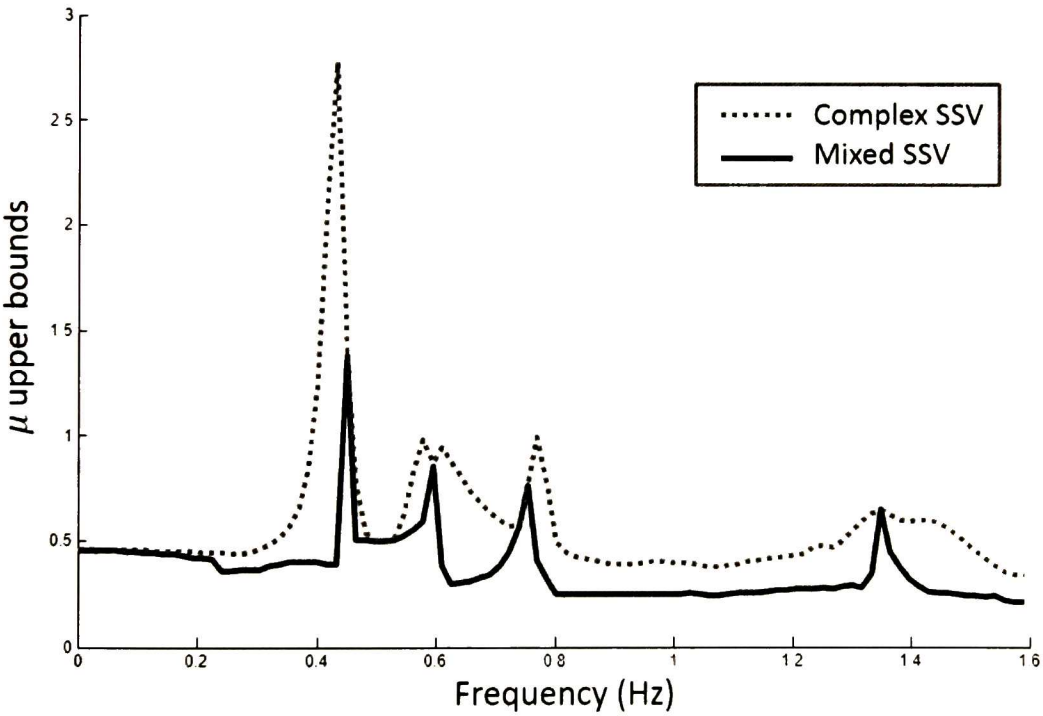

Fig. 5.2. Complex and mixed SSV of the MIS without controllers.

Figure 5.4 shows the results of the upper bound and the lower bound of the mixed SSV without and with 1% and 4% of complex uncertainty; the

differences are imperceptible for the upper bounds with and without 1%. Nevertheless, the lower bounds of the mixed SSV with a percent of complex uncertainty (dotted line) are not zero.

From Fig. 5.4 the lower bound and the upper bound are close with 4% percent of complex uncertainty near the inter-area and local mode at 0.4501 Hz and 1.3504 Hz, respectively, which means that the accuracy is good.

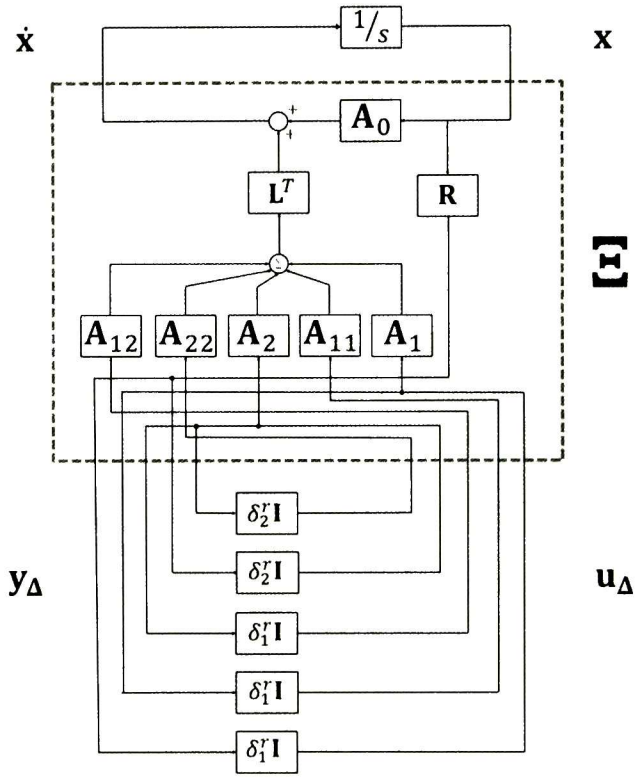

Fig. 5.3. LFT form of $\dot{\mathbf{x}}(t) = \mathbf{A}[\boldsymbol{\Delta}]\mathbf{x}(t)$.

The dimension of the perturbations matrix for the mixed case with 1% and 4% of complex uncertainty is given by

$$\boldsymbol{\Delta} := \{\text{diag}[\delta_1^r \mathbf{I}_{417\times417},\ \delta_2^r \mathbf{I}_{278\times278}, \delta_1^c \mathbf{I}_{417\times417}, \delta_2^c \mathbf{I}_{278\times278}] : \delta_1^r,\ \delta_2^r \in \mathbb{R}, \delta_1^c,\ \delta_2^c \in \mathbb{C}\}$$

With this representation of the perturbation, the differential equation $\dot{\mathbf{x}}(t) = \mathbf{A}\mathbf{x}(t)$ and the uncertainty, $\boldsymbol{\Delta}$, can be represented as in Fig. 5.5. Finally, the peak of the μ-plot over $\propto^2$ from $\propto = 0\,\%$ to $\propto = 4\,\%$, which represents the percent of complex uncertainty, is listed in Table 5.2. The upper bound is always larger than 1. However, for the particular cases $\propto^2 = 1\,\%$ and $\propto^2 = 1.25\,\%$ ($\propto = 10\,\%$ and $\propto = 11.18\,\%$) the lower bound suffer of a discontinuity

near inter-area mode at 0.4501 Hz. In general the μ lower bound test with a percent complex uncertainty is a good approximation to approximate the SSV.

To summarize, the system without controllers does not have robust stability for the uncertainty range considered in the analysis using the complex and mixed SSV. Controllers are then designed to meet robust stability at each of the operating scenarios.

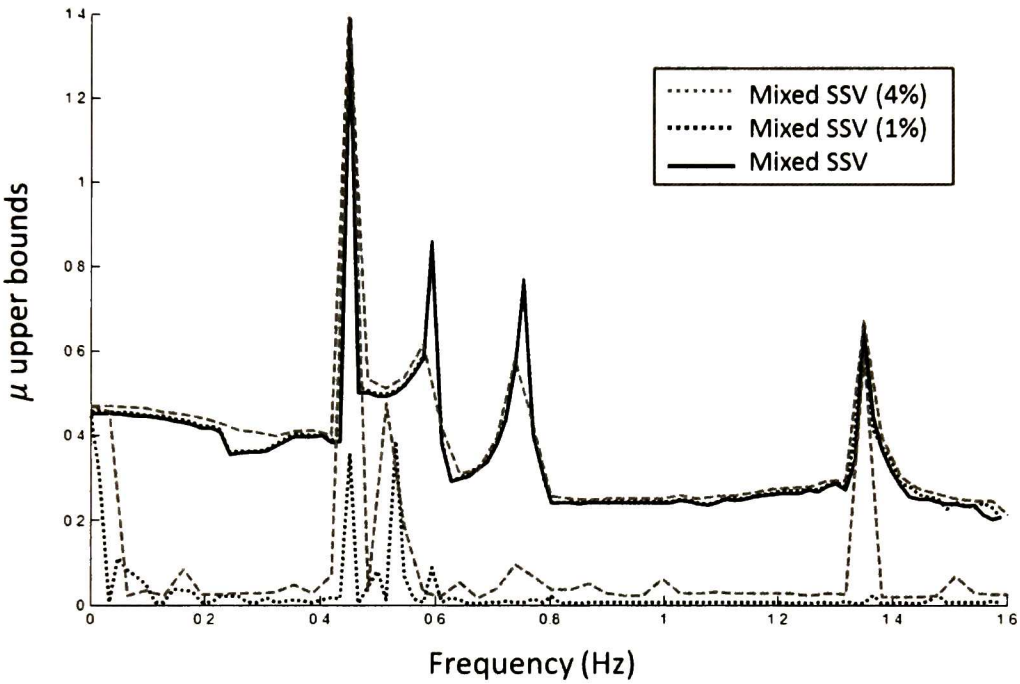

Fig. 5.4. Mixed SSV without and with 1% and 4% of complex uncertainty.

Table 5.2.

Mixed SSV with a percent of complex uncertainty $\propto^2$

$\propto^2$	Upper bound	Lower bound
0.0000 %	1.3813	0.0000
0.0625 %	1.3831	1.2246
0.2500 %	1.3870	1.3147
0.5600 %	1.3917	1.3305
0.7500 %	1.3950	1.3430
1.0000 %	1.3966	0.3616
1.2500 %	1.4000	0.4289
1.5600 %	1.4068	1.3546
2.2500 %	1.4167	1.3663
3.0600 %	1.4283	1.3795
4.0000 %	1.4415	1.3942

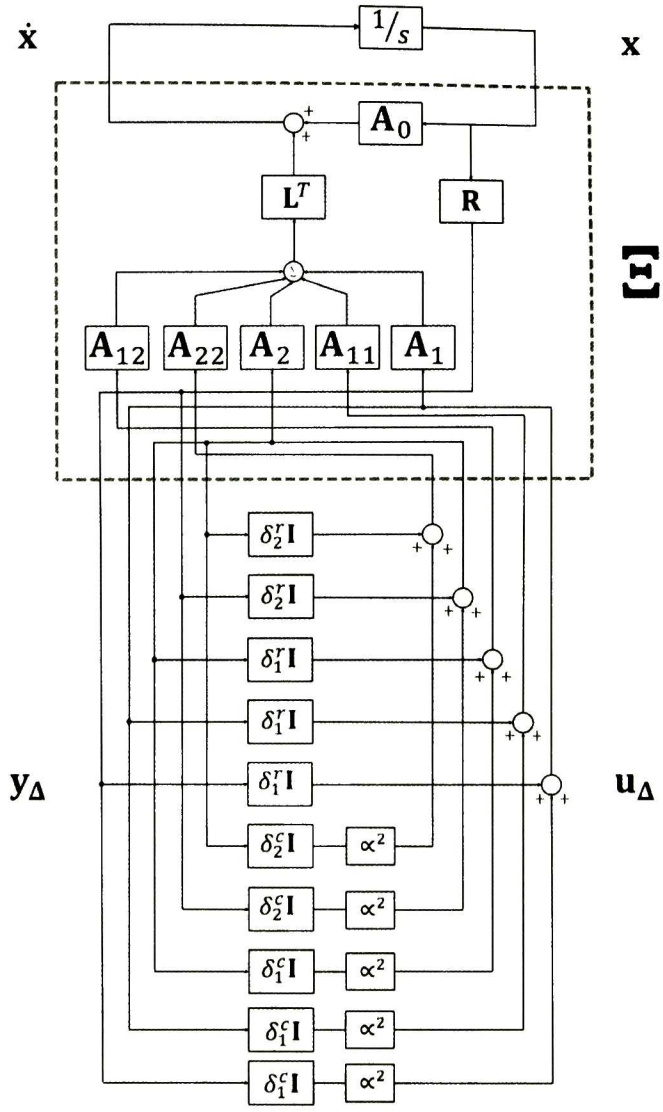

Fig. 5.5. LFT form of $\dot{\mathbf{x}}(t) = \mathbf{A}[\boldsymbol{\Delta}]\mathbf{x}(t)$ with a percent of complex uncertainty.

5.3.3 Controllability and observability analysis

Table 5.3 shows selected control sites and input signals to the WADCs. The analysis of controllability and observability measures in Table 5.2 indicates that machines in the southwestern (MPU) and northern (MTY, HUI,CRB) systems are expected to enhance damping of both, inter-area modes 1 and 2 at 0.42 Hz and 0.58 Hz, respectively.

Inter-area mode 2 is of little interest here because it has a low joint controllability/observability measure. Machines in the southwestern and

western systems, on the other hand, are the most efficient machines for damping inter-area mode 3 at 0.77 Hz.

From this analysis, seven sets of input-output pairings are proposed to allocate two MIMO WADCs. For this particular case, each MIMO control only has two-input two-output channels from PMUs to generators.

Table 5.3.

Geometric measures of controllability and observability

Mode	Maximum m_{ci}	Maximum m_{oi}
Inter-area mode 1	Gen_{MPU} (0.1667E-4), Gen_{MTY1} (0.2735E-4), Gen_{MTY4} (0.4035E-4), Gen_{HUI} (0.2026E-4), Gen_{CRB} (0.2996E-4)	$I_{GUZ4\text{-}ALT4}$ (0.1333), $I_{GUZ4\text{-}HUI4}$ (0.1329), $I_{HUI4\text{-}LAJ4}$ (0.1276), $I_{LAJ4\text{-}GUZ4}$ (0.1319), $I_{PRD4\text{-}ALT4}$ (0.0753)
Inter-area mode 2	Gen_{SYC} (0.2973E-4), Gen_{MTY1} (0.2785E-4), Gen_{MTY4} (0.4741E-4), Gen_{HUI} (0.2734E-4), Gen_{CRB} (0.4139E-4)	$I_{GUZ4\text{-}ALT4}$ (0.1152), $I_{GUZ4\text{-}HUI4}$ (0.1165), $I_{HUI4\text{-}LAJ4}$ (0.1099), $I_{LAJ4\text{-}GUZ4}$ (0.1138), $I_{RES2\text{-}ARC2}$ (0.1207), $I_{ARC1\text{-}NUL1}$ (0.1149), $I_{MTY13\text{-}FAL1}$ (0.1244), $I_{MTY13\text{-}MTY11}$ (0.1244), $I_{PRD4\text{-}ALT4}$ (0.0680), $I_{ARC2\text{-}ARC1}$ (0.1191)
Inter-area Mode 3	Gen_{CHI} (0.1416E-4), Gen_{MPU} (0.3628E-4), Gen_{SLM} (0.2948E-4), Gen_{SLP} (0.3579E-4), Gen_{MZN} (0.3268E-4), Gen_{MAD} (0.2437E-4)	$I_{MPU4\text{-}MNDC}$ (0.0647), $I_{MNDC\text{-}MND4}$ (0.0625), $I_{CHI4\text{-}JUI4}$ (0.0786), $I_{JUIC\text{-}TMD4}$ (0.0787), $I_{JUIC\text{-}JUI4}$ (0.0787), $I_{TMD4\text{-}PBDC}$ (0.0770), $I_{PBDC\text{-}PBD4}$ (0.0755), $I_{TMD4\text{-}TECC1}$ (0.0774), $I_{TEC4\text{-}TECC1}$ (0.0755), $I_{TEC4\text{-}TECC2}$ (0.0788), $I_{TECC2\text{-}TOP4}$ (0.0788), $I_{PBD4\text{-}TEX2}$ (0.0767), $I_{SNB4\text{-}TOP4}$ (0.0772)
Local Mode 4	Gen_{CAR1} (0.4869E-4)	$I_{MEZ2\text{-}ZAP2}$ (0.1142), $I_{MEZ2\text{-}CAR2}$ (0.1053), $I_{ZAP2\text{-}ARC1}$ (0.1094), $I_{CAR2\text{-}CAR1}$ (0.1057)
		ω_{CAR1} (0.0030)
Local Mode 5	Gen_{LGV1} (0.6709E-4)	$I_{TEM4\text{-}TMD2}$ (0.1010)
		ω_{LGV1} (0.0014)
Local Mode 6	Gen_{RIB1} (1.1230E-4)	$I_{AER1\text{-}RIB1}$ (0.1118), $I_{AER2\text{-}RIB2}$ (0.1055), $I_{HUI4\text{-}AER2}$ (0.1311)
		ω_{RIB2} (0.0032)

5.3.4 BRG analysis for the proposed candidate sets

Fig. 5.6 shows the largest singular values of the BRG for the sets described in Table 5.4. In each case, the horizontal axis represents the frequency given in Hz and the vertical axis is the magnitude of the largest singular values of BRG described by $\bar{\sigma}[\boldsymbol{\lambda}]_{ii}$.

Thus, for instance, the set 1 represents the inputs-outputs from $I_{GUZ4\text{-}ALT4}$-$I_{LAJ4\text{-}GUZ4}$ to Gen_{MTY4}-Gen_{CRB} and the inputs-outputs from $I_{MPU\text{-}MNDC}$–$I_{MNDC\text{-}MND2}$ to Gen_{CHI}-Gen_{MPU}; the corresponding BRG is described by $\bar{\sigma}[\lambda]_{11}$ and $\bar{\sigma}[\lambda]_{22}$, respectively. Examination of these results shows that the sets 1 and 2 are the most suitable block input-output pairings because they have strong interaction near inter-area modes which is located at 42 Hz.

Sets 3 to 7, on the other hand, have low interactions but these input-output pairings can have a degradation in the performance which is an undesirable characteristic when damping inter-area oscillations, but it is necessary to study the closed-loop interaction without integral feedback. Furthermore, local modes present a strong interaction of the described set 1 by the BRG analysis; these frequency characteristics must be considered if local modes are being modified by means of supplementary local controllers.

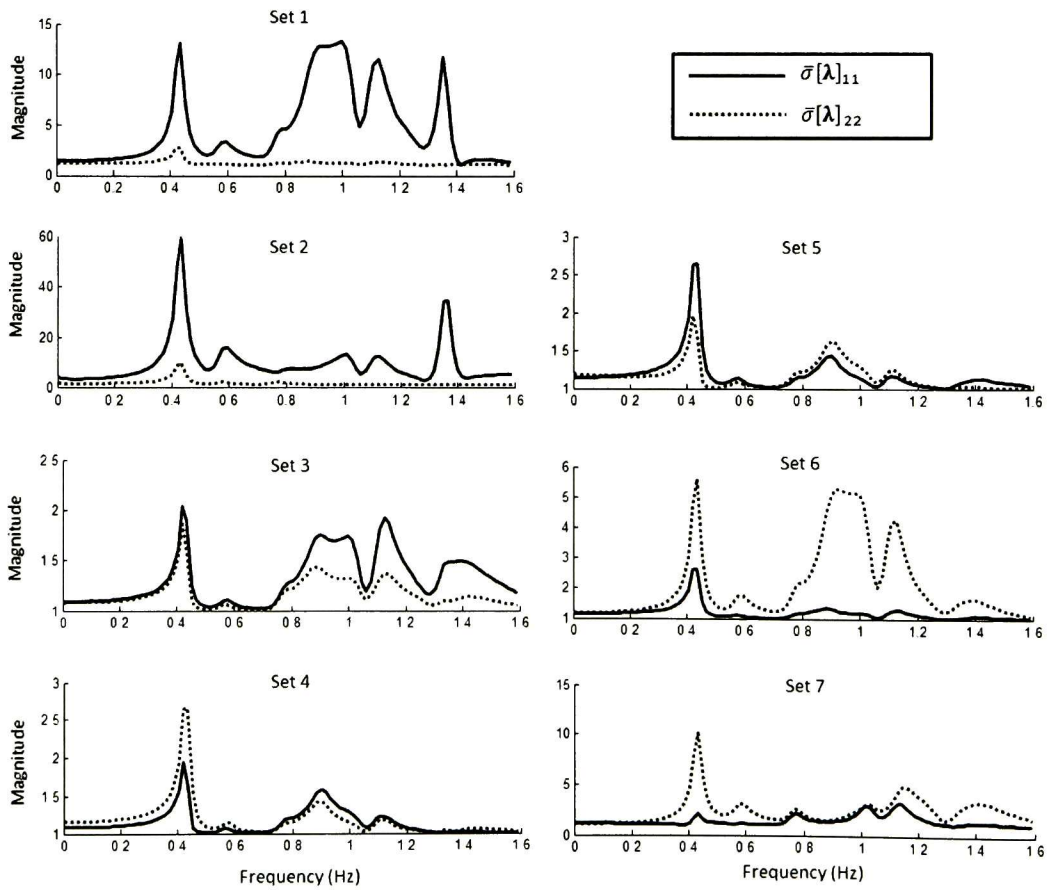

Fig. 5.6. Frequency response of the BRG for the candidate sets.

Table 5.4.

Peak of the BRG for the candidate sets of WADCs

Set No.	Output signals from WADC to u	Input signals to WADCs	$\|[\lambda(s)]_{ii}\|_\infty$
Set 1	Gen_{MTY4}-Gen_{CRB}	$I_{GUZ4\text{-}ALT4}$ - $I_{LAJ4\text{-}GUZ4}$	13.22
	Gen_{CHI}-Gen_{MPU}	$I_{MPU4\text{-}MNDC} - I_{MNDC\text{-}MND4}$	2.64
Set 2	Gen_{MTY4}-Gen_{CRB}	$I_{GUZ4\text{-}ALT4}$ - $I_{LAJ4\text{-}GUZ4}$	59.19
	Gen_{CHI}-Gen_{SLP}	$I_{MPU4\text{-}MNDC} - I_{TOP4\text{-}SNB4}$	9.67
Set 3	Gen_{MTY1}-Gen_{MTY4}	$I_{GUZ4\text{-}ALT4} - I_{GUZ4\text{-}HUI4}$	1.86
	Gen_{CHI}-Gen_{MPU}	$I_{CHI4\text{-}JUI4} - I_{JUI\text{-}TMD4}$	2.04
Set 4	Gen_{MTY1}-Gen_{MTY4}	$I_{PRD4\text{-}ALT4} - I_{GUZ4\text{-}ALT4}$	1.94
	Gen_{CHI}-Gen_{MPU}	$I_{MPU4\text{-}MNDC} - I_{MNDC\text{-}MND4}$	2.65
Set 5	Gen_{MZD}-Gen_{MTY4}	$I_{PRD4\text{-}ALT4} - I_{GUZ4\text{-}ALT4}$	1.97
	Gen_{CHI}-Gen_{MPU}	$I_{MPU4\text{-}MNDC} - I_{MNDC\text{-}MND4}$	2.65
Set 6	Gen_{MZD}- Gen_{CRB}	$I_{GUZ4\text{-}ALT4} - I_{LGV2\text{-}LAJ4}$	5.60
	Gen_{CHI}-Gen_{MPU}	$I_{MPU4\text{-}MNDC} - I_{MNDC\text{-}MND4}$	2.64
Set 7	Gen_{SLM}- Gen_{MZN}	$I_{GUZ4\text{-}ALT4} - I_{LGV2\text{-}LAJ4}$	10.07
	Gen_{CHI}-Gen_{MPU}	$I_{MPU4\text{-}MNDC} - I_{MNDC\text{-}MND4}$	3.21

5.3.5 Design of block decentralized controllers

The weighting functions used in the design of the WADCs of the sets 1 and 2, are given in Table 5.5. As discussed in the introductory section of the chapter, the test system has 249 states originally. To apply the synthesis process the system is reduced first to a 12-order model by the method of balanced reduction.

Following the optimization and synthesis procedure, the order of the first controller was reduced using a balanced realization and was absorbed in the transfer function of the full-order nominal model. A similar process was adopted for the design of the second controller for the set 1. Column 5 in Table 5.5 shows the size of the reduced-order model (in parenthesis) for each synthesis process and the size of each reduced-order controller.

Table 5.5.

Weighting functions for the sets 1 and 2 of WADCs

Set No.	$W_1(s)$	$W_2(s)$	$W_3(s)$	Reduced-order model
Set 1	$(s + 20)/(.1s + 100)$	1E-2	$100/(s + 10)$	(12) 9
	1	10	$11/(s + 10)$	(17) 7
Set 2	$(s + 20)/(.1s + 100)$	1E-2	$100/(s + 10)$	(12) 9
	1	10	$11/(s + 10)$	(18) 8

5.3.6 Assess control loop interaction using the magnitude of the block GDRG for the designed damping controllers

Fig 5.7 shows the largest singular values of the block GDRG for the sets 1 and 2 where the differences for inter-area modes are imperceptible. Table 5.6 identifies the set 1 as the most suitable option to damp the inter-area oscillations with good performance. Nevertheless note that the peaks, which are represented by $\left\|[\tilde{\lambda}(s)]_{11}\right\|_\infty$ and $\left\|[\tilde{\lambda}(s)]_{22}\right\|_\infty$ are near to local mode frequencies. This condition must be considered in the local controllers design.

Table 5.6.

Peak of the block GDRG for the candidate sets of WADCs

Set No.	Output signals from WADC to u	Input signals to WADC	$\left\|[\tilde{\lambda}(s)]_{ii}\right\|_\infty$
Set 1	Gen_{MTY4}-Gen_{CRB}	$I_{GUZ4\text{-}ALT4}$ - $I_{LAJ4\text{-}GUZ4}$	271.83
	Gen_{CHI}-Gen_{MPU}	$I_{MPU4\text{-}MNDC} - I_{MNDC\text{-}MND4}$	9.97
Set 2	Gen_{MTY4}-Gen_{CRB}	$I_{GUZ4\text{-}ALT4}$ - $I_{LAJ4\text{-}GUZ4}$	270.68
	Gen_{CHI} - Gen_{SLP}	$I_{MPU4\text{-}MNDC} - I_{TOP4\text{-}SNB4}$	9.88

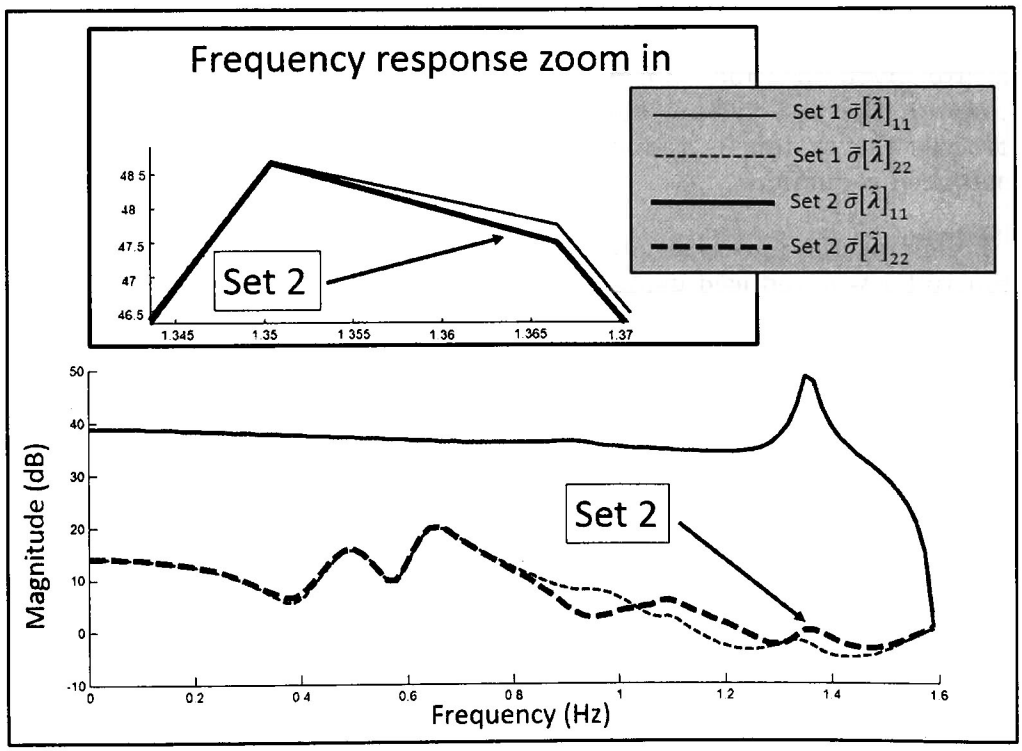

Fig. 5.7. Frequency response of the block GDRG for the sets 1 and 2.

5.3.7 Control performance under transient conditions

Detailed transient stability studies were performed to verify and compare the effect of WADCs on system dynamic performance under large disturbances. Cases of interest included three-phase faults applied at buses *CHI4* and *LAJ4* in the southeastern and northwestern systems, respectively.

These contingency scenarios are found to stimulate major inter-area modes. Fig 5.8 shows the system response following a three-phase stub fault with and without WADCs for each set on bus *CHI4*. Note that the set 2 is the most suitable option for this type of supplementary controllers since the damping characteristic is notorious while the set 1 presents a performance degradation in terms of damping the power oscillation. Furthermore, for purposes of clarity Fig. 5.9 represents the control configuration for the set 1.

Similar conclusions can be drawn from the analysis of Fig. 5.10. Both options show a good damping characteristic with the set 1 being a slightly better option. In general, the sets 1 and 2 demonstrate similar performance under both, steady-state and transient conditions.

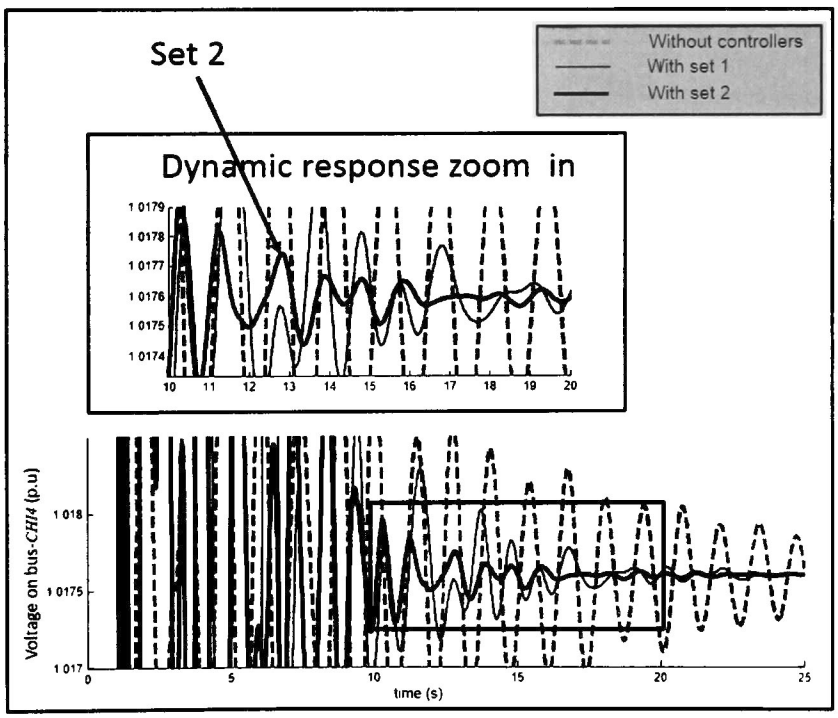

Fig. 5.8. Bus voltage magnitude at 400-kV bus *CHI4* for the sets 1 and 2.

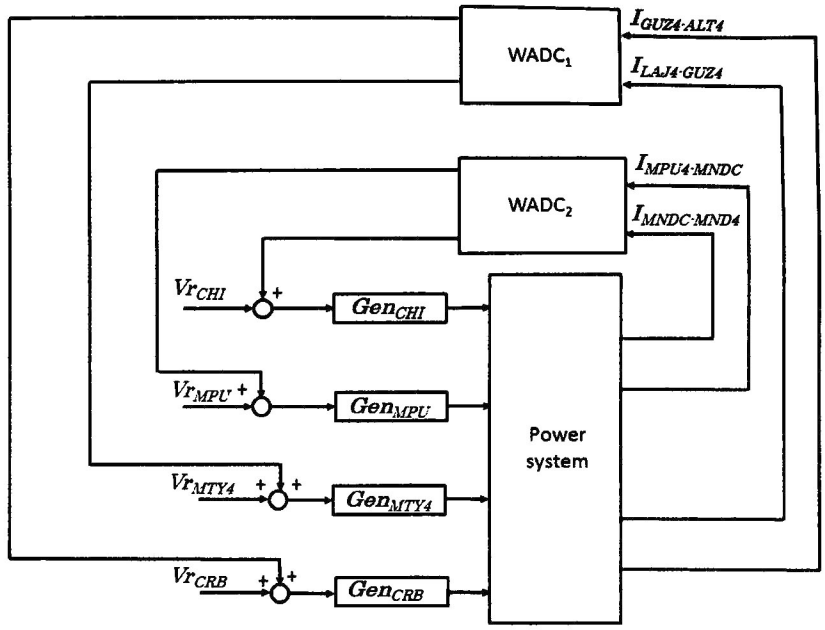

Fig. 5.9. Control configuration for the set 1.

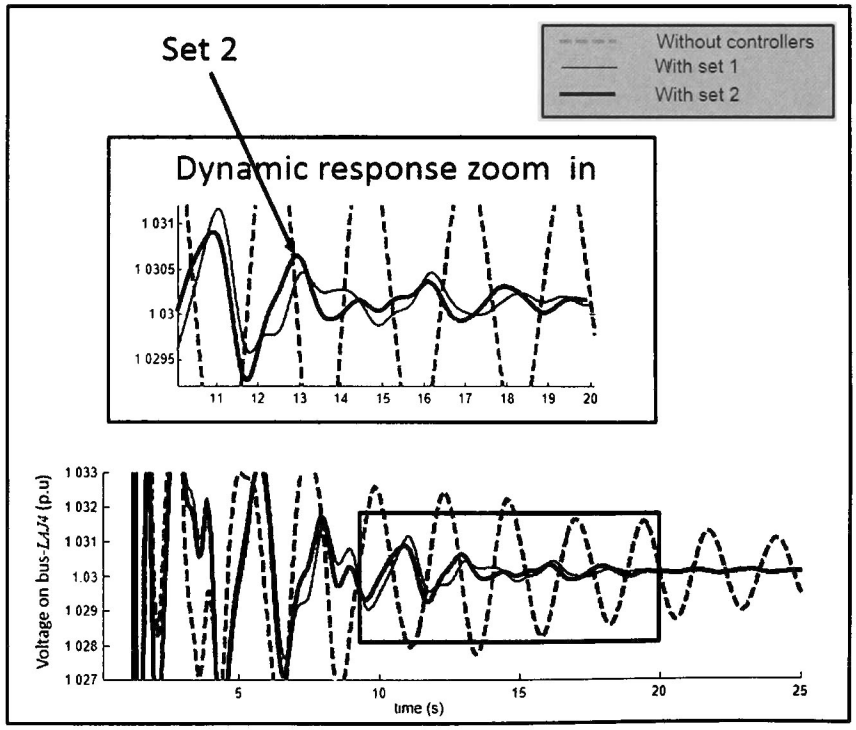

Fig. 5.10. Bus voltage magnitude at 400-kV bus *LAJ4* for the sets 1 and 2.

Table 5.7 compares the electromechanical modes of the system with and without WADCs. A minor adverse interaction with mode 2 can be observed for the set 2 but this is of little practical importance. On the other hand; the evaluation of the mixed SSV with and without controllers is shown in Fig. 5.11. In general, in terms of the robustness, the best option is given by the set 2, but it is possible to choose the set 1.

Table 5.7.

Comparison of system performance with and without control action

Mode	Control option	Eigenvalue	Freq. (Hz)	Damp. Factor
Inter-area Mode 1	Without controllers	-.0769±j2.6975	0.42	0.028
	With set 1	-.2861±j2.4756	0.39	0.114
	With set 2	-.2944±j2.5822	0.41	0.113
Inter-area Mode 2	Without controllers	-.1916±j3.6439	0.58	0.052
	With set 1	-.2161±j3.6250	0.57	0.059
	With set 2	-.1918±j3.6484	0.58	0.052
Inter-area Mode 3	Without controllers	-.1338±j4.8535	0.77	0.027
	With set 1	-.5429±j4.7536	0.75	0.113
	With set 2	-.5630±j4.4320	0.70	0.126

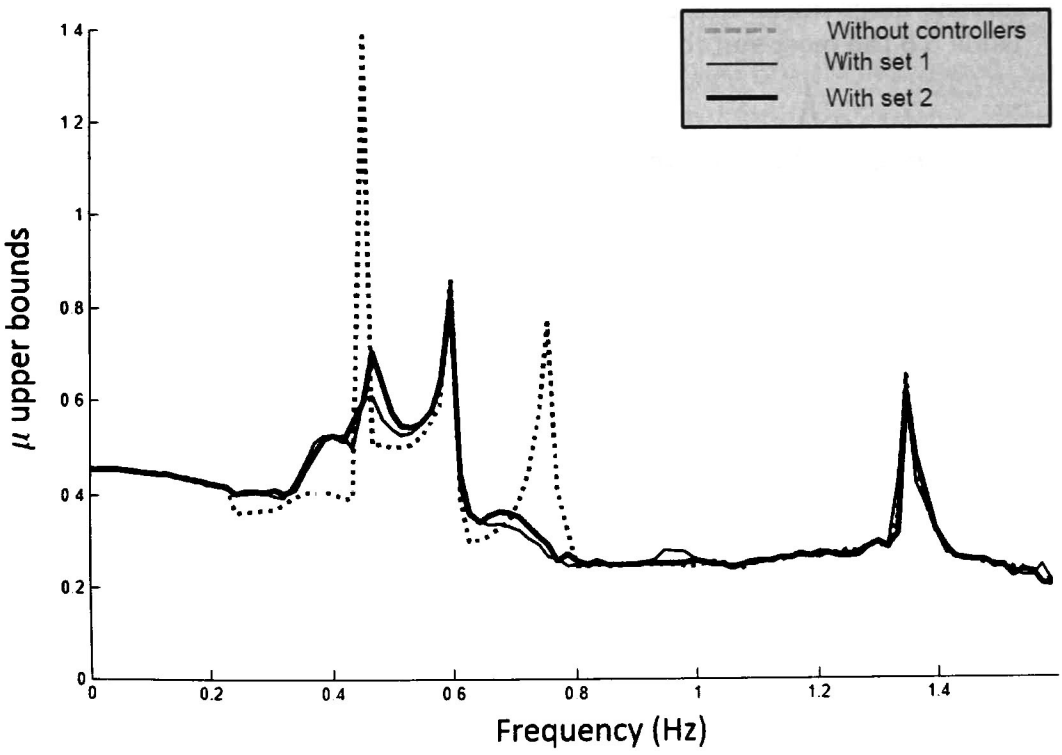

Fig. 5.11. Mixed SSV without and with controllers.

5.4 Design of a hierarchical control configuration (Case 2)

In order to make an effective comparison between the configuration of the last section and a hierarchical control configuration using the BRG analysis in this section, the following procedure is followed. Two WADCs are designed for the MIS using the same nominal model described in last section, then the modal and SSV analysis are omitted, but the first controller configuration $WADC_1$ has three input signals and two output signals.

The second controller configuration $WADC_2$ has only two input signals and two output signals.

5.4.1 BRG analysis for the proposed candidate sets

The candidate sets for the selection of input-output signals using the BRG analysis is shown in Table 5.8. As mentioned before, the magnitude of line currents are chosen as the input signals to the WADC since enables substantial damping for all operating conditions. Furthermore, Table 5.8 list the peak of the BRG in the fourth column. For example, it can be seen that for the first WADC of the set 1, the current magnitude in lines $I_{TOP4\text{-}SNB4}$, $I_{GUZ4\text{-}ALT4}$ and $I_{LAJ4\text{-}GUZ4}$ are the most suitable signals to damp electromechanical oscillations with strong interaction. For the second WADC of the set 1, the current magnitudes are given by $I_{MPU\text{-}MND}$ and $I_{MND\text{-}MND4}$. In general, from Table 5.8 the most suitable options are given by the sets 1 and 2.

Table 5.8.

Peak of the BRG for the case 2 of the candidate sets of WADCs

Set No.	Output signals from WADC to u	Input signals to WADCs	$\|[\lambda(s)]_{ii}\|_\infty$
Set 1	Gen_{MTY4}-Gen_{CRB}	$I_{TOP4\text{-}SNB4}$ - $I_{GUZ4\text{-}ALT4}$ - $I_{LAJ4\text{-}GUZ}$	6.53
	Gen_{CHI}-Gen_{MPU}	$I_{MPU4\text{-}MNDC} - I_{MNDC\text{-}MND4}$	3.26
Set 2	Gen_{MTY4}-Gen_{CRB}	$I_{RES2\text{-}ARC2}$ - $I_{GUZ4\text{-}ALT4}$ - $I_{LAJ4\text{-}GUZ}$	6.06
	Gen_{CHI}-Gen_{SLP}	$I_{MPU4\text{-}MNDC} - I_{TOP4\text{-}SNB4}$	9.45
Set 3	Gen_{MTY1}-Gen_{MTY4}	$I_{RES2\text{-}ARC2}$ - $I_{GUZ4\text{-}ALT4} - I_{GUZ4\text{-}HUI4}$	1.79
	Gen_{CHI}-Gen_{MPU}	$I_{CHI4\text{-}JUI4} - I_{JUIC\text{-}TMD4}$	2.04
Set 4	Gen_{CHI}-Gen_{MPU}	$I_{MPU4\text{-}MNDC}$ - $I_{MNDC\text{-}MND4}$ -$I_{CHI4\text{-}JUI4}$	2.67
	Gen_{MTY1}-Gen_{MTY4}	$I_{PRD4\text{-}ALT4} - I_{GUZ4\text{-}ALT4}$	1.93
Set 5	Gen_{CHI}-Gen_{MPU}	$I_{MPU4\text{-}MNDC}$ - $I_{MNDC\text{-}MND4}$ -$I_{JUIC\text{-}TMD4}$	2.46
	Gen_{MZD}-Gen_{MTY4}	$I_{PRD4\text{-}ALT4} - I_{GUZ4\text{-}ALT4}$	1.93
Set 6	Gen_{MZD}- Gen_{CRB}	$I_{RES2\text{-}ARC2}$ - $I_{GUZ4\text{-}ALT4} - I_{LGV2\text{-}LAJ4}$	4.94
	Gen_{CHI}-Gen_{MPU}	$I_{MPU4\text{-}MNDC} - I_{MNDC\text{-}MND4}$	2.99
Set 7	Gen_{SLM}- Gen_{MZN}	$I_{TOP4\text{-}SNB4} - I_{GUZ4\text{-}ALT4} - I_{LGV2\text{-}LAJ4}$	6.38
	Gen_{CHI}-Gen_{MPU}	$I_{MPU4\text{-}MNDC} - I_{MNDC\text{-}MND4}$	3.06

Figure 5.12 shows the frequency response of the BRG analysis for system where the resonance peaks confirm that the best options are obtained for the

sets 1 and 2. Nevertheless, the set 7 is a more suitable option for local modes due to the fact the resonances peak of the BRG is near local frequencies.

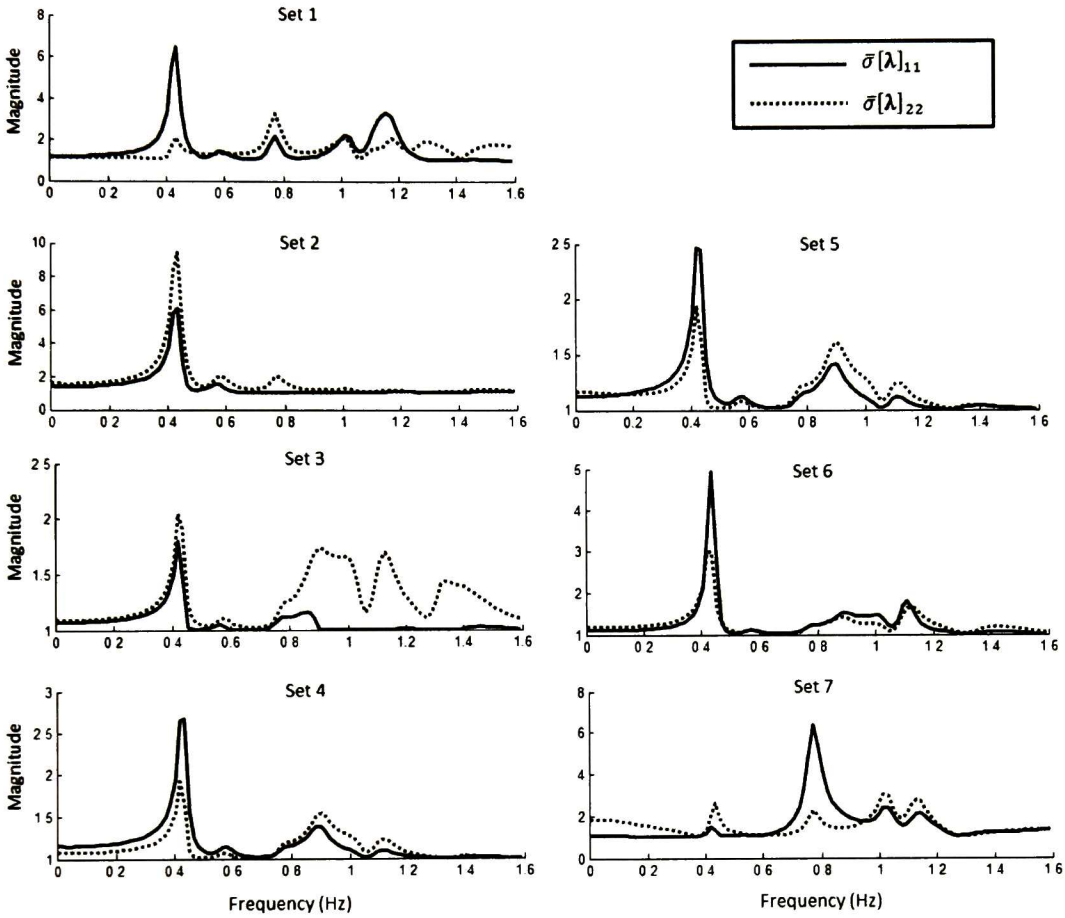

Fig. 5.12. BRG for the case 2 of the candidate sets.

5.4.2 Design of block decentralized controllers and evaluation of the performance under transient conditions

The weighting functions of block decentralized controllers are described in Table 5.9. The MIMO controllers can be approximated by a lower order state space representation given in the fifth column of Table 5.9 where it is shown the size of the reduced-order model in parenthesis.

Fig 5.13 shows the largest singular values of the block GDRG for the sets 1 and 2 of the case 2, where the differences for inter-area modes are clear. The set 1 is the most suitable option to damp the inter-area oscillations with good performance due to the high interactions among control loops.

Table 5.9.

Weighting functions for the case 2 of the sets 1 and 2

Set No.	$W_1(s)$	$W_2(s)$	$W_3(s)$	Reduced-order model
Set 1	$(s+20)/(.1s+100)$	1E-2	$100/(s+10)$	(14) 10
	1	10	$11/(s+10)$	(16) 9
Set 2	$(s+20)/(.1s+100)$	1E-1	$100/(s+10)$	(15) 8
	3	5.3	$.1/(s+10)$	(19) 7

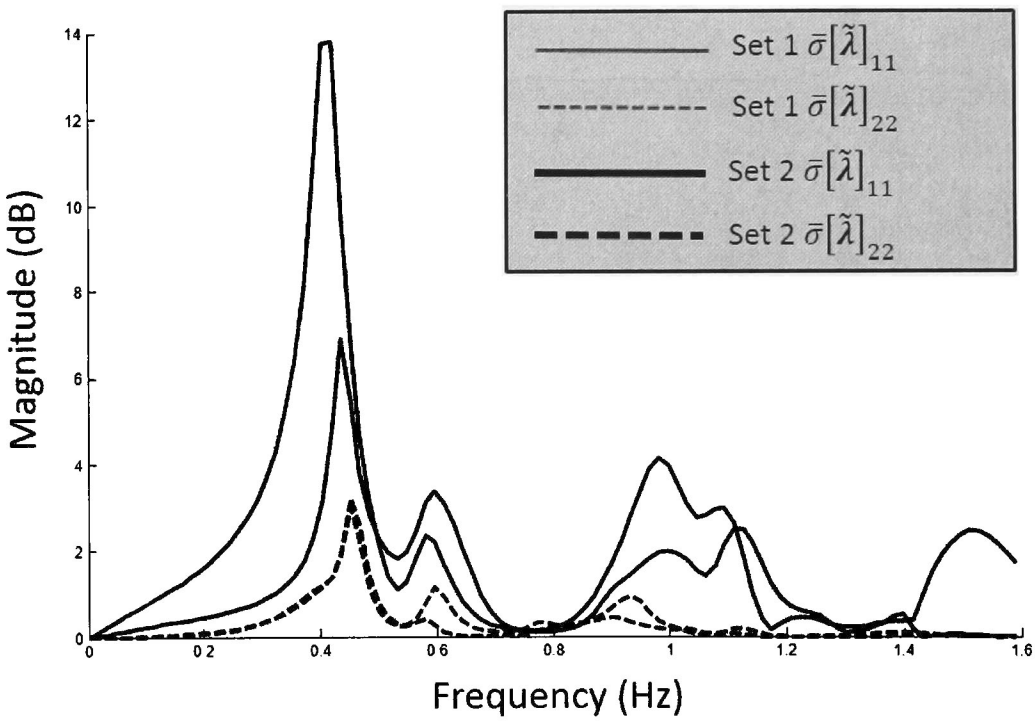

Fig. 5.13. Frequency response of the block GDRG for the sets 1 and 2 of the case 2.

At this point, it must be noticed that the developed control configuration only has WADCs to damp inter-area oscillations. In general, Table 5.10 shows the modes of the MIS with controllers and without non-square WADCs for the sets 1 and 2, where the best option is the set 1. Note that for mode 2, the set 2 shows an undesirable damping. This means that the interaction of frequency domain affects both the stability and the damping performance of the set 2. In general, the most suitable input-output signals is given by the set 1. Moreover, simulations are carried out to evaluate the performance of the designed

controller corresponding to some fault scenarios in the MIS. Figure 5.14 and 5.15 show the transient conditions of the sets 1 and 2, where the set 2 does not have a good damping, as was observed from linear analysis.

Table 5.10.

Comparison of system performance with and without WADCs

Mode	Control option	Eigenvalue	Freq. (Hz)	Damp. factor
Inter-area Mode 1	Without controllers	-.0769±j2.6975	0.42	0.028
	With set 1	-.2985±j2.4846	0.39	0.119
	With set 2	-.2957±j2.6608	0.42	0.110
Inter-area Mode 2	Without controllers	.1916±j3.6439	0.58	0.052
	With set 1	-.2716±j3.6645	0.58	0.073
	With set 2	.1644±j3.6759	0.58	0.044
Inter-area Mode 3	Without controllers	.1338±j4.8535	0.77	0.027
	With set 1	-.5622±j4.6880	0.74	0.119
	With set 2	-.2921±j4.9864	0.79	0.058
Local Mode 4	Without controllers	.1926±j6.4254	1.02	0.030
	With set 1	-.2998±j6.8417	1.08	0.043
	With set 2	-.3115±j6.9678	1.10	0.044
Local Mode 5	Without controllers	-.2636±j7.0585	1.12	0.037
	With set 1	.3767±j7.7809	1.23	0.048
	With set 2	-.4278±j7.5332	1.19	0.056
Local Mode 6	Without controllers	-.2536±j7.7506	1.23	0.032
	With set 1	-.2561±j7.7436	1.23	0.033
	With set 2	-.3738±j7.5947	1.20	0.049

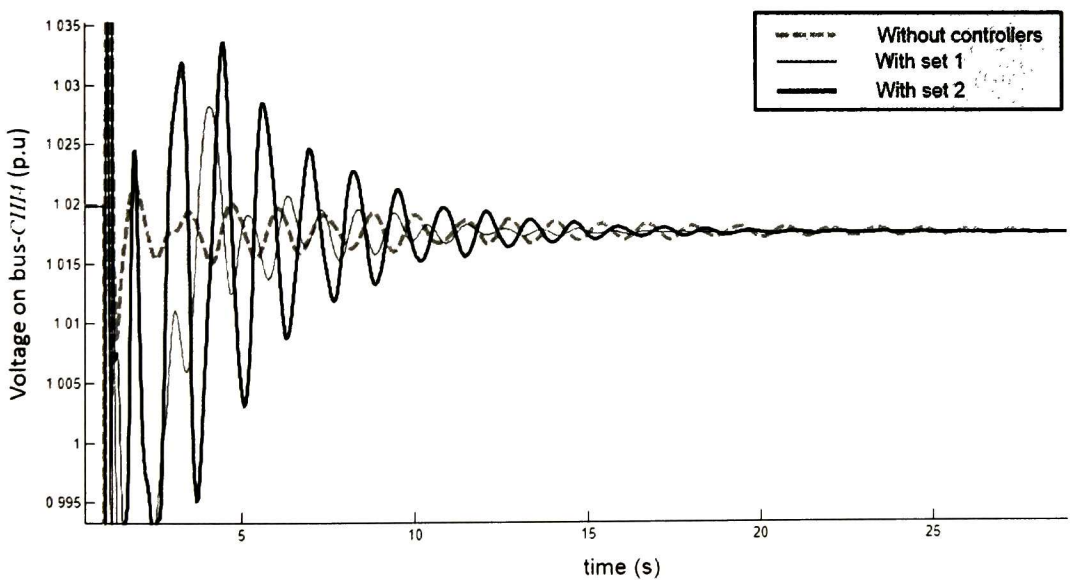

Fig. 5.14. Bus voltage magnitude at 400-kV bus *CHI4* for the non-square MIMO WADCs of the sets 1 and 2.

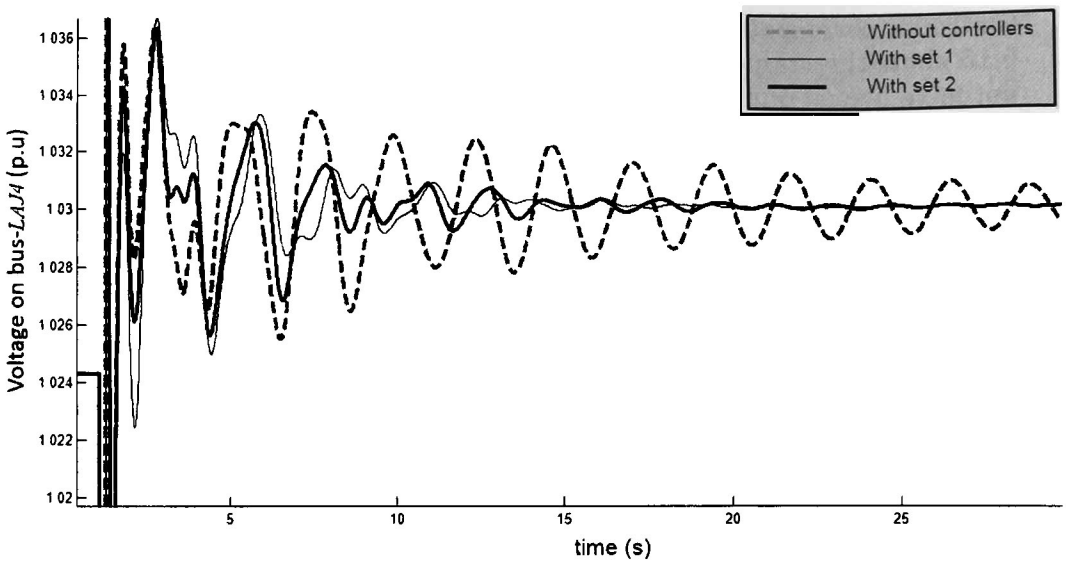

Fig. 5.15. Bus voltage magnitude at 400-kV bus *LAJ4* for the non-square MIMO WADCs of the sets 1 and 2.

Adding damping to local modes can be achieved by means of placing PSSs to increase power system performance. Incorporation of this type of controllers leads to a hierarchical control configuration. Table 11 describes input-output signals for PSSs and Fig. 5.16 shows the hierarchical configuration. Details of the coordination of local PSSs are omitted but can be find in [10-11].

As a comparison, Fig. 5.17 and 5.18 show the test cases for the sets 1 and 2 with and without hierarchical control configuration. From this case, it is shown that the set 1 is the best control hierarchical configuration. The same results can be confirmed in Table 5.12 where the eigenvalue analysis of the system was carried out to verify the stability of the MIS. Furthermore, the mixed SSV, described by Fig. 5.19, confirms the robust stability of the system.

Table 5.11.

Input-output signals for PSSs of sets 1 and 2

Set No.	Input-output signals
Set 1	ω_{LGV} - Gen_{LGV}
	ω_{SLP} - Gen_{SLP}
	ω_{RIB} - Gen_{RIB}
	ω_{CAR1} - Gen_{CAR1}
	ω_{DBO} - Gen_{DBO}
Set 2	ω_{SLP} - Gen_{SLP}
	ω_{MTY4} - Gen_{MTY4}
	ω_{CRB} - Gen_{CRB}

Table 5.12.

Comparison of system performance with and without WADCs and PSSs

Mode	Control option	Eigenvalue	Freq. (Hz)	Damp. factor
Inter-area Mode 1	Without controllers	-.0769±j2.6975	0.42	0.028
	With set 1	-.3575±j2.4627	0.39	0.143
	With set 2	-.3753±j2.6487	0.42	0.140
Inter-area Mode 2	Without controllers	.1916±j3.6439	0.58	0.052
	With set 1	.2818±j3.6498	0.58	0.077
	With set 2	-.2343±j3.660	0.58	0.063
Inter-area Mode 3	Without controllers	.1338±j4.8535	0.77	0.027
	With set 1	.7533±j4.8719	0.77	0.152
	With set 2	.3033±j4.9912	0.79	0.060
Local Mode 4	Without controllers	-.1926±j6.4254	1.02	0.030
	With set 1	-1.3061±j6.9586	1.10	0.184
	With set 2	-.2773±j6.2376	0.99	0.044
Local Mode 5	Without controllers	-.2636±j7.0585	1.12	0.037
	With set 1	-.7520±j8.6882	1.38	0.086
	With set 2	-.4054±j7.7643	1.23	0.052
Local Mode 6	Without controllers	-.2536±j7.7506	1.23	0.032
	With set 1	-.9544±j8.4562	1.34	0.112
	With set 2	-.3901±j7.6033	1.21	0.051

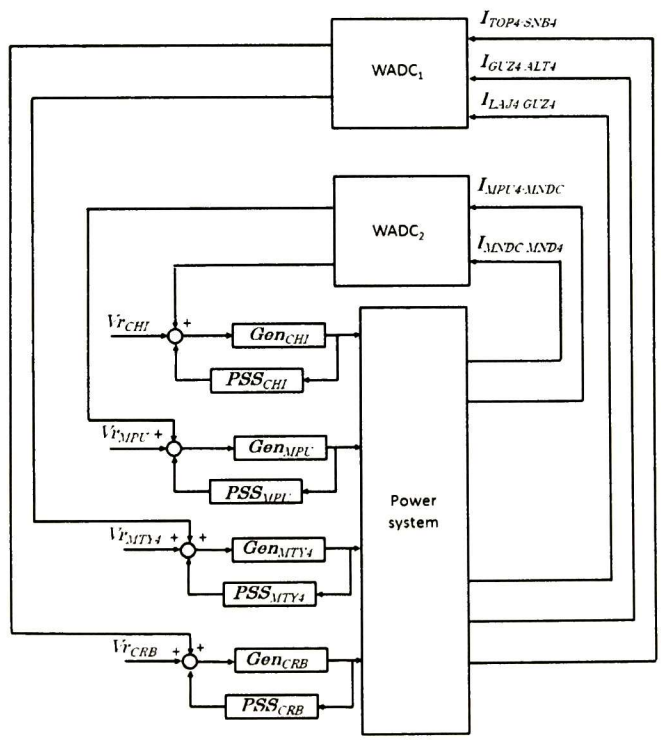

Fig. 5.16. Hierarchical control configuration for the set 1.

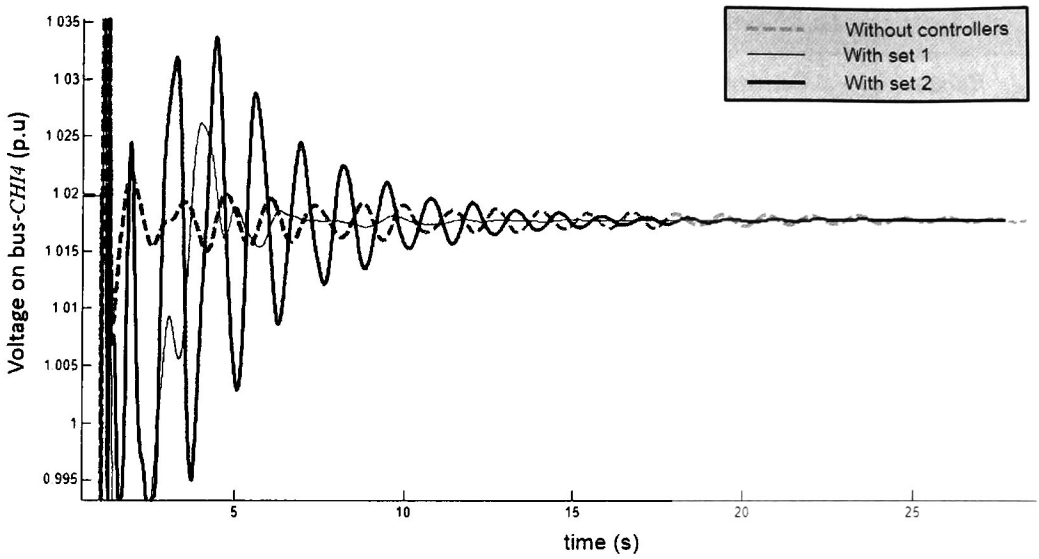

Fig 5.17. Bus voltage magnitude at 400-kV bus *CHI4* for the non-square MIMO WADCs and PSSs of the sets 1 and 2.

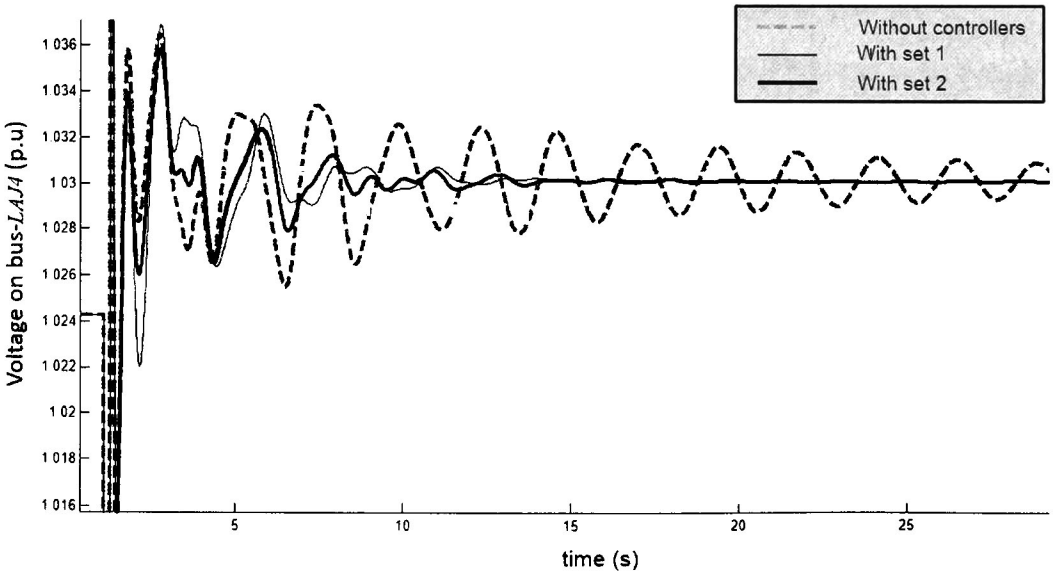

Fig 5.18. Bus voltage magnitude at 400-kV bus *LAJ4* for the non-square MIMO WADCs and PSSs of the sets 1 and 2.

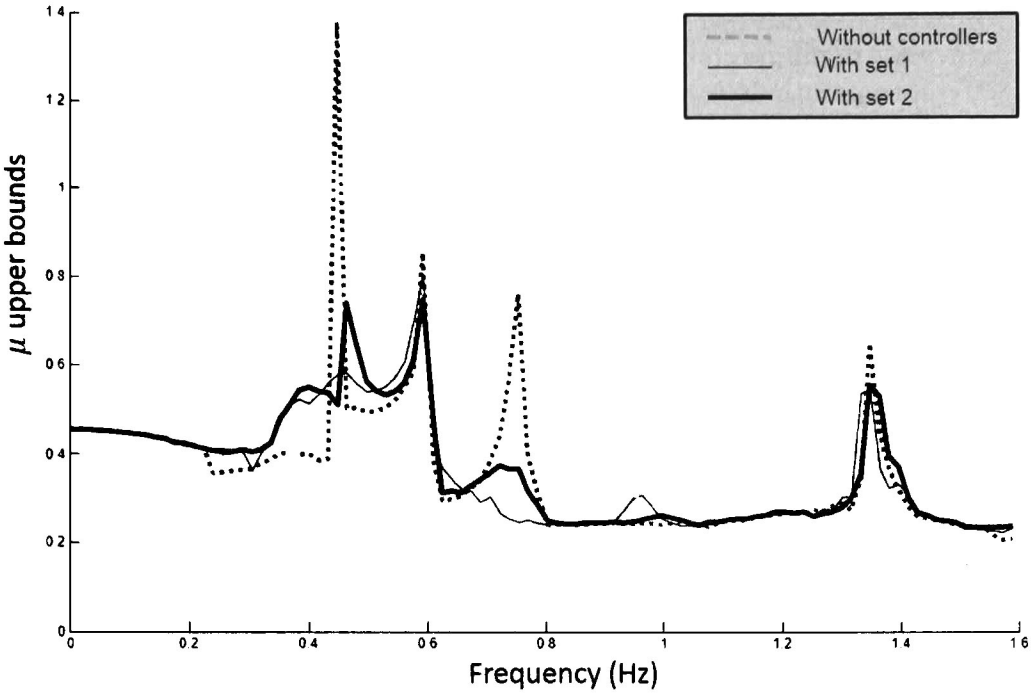

Fig. 5.19. Mixed SSV without and with controllers.

5.5 Comparison of the block decentralized configuration versus the hierarchical control configuration

As a general comparison, non-linear simulations are performed, to test the efficacy of the designed control configurations: block decentralized and hierarchical configuration. Fig. 5.20 and 5.21 show the results for the two proposed control configurations, it is clear that the MIS under the hierarchical configuration presents most satisfactory damping. In general, these non-linear simulations provide clear evidence that the WADCs obtained using LMI techniques provides excellent damping.

To further validate the robust stability of the designed control configurations, the upper bound of the mixed SSV is computed on the linear system. The dimensions of the perturbations matrices are given by := $\{\text{diag}[\delta_1^r \mathbf{I}_{417\times417}, \delta_2^r \mathbf{I}_{278\times278}]: \delta_1^r,\ \delta_2^r \in \mathbb{R}\}$. Fig. 5.22 shows the upper bounds of the μ analysis for the MIS under three scenarios: the dotted line belongs to case without controllers and the thin line belongs to the set 1 case 1 and the thick line to the hierarchical configuration. It is clear that the system achieves robust stability with controllers and the results are consistent with the non-linear simulations.

In general, it can be concluded that the proposed configurations can provide sufficient damping to the MIS and has satisfactory robustness against different operations conditions. Finally, these results confirm the validation of the systematic methodology.

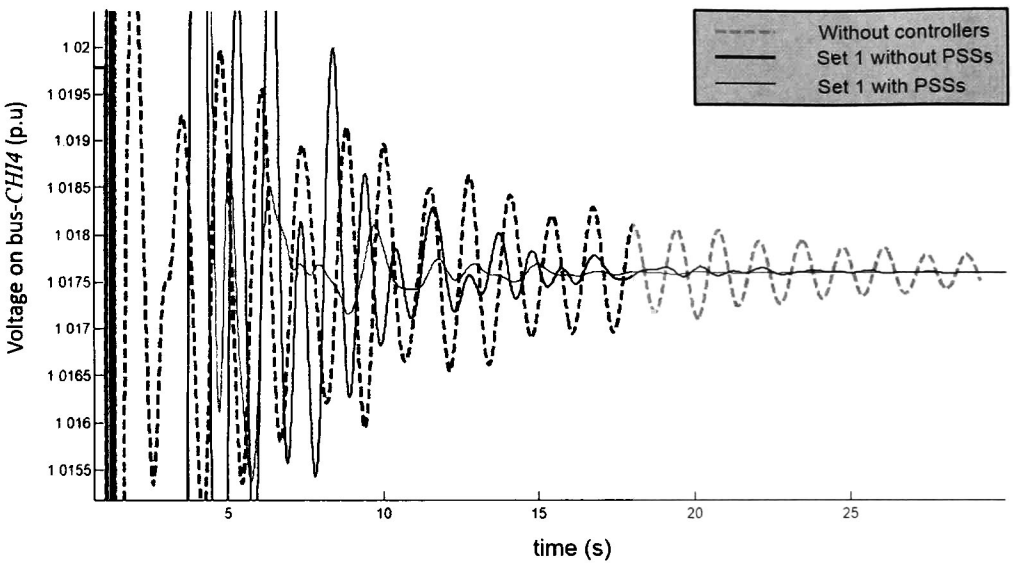

Fig 5.20. Bus voltage magnitude at 400-kV bus *CHI4* for the block decentralized and hierarchical configuration of the set 1.

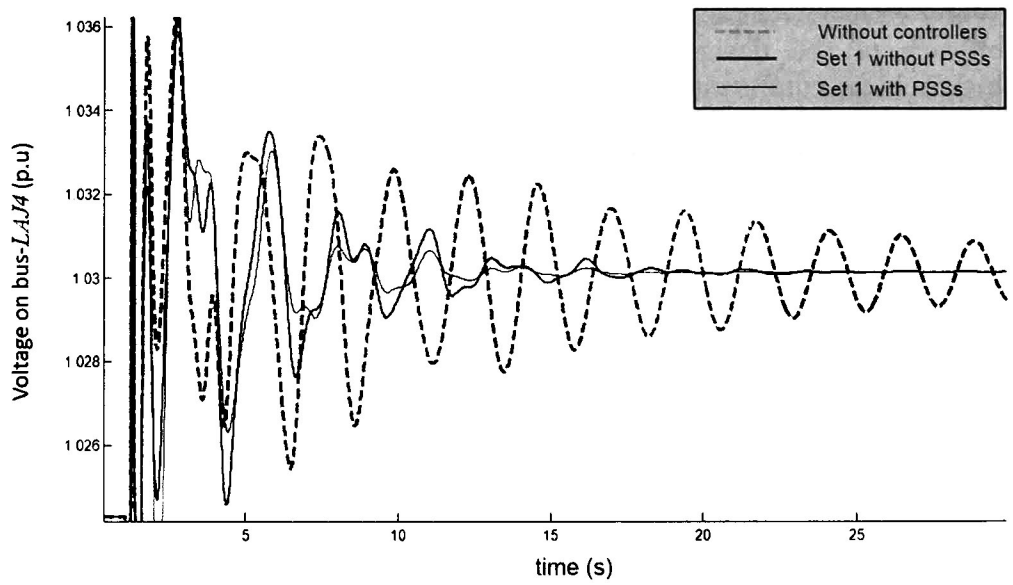

Fig 5.21. Bus voltage magnitude at 400-kV bus *LAJ4* for the block decentralized and hierarchical configuration of the set 1.

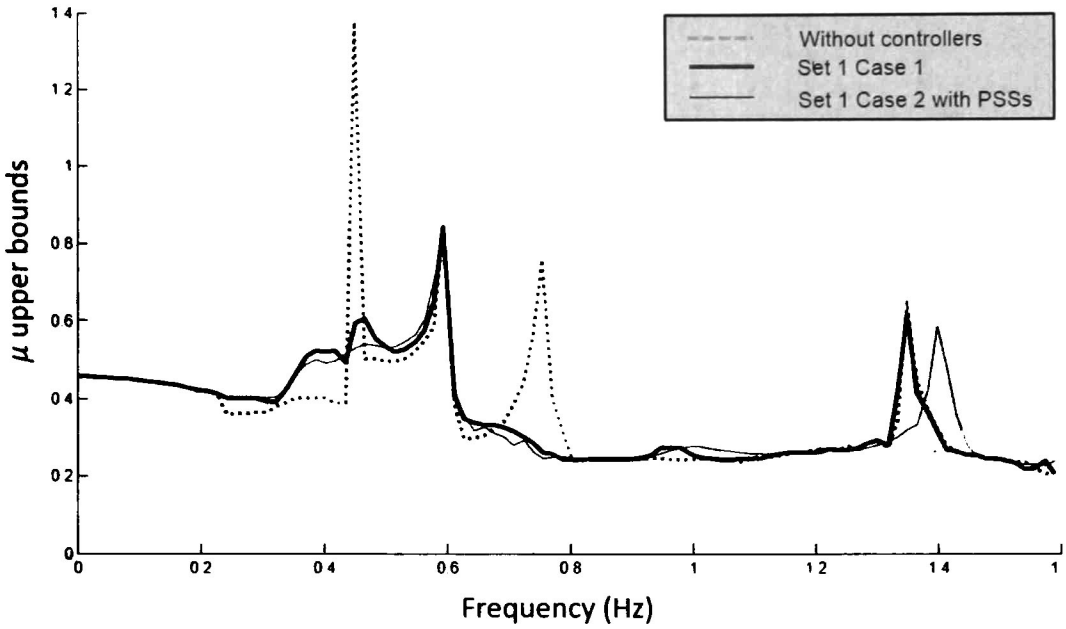

Fig 5.22. Mixed SSV for the block decentralized and hierarchical control configuration of the set 1.

5.6 Effect of communication time-delays

To evaluate the performance of the designed controllers with time-delays in different fault scenarios, non-linear time simulations are computed. Three types of faults are simulated in the MIS. The responses under time-delays, 30, 50 and 100 ms, are given in Fig. 5.23, 5.24 and 5.25. It can be seen that the damping effect of hierarchical configuration does not achieve a satisfactory performance in 100ms.

In general, the degradation of inter-area modes is sever. From these results, with the increased dependence on controls to maintain power system stability and security, significant new requirements are necessary on communication networks in terms of service quality and reliability for the MIS.

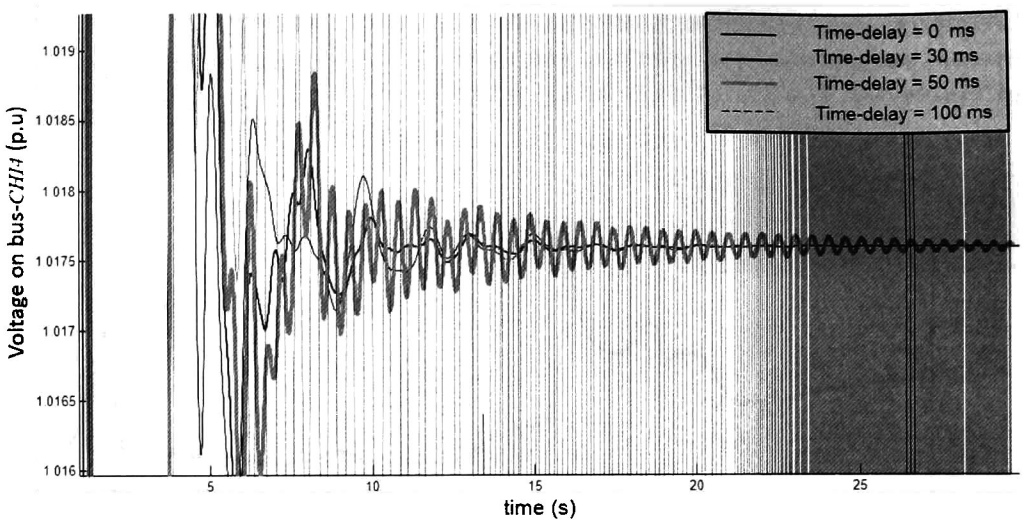

Fig 5.23. Bus voltage magnitude at 400-kV bus *CHI4* for the hierarchical configuration of the set 1 with different time-delays.

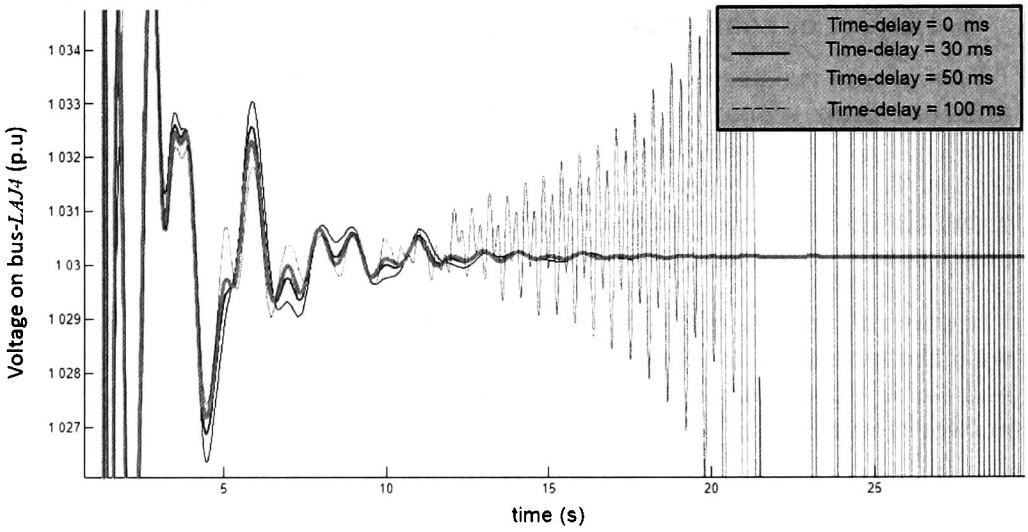

Fig 5.24. Bus voltage magnitude at 400-kV bus *LAJ4* for the hierarchical configuration of the set 1 with different time-delays.

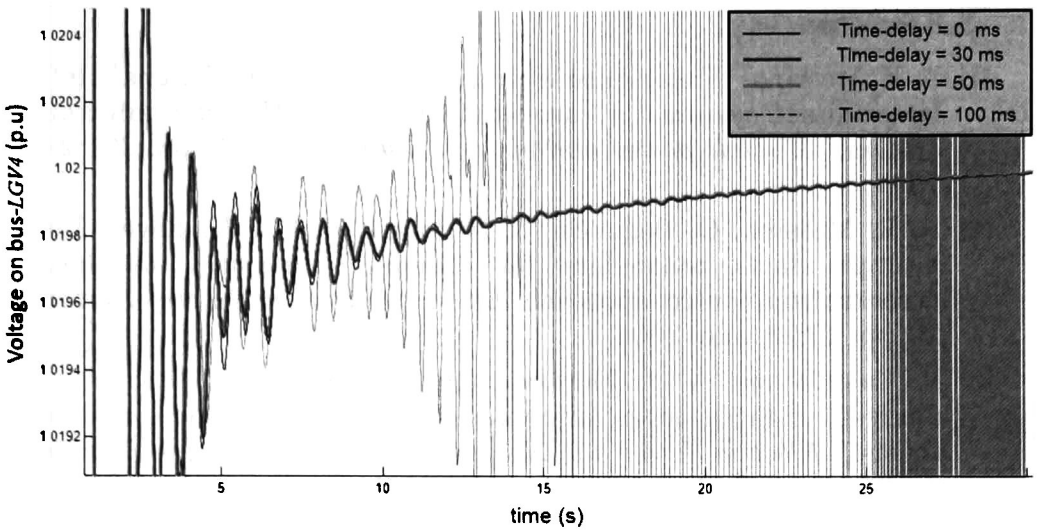

Fig 5.25. Bus voltage magnitude at 400-kV bus *LGV4* for the hierarchical configuration of the set 1 with different time-delays.

5.7 Conclusions

In this chapter, a general method to find suitable input-output variable pairings for block decentralized controllers of large interconnected power systems based on the BRG and the block GDRG methods is proposed. The research extends existing theory to the case of WADCs with MIMO characteristics. In addition, the incorporation of WADCs or block decentralized controllers offers better coordination among controllers and performance under transient conditions. Simulation results show that the proposed technique yields in better small and large signal performance than conventional controllers and suggests the importance of investigating control interactions in the design of WADC controllers.

The results are promising but they also show that the use of linear, continuous methods to design a controller, although very powerful, requires considerable tuning, testing and further development in the nonlinear, discontinuous real world. Furthermore, in order to transmit wide-area signals for use in controls, fast and reliable communication systems are required.

5.8 References

[1] A. R. Messina, "Experience with the analysis of small signal stability in longitudinal systems: a case study with the Mexican interconnected system," *Electric power and energy systems*, vol. 17, pp. 291-299, Oct. 1995.

[2] A. R. Messina, O. Begovich, J. H. López, and E. N. Reyes, Design of multiple facts controllers for damping inter-area oscillations: a decentralized control approach, *Electric Power and Energy Systems*, Vol. 26, pp. 19-29, Jan. 2004.

[3] R. Castellanos, A. R. Messina, and H. Sarmiento, "Robust stability analysis of large power systems using the structured singular value theory," *Electric Power and Energy Systems*, vol. 27, pp. 389-397, Jun. 2005.

Chapter 6
General Conclusions and Suggestions

This chapter gives the main conclusions with their respective original contributions. Finally, suggestions are given for future researches.

6.1 General conclusions

Very often, real-life systems are subject to parametric uncertainties by unknown parameters and measurement noise. At present, a valuable topic is the implementation of efficiently computational algorithms for large power systems to describe the structured uncertainty. Investigations of power system dynamic behavior typically involve numerous uncertain parameters from a vast number of generators and FACTS devices. On the other hand, the performance of a power system is described by their slow inter-area electromechanical eigenvalues. Then, the design of a controller to increase system damping is fundamental for a good performance.

In the last decade, phasor measurement unit (PMU) devices have offered wide-area measurement system (WAMS) by which large power systems can be stabilized by block decentralized controllers, quasi-decentralized controllers and centralized controllers. This new type of technology captures the dynamic information in near real time and resolution. Then, WAMS gives the opportunity to design multiple-input multiple-output (MIMO) WADCs to damp electromechanical oscillations for a good operation of power systems. In addition to the multiple measurement signals from a WAMS, there is usually a large amount of local available signals from generators to damp local modes.

In the literature classic control methods has been proved for small power systems to design PSSs: the conventional root-locus and multi-variable root locus. However, the robustness is not directly considered in the design approach and, some occasions, the system might not be operating under a nominal point. In real power systems the problem is more complex due to size of the network.

To address the above problem in this research, a design procedure based on the structural singular value (SSV), the block relative gain (BRG) methodology and the joint controllability-observability to choose the most suitable input-output parings in MIMO wide-area damping controllers (WADCs) has been proposed. To design the block decentralized controllers the linear matrix inequality (LMI) techniques for block decentralized controllers and hierarchical control configurations have been applied. It should be pointed out that the implementation of the designed controllers in this document based on a balanced reduced-order model has been implemented.

On the other hand, the extra information provided by the structured uncertainty has established a clear framework with the SSV technique which has included a percent of complex uncertainty into the parameters. Nevertheless, the computational burden has been increased due to high dimensional of block matrices, but the results are promising for futures researches.

A similar argument holds for the BRG which has given a new general perspective for interacting control loops in MIMO controls. In addition, the BRG technique generalizes the described concept by the classic definition of the RGA. The developed theory is then used to define the block GDRG which opens new concepts in the theory of interaction measures. Finally, non-linear simulation results confirm the efficacy of the proposed systematic method.

The following advantages and contributions of this dissertation are:

- A systematic method is derived to design MIMO WADCs in power systems to damp electromechanical modes which take into account the most sensitivity global signals.

- The implementation and use of the BRG to describe interactions among MIMO controllers for large power systems. The BRG generalizes the concept of the relative gain array (RGA) analysis.

- A general framework based on the SSV is developed to evaluate the robust stability in power systems, which includes a percent of complex uncertainty to avoid the discontinuity of the lower bound of the mixed SSV.

- A sequential method is proposed which takes into account hierarchical and block decentralized configurations.

- A rigorous review of the theory of interaction measures to describe new ideas in power systems.

6.2 Suggestions for future works

This desertion has considered a systematic method to design WADCs taking into account MIMO interactions though the BRG analysis. In addition, the use of the complex and mixed SSV has been used to evaluate the robust stability of large power systems. Nevertheless, the next aspects require further investigation:

- A method which takes into account the time-delays for the MIMO signals in WADCs to explore the interactions of control loops.

- A modal analysis method to select the most suitable multiple input-output signals to design WADCs.

- There are instances where it is appropriate to represent parameter uncertainties into a sector of the Nyquist plot. This sector can be described by $2\theta < \pi$. This means that the Nyquist plot can lie in a sector of the unit-disk and this idea would result in significant computational savings in comparison with the direct approach described by the standard SSV

- It is a necessity to explore conditions to characterize phase uncertainty in multivariable systems, but also to provide a practical computational method for large power systems. In general, a method that uses uncertainty phase information in robustness analysis, such as bounds on the phase of the uncertain dynamics blocks, and a criterion for stability analysis of time-delay systems

- Development of efficient algorithms for the upper bound and the lower bound of the skew SSV in large power systems. This problem in large networks can preset due to the fact that some problems are re-scaled in the analysis of performance: The physical uncertainties have a fixed range and the performance block is allowed to vary to determine the point where the system could become unstable. Finally, the incorporation of phase uncertainty into the algorithm of the skew SSV to describe the communication time-delay.

- Development of an efficient algorithm to compute a model reduction method for uncertain systems. This model reduction could provide a framework in large power systems to implement the D-G-K, the μ-K and the standard D-K iteration. On the other hand, model reduction also may interpreted as state order reduction for multi-dimensional systems.

- A method to compute solutions of the structured $\mathcal{H}_\infty$-problem with time delays.

- Efficient computation of a general framework for the standard D-K iteration including the structured $\mathcal{H}_\infty$-problem for large power systems.

CENTRO DE INVESTIGACIÓN Y DE ESTUDIOS AVANZADOS DEL I.P.N.
UNIDAD GUADALAJARA

El Jurado designado por la Unidad Guadalajara del Centro de Investigación y de Estudios Avanzados del Instituto Politécnico Nacional aprobó la tesis

Diseño de la estructura y el control de área amplia del sistema de potencia

Wide-area power system control and structure design

del (la) C.

Evaristo Noé REYES PÉREZ

el día 06 de Febrero de 2015.

Dr. José Manuel Cañedo Castañeda
Investigador CINVESTAV 3C
CINVESTAV Unidad Guadalajara

Dr. José Javier Ruíz León
Investigador CINVESTAV 3C
CINVESTAV Unidad Guadalajara

Dr. Alexander Georgievich Loukianov
Investigador CINVESTAV 3C
CINVESTAV Unidad Guadalajara

Dr. Arturo Román Messina
Investigador CINVESTAV 3C
CINVESTAV Unidad Guadalajara

Dr. Ramon Octavio Jimenez Betancourt
Profesor Investigador
Universidad de Colima